Phase transitions under shock-wave loading*

G. E. Duvall

Washington State University, Pullman, Washington

R. A. Graham

Sandia Laboratories, Albuquerque, New Mexico

First-order polymorphic, second-order, melting, and freezing transitions induced by shock-wave loading are reviewed. Comprehensive tabulations of the experimental observations are presented and materials that have been subjected to in-depth study are reviewed in more detail. Theories of the mechanics, thermodynamics, kinetics, and shear strength of shock-loaded materials are described and experimental techniques are briefly reviewed.

CONTENTS

*This work was supported in part by the U. S. Energy Research and Development Administration, ERDA, under Contract E(29-1)789, by the National Science Foundation under Grant DMR72-03171 A02, and by the U. S. Air Force Office of Scientific Research under Grant AFOSR-76-2898.

I. INTRODUCTION

Shock phenomena most commonly experienced by an individual are the boom from supersonic aircraft, the crack of a rifle, and automobile pileups on crowded freeways. The fact that the last-named event produces a shock wave suggests what is indeed true: that shock waves are very general and are, if not ubiquitous, at least pervasive. Extensive use has been made of the shock wave as a scientific tool in the study of gases, but there has been limited application to solids. Even so, considerable data have accumulated in the last twenty years on miscellaneous problems, even though there has not yet been concentrated study of many subjects. One area which has received considerable attention is the pressure-induced phase transition. Testimony to this attention lies in the entries of Table AI of the Appendix. Even here, however, efforts are in general fragmented, and few materials have been studied in detail compared to static high-pressure investigations. (See, for example, Klement and Jayaraman, 1967 and Rooymans, 1969.)

The purposes of this review are to present some elementary things about shock waves, to explain how they relate to phase transitions, to tell what measurements can be made and how, to list and discuss measurements that have been made, and to point out some areas for future work.

Shock waves in solids are ordinarily produced by impact of a projectile on the sample or by detonation of an explosive in contact with it. In either case, the result is the introduction of a step pressure that propagates through the sample, changing shape as it goes; these changes in shape result from the action of inertial forces derived from mechanical properties of the sample. When shock waves are used to probe material properties, the challenge to the experimenter is to accurately measure changes in shock-wave shape and to interpret them in terms of material properties. The philosophy is analogous to that involved when response of an electrical network to a step in voltage is used to determine network parameters. But the shock-wave problem is more complicated because the sample is a continuum and because relations between impressed force and mechanical response are nonlinear.

A stress pulse produced by sudden application and

subsequent release of pressure on the surface of a solid has a beginning, a middle, and an end. The beginning is a shock front, i.e., a near-discontinuous compression. The middle is a region of uniform or slowly varying pressure, density, and temperature; the end is a rarefaction that returns the material to something approaching its original state. In some experiments the middle region is so abbreviated that only beginning and end are apparent. A representation of an unusually complicated pressure profile is shown in Fig. 1. All these features, developing from a step in pressure loading and a subsequent unloading applied at a plane boundary, may exist in a single sample, but are not apt to be recorded in a single measurement. $\mathcal{S}_1$ is an elastic shock travelling at the dilatational wave velocity and limited in amplitude by the shear strength of the material. In an ideal elastic–plastic solid, $\mathcal{S}_1$ brings the material to the point of permanent deformation, but no deformation occurs until $\mathcal{S}_2$ arrives. The second shock $\mathcal{S}_2$ is a wave of plastic deformation, often called the "Plastic I Wave," limited in amplitude by the pressure at which the phase transformation takes place. In a reversible transformation, $\mathcal{S}_2$ compresses the material to the boundary of the mixed phase region, but transformation is delayed until arrival of $\mathcal{S}_3$, the "Plastic II Wave." Transformation occurs in the shock front $\mathcal{S}_3$, going to completion if the driving pressure is large enough. The amplitude of $\mathcal{S}_3$ is determined by driving pressure. $\mathcal{S}_3$ travels more slowly than $\mathcal{S}_2$, which, in turn, travels more slowly than $\mathcal{S}_1$. In real materials the regions bounded by $\mathcal{S}_1$, $\mathcal{S}_2$, and $\mathcal{S}_3$ are regions of relaxation toward equilibrium. Immediately following $\mathcal{S}_3$ is a "rarefaction fan" $\mathcal{R}_1$. $\mathcal{R}_2$ is a "rarefaction shock," associated with the phase transformation which separated $\mathcal{S}_2$ and $\mathcal{S}_3$. Another nominally uniform region follows $\mathcal{R}_2$ and is bounded by the final rarefaction fan $\mathcal{R}_3$.

A shock wave results from inertial response of the material to sudden changes in pressure or particle velocity at a boundary. Pressures in laboratory shock experiments commonly range from about 10^9 to 10^{11} Pa.[1] Measurements have been made at pressures as small as 10^7 Pa and as great as 3×10^{12} Pa. The latter measurement was made near an underground nuclear explosion (Al'tshuler *et al.*, 1968a). Duration of the high-pressure state produced by a shock wave is determined by characteristic dimensions that commonly range from 1 to 50 cm in diameter, corresponding to durations of about 0.5 to 25 μs. Most quantitative experiments are performed with plane-wave loading.

The possibility that phase transformations might be induced by shock waves was suggested at least as early as 1941 (Schardin, 1941), but the first serious experimental study of the subject was stimulated by an apparent anomaly in shock-wave compression of iron at high and low pressures (Bancroft *et al.*, 1956), arising from a phase transition at 13 GPa.

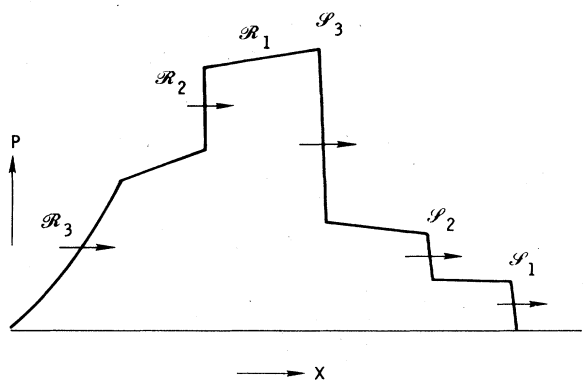

FIG. 1. Pressure distribution in a pulse propagating through a material undergoing a phase transformation and a transition from elastic to inelastic behavior.

Discovery of the 13 GPa polymorphic transition was a notable scientific achievement. Since the transition had not been observed before, unique capabilities of shock-wave experimentation were clearly demonstrated. This discovery stimulated further static high-pressure research and has played a major role in establishing a pressure calibration scale for static experiments. Shock experiments by Johnson *et al.* (1962) gave the first evidence for a triple point in the pressure–temperature phase diagram of iron. Detection of the well-known Bi I – Bi II transition under shock loading by Duff and Minshall (1957) confirmed the importance of shock loading experimentation in the study of polymorphic phase transitions.

Shock-induced polymorphic transitions are important for their applications. A particularly notable application is in material synthesis, exemplified by production of diamonds in shock-loaded graphite (DeCarli and Jamieson, 1961) and of cubic and wurtzite forms of BN from shock compression of hexagonal BN (Batsanov *et al.*, 1965; Coleburn and Forbes, 1968). Diamonds of industrial quality are now produced commercially by E. I. Dupont de Nemours Co. and Allied Chemical Corp. (Trueb, 1970, 1971). Scientists in the Soviet Union have undertaken an extensive program in material synthesis with shock loading techniques (Ruchkin *et al.*, 1968; Kirkinsky, 1968; Batsanov, 1968; Boreskov *et al.*, 1968; and Batsanov *et al.*, 1969). Material synthesis, not necessarily involving polymorphic phase transitions, includes polymerization (Al'tshuler *et al.*, 1968b; Adadurov *et al.*, 1965) and synthesis of superconducting intermetallic compounds (Barskii *et al.*, 1972; and Otto *et al.*, 1971). It has also been demonstrated that damage due to hypervelocity impact may be strongly influenced by phase transitions (Shockey *et al.*, 1975; Bertholf *et al.*, 1975). The possibility of producing metallic hydrogen in explosively driven magnetic compression experiments has been explored. (See, for example, *Physics Today*, Vol. 26, No. 3, p. 17, 1976).

Many measurements of shock transition pressure have now been reported. Many of them are isolated measurements that neither exploit nor illustrate the full capabilities of shock compression techniques. The novelty of shock-induced transition measurements has given way

[1]One pascal equals one newton/meter^2 or 10 dynes/cm^2. Multiples of the pascal used here are the terapascal (TPa), gigapascal (GPa), and the megapascal (MPa), which are equal to 10^{12}, 10^9, and 10^6 newtons/meter^2, respectively. One GPa = 10 kilobars or about 10 000 atmospheres.

to realism concerning difficulties in interpreting measurements and the necessity for more detailed measurements if scientifically useful data are to be obtained. In this review, we hope to bring the present state of knowledge of shock-induced phase transition into perspective in hopes that major problems will come into focus for further work.

The results of experimental observations of shock-induced transformation are shown in Tables AI and VII of this review. Some discussion of these results is contained in Secs. IV and VI. Section II provides an introduction to the necessary mechanics, thermodynamics, and kinetics of shock-wave propagation; Sec. III describes various experimental methods used to study transformation; and Sec. VII contains concluding remarks and some suggestions for future efforts.

If the reader is totally unfamiliar with shock-wave phenomena and experimentation, he may find it helpful to consult some general references (Duvall, 1968; Duvall and Fowles, 1963; Al'tshuler, 1965; Zeldovich and Raizer, 1966 and 1967; Glass, 1974; Courant and Friedrichs, 1948).

II. MECHANICS OF SHOCK-WAVE PROPAGATION

A. Stress and strain conventions

We shall be dealing almost exclusively with plane waves in one space dimension. Cartesian coordinates are used with x axis in the direction of propagation. All equations will refer to mechanically isotropic materials. Shock waves in anisotropic elastic and plastic media have been treated (Pope and Johnson, 1975), but effects of anisotropic properties on phase transition phenomena have received little consideration though they appear to exist, even at relatively high pressure (Fritz *et al.*, 1971). Materials of interest are solids or viscous fluids, so shear stresses commonly exist. Diagonal stress components will be exclusively compressive, so it is convenient to follow the practice of fluid dynamics and use the pressure tensor p_{ij}, which is the negative of the stress tensor σ_{ij} commonly used in solid body mechanics[2]:

$$p_{ij} = -\sigma_{ij} . \tag{1}$$

With the coordinate convention described above, x,y,z are principal coordinates; off-diagonal components of p_{ij} vanish, and diagonal components can be described by a single subscript: $p_x \equiv p_{xx}, p_y \equiv p_{yy}, p_z \equiv p_{zz}$. Because of the symmetry of one-dimensional plane waves, $p_y = p_z$. No motions parallel to wave fronts will be considered, so the only nonvanishing component of strain is $\eta_x \equiv \eta_{xx}$; this is called a "state of uniaxial strain."

The only pressure component normally measured in experiments with plane shock waves is p_x, which can be looked upon as composed of mean pressure,

$$\begin{aligned} \bar{p} &= (p_x + p_y + p_z)/3 \\ &= (p_x + 2p_y)/3 , \end{aligned} \tag{2}$$

and a shearing stress τ. This useful resolution is a simple identity:

$$\begin{aligned} p_x &= (p_x + 2p_y)/3 + 2(p_x - p_y)/3 \\ &= \bar{p} + 4\tau/3 , \end{aligned} \tag{3}$$

where

$$\tau = (p_x - p_y)/2 . \tag{4}$$

Often called "maximum resolved shear stress," τ is shear stress on planes with normals at 45° to the x axis. When dealing with hydrodynamic states, or when shock-wave results are to be compared with static measurements, $\bar{p}$ will be identified with hydrostatic pressure P.

B. Equations of propagation

The differential equations of motion and mass conservation in one-dimensional plane geometry are

$$\rho \frac{\partial u}{\partial t} + \rho u \frac{\partial u}{\partial x} + \frac{\partial p_x}{\partial x} = 0 , \tag{5}$$

$$\frac{\partial \rho}{\partial t} + u \frac{\partial \rho}{\partial x} + \rho \frac{\partial u}{\partial x} = 0 , \tag{6}$$

where ρ is mass density and u is particle velocity. Another quantity commonly used is specific volume,

$$V \equiv 1/\rho . \tag{7}$$

The equation of energy conservation, when combined with Eqs. (5) and (6), reduces to the first law of thermodynamics:

$$\frac{dE}{dt} = -p_x \frac{dV}{dt} + \frac{dQ}{dt} , \tag{8}$$

where E is internal energy per unit mass, dQ is heat added per unit mass, and $d/dt = \partial/\partial t + u\partial/\partial x$ is the convective derivative. Equations (5), (6), and (8) are often called "the flow equations."

The flow equations do not of themselves define a physical problem. The description of the material in which propagation is to occur and initial and boundary conditions serve to complete the problem definition. The material description is stated as a set of *constitutive relations*. In the simplest case this set is the equation of state alone. More generally it includes equations describing various irreversible and rate-dependent processes important to the problem at hand. For example, constitutive relations for a ductile solid would include an equation of state, specification of the yield stress, specification of the plastic flow rule following yield, and a recipe for calculating shear stresses. The equation of state might consist of a relation among P, V, E, but is not necessarily limited to such a relation.

The simplest problem of shock-wave propagation is that in which a uniform pressure P_1 is suddenly applied to the surface of half-space and thereafter held constant. Figure 2 portrays the resulting flow field for a simple

[2]Writers on shock-wave problems sometimes use the term "stress" to denote the term p_{ij} and the term "pressure" to denote mean pressure $\bar{p}$ and hydrostatic pressure P alone. Since some of the figures in this paper are derived from other work, coordinates are sometimes labeled "stress" to indicate that the quantity being plotted is p_x, not $\bar{p}$ or P. Whether "pressure" or "stress" is used, the quantity is positive in compression.

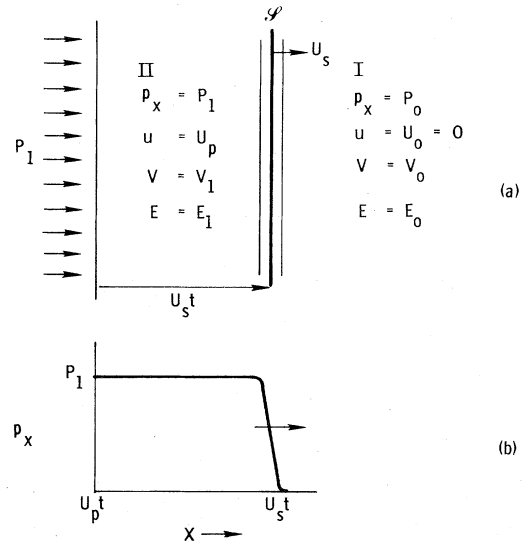

FIG. 2. A uniform pressure is applied to the plane surface, $x = 0$, at $t = 0$. (a) After time t the shock front divides the space into two uniform regions: I, undisturbed, and II compressed and accelerated. (b) $p_x(x)$ at time t. S is the shock front. The relation between P and V is shown in Fig. 3.

fluid with the isentropic compression curve shown in Fig. 3. In Fig. 2(a) is shown a section of a half-space to the surface of which a constant pressure P_1 has been applied since zero time. The shock front S is a region of rapid but not discontinuous change of state variables. It divides the half-space into two regions: I, in which the effects of applied pressure P_1 have not yet been experienced, and II, which is a constant state between surface and shock front. The corresponding pressure profile is shown in Fig. 2(b). Constitutive relations in this case consist of a single equation, $P = P(V, E)$.

If the shock front of Fig. 2 is unchanging in form as it propagates, the flow equations can be reduced to a set of jump conditions connecting compressed and undisturbed states (Band and Duvall, 1961):

$$P_1 - P_0 = (U_s - U_0)(U_p - U_0)/V_0 , \tag{9}$$

$$1 - V_1/V_0 = (U_p - U_0)/(U_s - U_0) , \tag{10}$$

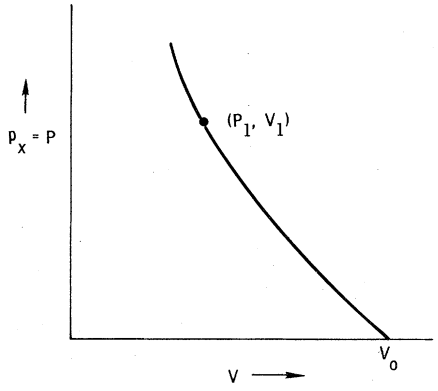

FIG. 3. Isentropic compression curve for a normal liquid.

$$E_1 - E_0 = (P_1 + P_0)(V_0 - V_1)/2 . \tag{11}$$

Here U_s is propagation velocity of the shock front; U_0 and U_p are particle velocities ahead of and behind the shock, respectively. Equations (9)–(11) apply even if connected states are not uniform, provided the shock front is a discontinuity in P, V, U_p, and E (Courant and Friedrichs, 1948). As a practical matter, the jump conditions are assumed to apply if field variables are changing much more rapidly in the shock front than before or behind it. Some caution must be exercised in defining shock propagation velocity if the shock front is not steady (Barker, 1975). If resolved shear stresses are significant, hydrostatic pressures P_1 and P_0 are replaced by p_{x1} and p_{x0}. The thermodynamics of compression are then complicated by irreversible processes like plastic flow and fracture (Duvall, 1973).

Equation (11) is called the "Rankine–Hugoniot Equation." When combined with an equation of state of the form $E_1 = E(P_1, V_1)$, and P_1 is varied, it produces a set of curves in the (P, V) plane, one for each set of initial points (P_0, V_0). The curve through (P_0, V_0) is said to be "centered" at P_0, V_0 and is known variously as the "Rankine–Hugoniot P–V curve," "Hugoniot P–V curve," "Hugoniot" or "R–H curve" centered at P_0, V_0. It will be called R–H curve in this review. The shock process is adiabatic but not isentropic (Courant and Friedrichs, 1948). The R–H curve lies above the isentrope centered at the same point. It is usually called the "shock adiabat" or "dynamic adiabat" in Russian literature.

Equations (9) and (10) can be combined to give expressions for U_s and U_p in terms of P_1, V_1, P_0, V_0, and U_0:

$$U_s - U_0 = V_0[(P_1 - P_0)/(V_0 - V_1)]^{1/2} , \tag{12}$$

$$U_p - U_0 = [(P_1 - P_0)(V_0 - V_1)]^{1/2} . \tag{13}$$

The R–H curve centered at P_0, V_0 thus maps into a curve in the $U_s - U_p$ plane. This is also called an R–H curve and provides a convenient representation of shock-wave data when U_s and U_p are measured quantities, which is frequently the case. In the absence of phase transformations, the U_s vs U_p curve can usually be fitted to a straight line:

$$U_s - U_0 = C_0 + s(U_p - U_0), \tag{14}$$

where C_0 is equal to, or very nearly equal to, the bulk sound velocity at $P = P_0$, s is the slope of the $U_s - U_P$ relation, and

$$C_0 = \sqrt{K_0 V_0} , \tag{15}$$

where K_0 is bulk modulus at P_0.

Elimination of $U_s - U_0, U_p - U_0$ from Eqs. (12)–(14) yields a form of P–V relation frequently used to describe R–H curves:

$$P - P_0 = \frac{C_0^2(V_0 - V)}{[V_0 - s(V_0 - V)]^2} . \tag{16}$$

Temperature in a shock wave can be calculated by integrating the differential equations of the R–H curve (Duvall, 1973) or by comparison with temperature on the isentrope at the same volume (Goranson *et al.*, 1955; Duvall and Zwolinskii, 1955). Temperature on the isentrope through the initial state is given by the expression:

$$\ln(T_S/T_0) = \int_V^{V_0} \Gamma\, dV/V, \tag{17}$$

where

$$\Gamma \equiv \frac{V}{C_V}\left(\frac{\partial P}{\partial T}\right)_V, \tag{18}$$

is the Gruneisen ratio. The additional temperature increment at the same volume arising from shock compression is $T_D - T_S$, where

$$\ln T_D/T_S = \int_{S_0}^{S_D} dS/C_V. \tag{19}$$

Entropy, S_D, can be expressed as a series in powers of the volume compression, $\eta = (1 - V/V_0)$:

$$S_D - S_0 = \frac{V_0^3}{12T_0}\eta^3\left(\frac{\partial^2 P}{\partial V^2}\right)_0 + \cdots, \tag{20}$$

where the second derivative is evaluated for the initial state on the isentrope or the R–H curve. If C_V and Γ/V are assumed constant, Eqs. (17), (19), and (20) can be combined to give

$$\ln T_D/T_0 = \Gamma_0\eta\left[1 + \frac{V_0^2\eta^2}{12\alpha T_0 K_0}\left(\frac{\partial^2 P}{\partial V^2}\right)_0 + \cdots\right], \tag{21}$$

where α is the thermal expansion coefficient, K_0 is the isothermal bulk modulus at (V_0, T_0) and Γ_0 has been evaluated by Eq. (18). For an R–H curve given by Eq. (16), Eq. (21) becomes

$$\ln T_D/T_0 = \Gamma_0\eta\left[1 + \frac{1+s}{6T_0\alpha}\eta^2 + \cdots\right]. \tag{22}$$

Coefficients of η^2 range from 10 to 100 for a variety of solids, so the temperature increment from irreversible shock heating is negligible for volume compressions of a few percent.

The problem represented by Figs. 2 and 3 is not realized in practice. Half-spaces do not exist, and uniform pressure cannot be instantly applied over a surface. Limitations imposed by real conditions are discussed in Sec. III.

C. Shock-wave stability

In general the R–H curve is not so simple as that shown in Fig. 3. A more common type for a solid has a cusp where elastic failure occurs, and a solid which fails elastically and also transforms to a new phase under pressure has two cusps, as shown in Fig. 4. In such a case the simple wave structure of Fig. 2(b) no longer applies. Instead the wave may consist of one, two, or three shock fronts, each one separating uniform states, depending on location of cusps and the magnitude of P_1, Fig. 5. In that case the jump conditions, Eqs. (9)–(11), are written for the ith shock:

$$p_x^i - p_x^{i-1} = (U_s^i - U_p^{i-1})(U_p^i - U_p^{i-1})/V_{i-1}, \tag{23}$$

$$1 - V_i/V_{i-1} = (U_p^i - U_p^{i-1})/(U_s^i - U_p^{i-1}), \tag{24}$$

$$E_i - E_{i-1} = (p_x^i + p_x^{i-1})(V_{i-1} - V_i)/2, \tag{25}$$

where p_x^i, V_i, U_p^i, and E_i are values of state variables behind the shock; p_x^{i-1}, V_{i-1}, U_p^{i-1}, and E_{i-1} are values ahead of it; and U_s^i is its velocity of propagation.

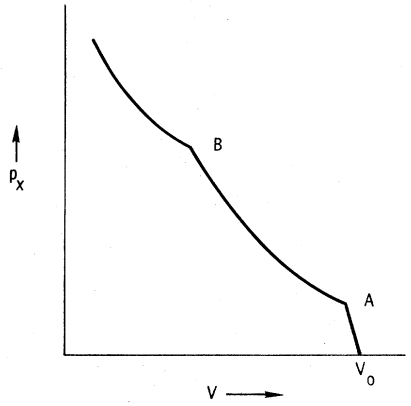

FIG. 4. R–H curve centered at (P_0, V_0) for a solid which fails elastically at A and transforms to a new phase starting at B.

Division of the shock wave into multiple waves hinges on questions of stability. Whether or not a given shock wave configuration is stable can be simply expressed by determining whether following shock waves will overtake those in front (Rice *et al.*, 1958). For example, in Fig. 6 are represented two shock waves in sequence. The leading shock $\mathcal{S}_1$ is traveling with speed $U_s^{(1)}$ relative to the material ahead of it, which is at rest. Material between $\mathcal{S}_1$ and $\mathcal{S}_2$ is compressed to specific volume V_1 and accelerated to particle velocity $U_p^{(1)}$. With respect to this material the first shock speed is $U_s^{(1)} - U_p^{(1)}$. With respect to this same material the second shock has speed $U_s^{(2)} - U_p^{(1)}$. If $U_s^{(2)} - U_p^{(1)} < U_s^{(1)} - U_p^{(1)}$, the second shock falls continually farther behind the first shock, and the two-shock system is stable. If the inequality is reversed, the second shock overtakes the first, forming a single stable shock.

From Eqs. (9) and (10) the equation for shock propagation speed is obtained

$$(U_s^i - U_p^{i-1})^2 = V_{i-1}^2(p_x^i - p_x^{i-1})/(V_{i-1} - V_i) \tag{26}$$

also

$$U_s^i - U_p^i = (V_i/V_{i-1})(U_s^i - U_p^{i-1}). \tag{27}$$

Applying these equations to the two shocks of Fig. 6, we see that the double shock is stable if

$$\frac{p_x^{(2)} - p_x^{(1)}}{V_1 - V_2} < \frac{p_x^{(1)} - P_0}{V_0 - V_1}. \tag{28}$$

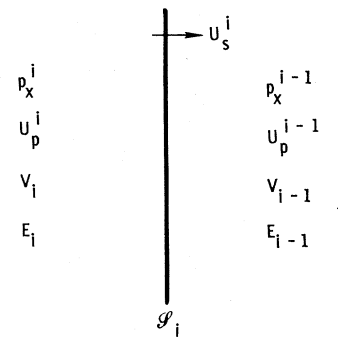

FIG. 5. Parameters of a shock preceded by moving material.

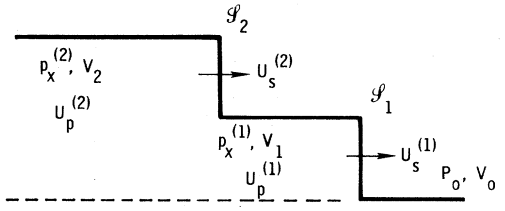

FIG. 6. Double shock configuration.

To see the meaning of this inequality, consider the (p_x, V) curve shown in Fig. 7 and suppose that the final shock state $(p_x^{(2)}, V_2)$ of Fig. 6 is at B. The negative slope of chord AB is given by the lhs of Inequality (28); that of OA is given by the rhs. Since OA is steeper than AB, Inequality (28) is satisfied and a double shock to B, with break at A, is stable. Chords like OA and AB of Fig. 7 which connect initial and final states are sometimes called "Rayleigh lines." If the driving pressure $p_x^{(2)}$ lies between O and A or above C, a single shock is stable. If it lies between A and C, a double shock is stable.

The shock stability problem can be couched more fundamentally in terms of the curvature of isentropes for a fluid medium (Bethe, 1942; Duvall, 1962). If

$$(\partial^2 P/\partial V^2)_s < 0$$

in some region, then there exist initial and final states for which a single shock wave is not stable. The general theory of stability is complicated (Fowles, 1976), but Inequality (28) is an adequate rule for practical experimental purposes.

D. Transformation thermodynamics

Gibbs (1925) was among the earliest thermodynamicists to point out the utility of geometric representations in thermodynamics. Such representations are particularly appropriate for discussion of shock phenomena since many important qualitative aspects of shock-wave representation are related to topological features of equation of state surfaces, without reference to particular analytical forms or numerical values. Some equilibrium relations pertaining to shock-induced phase transformations are described in this section.

Consider only a material that retains its chemical identity but can exist in two distinguishable physical forms, e.g., red and black phosphorus. Consider further that stress is limited to hydrostatic pressure. Then there exists a Gibbs function for each phase

$$G_i(P, T) = E_i - TS_i + PV_i, \quad i = 1, 2, \tag{29}$$

where S_i is specific entropy for phase i. The high-density phase will be referred to as "phase 2" throughout this paper.

Equations (29) represent two surfaces in a three-dimensional space with coordinates G, P, T, where $G = G_1$ for phase 1 and G_2 for phase 2. Transition between phases occurs where the two surfaces are in contact. If they intersect, the transition is first order and the Clausius–Clapeyron equation is the differential equation of the curve of intersection projected on the $P-T$ plane

$$dP/dT = (S_2 - S_1)/(V_2 - V_1) \equiv \Delta S/\Delta V . \tag{30}$$

The discontinuities in V and S arise from their identity as derivatives of G

$$V = \partial G/\partial P, \quad S = -\partial G/\partial T,$$

where the underlying surface represents the equilibrium state. This is illustrated in Fig. 8, where $G_1(P, T_0)$ and $G_2(P, T_0)$ are shown. $G(P, T_0)$ is the curve ABC.

If the two surfaces do not intersect, but are tangent along a curve, the transition is second order and second derivatives of G are discontinuous. Higher-order contacts define higher-order transitions, but these are hard to detect experimentally (Temperley, 1956). Our primary concern is with first-order transitions, though second-order transitions will be discussed briefly in Sec. V.

Discontinuities in V and S define a "mixed phase" region in $P-V-T$ space where phases 1 and 2 coexist. The mixed phase region is a cylindrical surface with generatrix normal to the $P-T$ plane. The phase diagram in the $P-T$ plane is the projection of this cylinder onto the $P-T$ plane. On the cylindrical surface Eq. (30) applies. If phase 2 is the high-pressure phase, $\Delta V < 0$ and ΔS may be either negative or positive. In the former case, $dP/dT > 0$; in the latter, $dP/dT < 0$. These two equilibrium cases are illustrated in Figs. 9 and 11, respectively. It can be seen from these figures that both cases

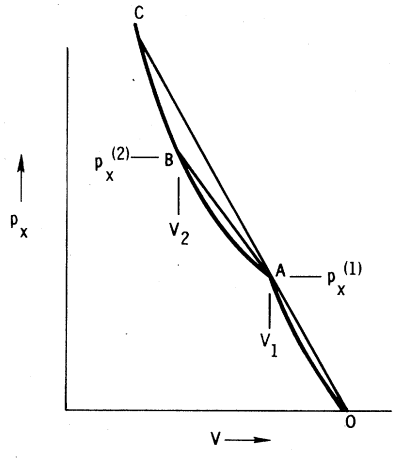

FIG. 7. Stability considerations for a double shock.

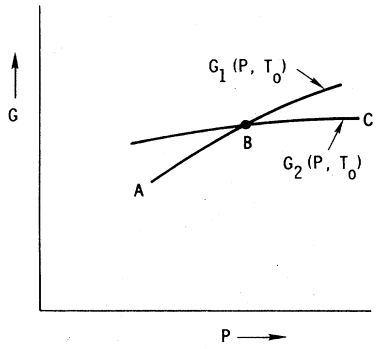

FIG. 8. Gibbs functions for a first-order transition.

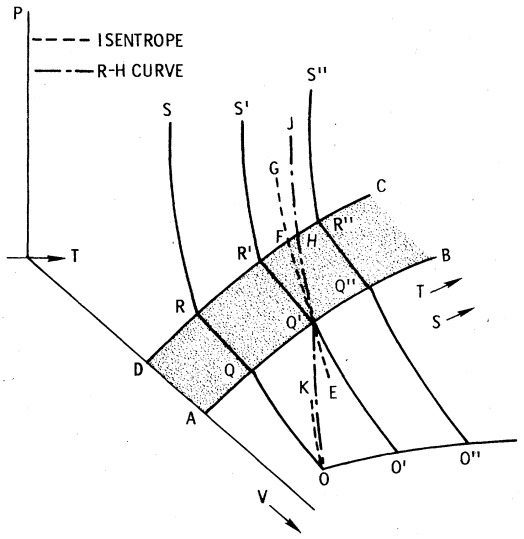

FIG. 9. P–V–T surface for a normal polymorphic transition. $\Delta S<0$, $\Delta V<0$, $dP/dT>0$. $O'Q'R'S'$, etc., are isotherms; OK and $EQ'FG$ are isentropes. $OQ'HJ$ is an R–H curve centered at 0.

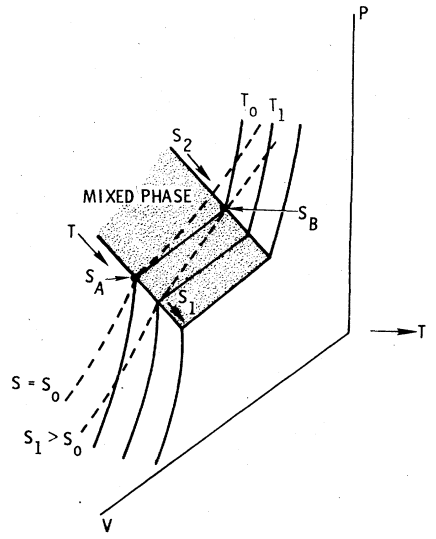

FIG. 11. Equation of state surface for $\Delta V<0$, $\Delta S>0$, $dP/dT<0$.

conform to the rule that on an isotherm the high-pressure phase has the lesser volume, and on an isobar the high-temperature phase has the greater entropy.

In Fig. 9, where $dP/dT>0$, $ABCD$ is the mixed phase region; $OQRS, O'Q'R'S', O''Q''R''S''$ are isotherms that start in phase 1 at $P=0$, cross the mixed phase region at constant pressure, and rise again in phase 2. $EQ'FG$ is an isentrope which experiences a break in slope at boundaries of the mixed phase region; $OQ'HJ$ is the R–H curve centered at O and recentered at Q'. It has a second-order contact with the isentrope OK at O; it intersects the phase boundary at Q', starts again with a second-order contact with $EQ'F$ at Q', continues on to intersect the second phase boundary at H, and turns sharply up in phase 2. Relative positions of phase boundaries, isotherm, isentropes, and R–H curve in the P–V plane are indicated in Fig. 10.

The discontinuity in slope of isentropes at the mixed phase boundary is given by (Duvall and Horie, 1965)

$$(\partial V/\partial P)_{S1}-(\partial V/\partial P)_{SM}=(T/C_p)(dS/dP)^2>0. \tag{31}$$

Subscript SM refers to the isentropic condition in the mixed phase region. All quantities are evaluated at the boundary between phase 1 and the mixed phase. The sign of the inequality in Eq. (31) insures that the isentrope in phase 1 is always steeper than that in the mixed phase. This implies that Inequality (28) is satisfied for some P_0, V_0 and $p_x^{(2)}, V_2$; i.e., under some conditions a double shock-wave structure will result from the cusp at A in Fig. 10. An analogous argument shows that the discontinuity in slope at B cannot produce a double wave. These statements apply only for $\Delta V<0$.

Some anomalous transitions exist for which $\Delta V<0$, $\Delta S>0$, $dP/dT<0$. The equation of state surface for such cases is illustrated in Fig. 11. For this case, $dS/dT<0$ on the phase boundary, so temperature decreases on the isentrope through the mixed phase region, as shown. Projections in the P–V plane are shown in Fig. 12. Inequality (31) is independent of the sign of dP/dT, so in this case, too, a double wave structure is possible.

There are discontinuities in slope of the R–H curve in the U_s-U_p plane which correspond to those illustrated in Figs. 9–12. Differentiation of Eqs. (9) and (10) yields the relation

$$\eta D'=(R-1)/(R+1), \tag{32}$$

where

$$\eta\equiv 1-V/V_0,$$
$$R\equiv(dP/d\eta)/[(P-P_0)/\eta],$$
$$D'\equiv d(U_s-U_0)/d(U_p-U_0).$$

R is the ratio of slope of the R–H curve at a point (P,V) to the slope of the chord drawn from (P_0,V_0) to (P,V). For a single shock from (P_0,V_0) to (P,V), $R>1$ and $d(U_s-U_0)/d(U_p-U_0)>0$, since $\eta>0$. If the R–H curve crosses a phase boundary at P_A, V_A and a single shock

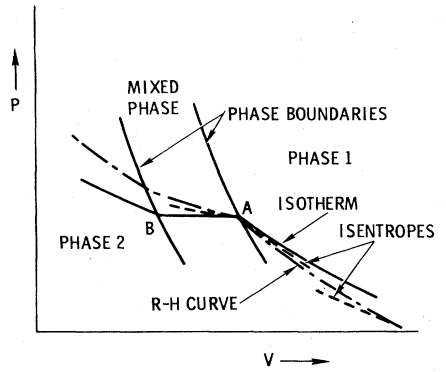

FIG. 10. Configuration of isentropes, isotherm, and R–H curves in the pressure–volume plane for a solid shock loaded through a normal polymorphic phase transition. Equation of state surface as in Fig. 9.

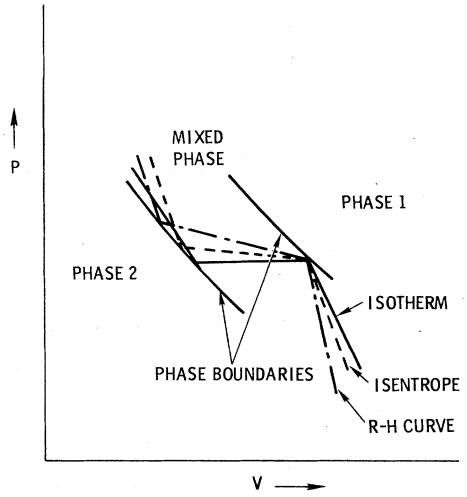

FIG. 12. Configuration of isentropes, isotherms, and R–H curves in the pressure–volume plane for $\Delta V<0$, $\Delta S>0$, $dP/dT<0$.

remains stable, $(P-P_0)/\eta$ is unchanged, but $dP/d\eta$ has a discontinuity which produces a discontinuity ΔR in R. The corresponding discontinuity in D' is

$$\Delta D' = 2\Delta R/[\eta(R+1)(R+1+\Delta R)]. \tag{33}$$

ΔR can be negative; if it is less than $1-R$, a single shock is unstable.

If the change in R–H curve slope at the phase boundary is great enough to produce a second shock, two cases must be distinguished: (1) the second shock is perceived as a second shock and data reduction proceeds accordingly; (2) the compression is still perceived as a single shock.

In the first case, if intersection with the phase boundary is at (P_A, V_A), Eqs. (9) and (10) still apply with P_0, V_0, U_0 replaced by P_A, V_A, and U_A. Then Eq. (32) is replaced by

$$\eta_A D'_A = (R_A-1)/(R_A+1), \tag{34}$$

where

$$\eta_A = 1-\frac{V}{V_A} = \frac{V_A-V}{V_0-V}\,\frac{V_0}{V_A}\,\eta,$$

$$R_A = \frac{(dP/d\eta_A)}{(P-P_A)/\eta_A},$$

$$D'_A = d(U_s^{(2)}-U_A)/d(U_p^{(2)}-U_A),$$

$U_s^{(2)}$ = propagation velocity of second shock,

$U_p^{(2)}$ = particle velocity behind the second shock.

At the intersection, $P=P_A, V=V_A, \eta_A=0$ and Eq. (34) is indeterminate. Let $P-P_A=C_1\eta_A+C_2\eta_A^2+\cdots$. Then Eq. (30) gives

$$D'_A = C_2/2C_1. \tag{35}$$

The change in slope in the U_s-U_p plane is

$$D'_A-D' = \frac{C_2}{2C_1} - \frac{dP/d\eta-[(P_A-P_0)/(V_0-V_A)]V_A}{dP/d\eta+[(P_A-P_0)/(V_0-V_A)]V_A}. \tag{36}$$

In the second case, which describes the "flash gap" experiments commonly used at the Los Alamos Scientific Laboratories (McQueen *et al.*, 1970), U_s does not change but U_p does since U_s is inferred from the time of first shock arrival. In that case $D'=0$ over the span of U_p from initial formation of the second shock until it overruns the first shock. This produces an uncertainty in the transition point which is noted in the literature (McQueen *et al.*, 1967).

Shock pressures measured in the mixed phase region are normally found to be greater than values calculated thermodynamically. Slope of the R–H curve in the mixed phase region at the boundary of phase 1 is given by the equation (Duff and Minshall, 1957),

$$\left.\frac{dV}{dP}\right|_{\text{R-H}} = -\beta_1 V_A + 2\alpha_1 V_A\frac{dT}{dP} - \frac{C_{p1}}{T_A}\left(\frac{dT}{dP}\right)^2, \tag{37}$$

where $\beta_1, \alpha_1, C_{p1}$ are isothermal compressibility, thermal expansivity, and specific heat at constant pressure, respectively, in phase 1, all evaluated at the transition point V_A, T_A, P_A; dP/dT is slope of the phase line. Measured values of $|dP/dV|$ are observed to be much greater than values calculated from Eq. (37) for iron and quartz (Duvall and Horie, 1965) and for KCl (Hayes, 1974). The difference is smaller for bismuth and may conform to the equilibrium value (Duff and Minshall, 1957; Duvall and Horie, 1965). Hayes (1972) and Podurets and Trunin (1974) have discussed possible causes for these differences. Both Hayes and Podurets and Trunin suggest surface energy as a cause for larger values of dP/dV, but means for establishing the validity of this proposal do not presently exist.

It is important to note that even though double wave structures are possible, they will not necessarily be found in a given experiment. Final pressure may be too high for the double shock to be stable, or initial pressure may be too low. The former case is illustrated in iron for final shock pressure greater than 33.0 GPa (Zukas and Fowler, 1961),[3] the latter in CCl_4 and liquid N_2 (Dick, 1970). Further discussion of shock waves and the geometry of phase transitions described in this section can be found in McQueen *et al.* (1970).

E. Effects of shear stress on phase transitions

According to Eq. (3) the stress component p_x in a shock wave is composed of mean pressure and a shear stress. No account of shear stress was included in the preceding section, and it is reasonable to suppose that it may complicate comparisons of shock-induced and static transformation parameters. In ductile solids τ is limited by the yielding process; it may be very small in soft metals like pure aluminum; in brittle materials, like sapphire, it may amount to several tens of GPa. The value of p_x at which elastic failure occurs in a shock wave is often called the "Hugoniot Elastic Limit," abbreviated HEL. When the HEL is large, τ may be large at the transition point, and the role of shear stress in transitions intrudes on the simplicity of hydrostatics. Unfortunately, it is not easy to account for the effects of shear.

[3] See also Fig. 18, this paper.

The hydrostatic Gibbs function cannot be generalized to produce a potential that defines equilibrium conditions for phase transition when shear stress is present, except in a few special cases of no interest here (Duvall, 1976; Paterson, 1973). The difficulties lie at two levels. In the first place, consider a finite mass of solid material which is systematically brought to the transformation point by application of forces to its outer boundaries. The mass does not transform homogeneously. Nuclei of the new phase begin to grow, transforming the original homogeneous mass into a heterogeneous mass with inhomogeneities in stress distribution produced by the growing nuclei. It is no longer possible to relate stress states in the new and old phases in any simple way and the first and second laws of thermodynamics for the finite mass are no longer satisfied by the simple expedient of setting $E_1 - TS_1 + PV_1 = E_2 - TS_2 + PV_2$, or by an obvious variant thereof.

At the microscopic level the difficulty persists, but in a different way. Consider, for example, only the region in the immediate vicinity of an interface between the nucleus of the new phase and the matrix of the old. The curvature of this interface presents difficulties, so consider a plane interface between the two phases. Is there a simple relation analogous to equality of the hydrostatic Gibbs function in a fluid which relates conditions on the two sides of such an interface? Paterson (1973) reviewed the entire problem. He suggested such a relation for the special case of coherent phase transitions, i.e., transitions in which the new phase can be constructed from the old through imposition of a set of strains $\Delta\eta_{ij}$ across an interface between old and new phases. If $\Delta\eta_{ij}$ is small, he gives the condition of equilibrium as

$$\Delta E - T\Delta S - V_0\sigma_{ij}\Delta\eta_{ij} = 0. \tag{38}$$

This gives for the analog of the Clausius–Clapeyron equation

$$\partial T/\partial\sigma_{kl} = -V_0\Delta\eta_{kl}/\Delta S, \quad k, l = 1, 2, 3. \tag{39}$$

Robin (1974) finds even this to be untrue. Instead, equilibrium of the interface depends on its orientation relative to the lattice, so the above equations are not general, even under the very restrictive assumptions made.

It is evident that if experimental data on phase transformations in solids are to be organized, some simple approximation to transformation theory is required, even if it be inexact. In reduction of shock data it is usually assumed that only hydrostatic or mean pressure is significant, and that fluid thermodynamics, including the Clausius–Clapeyron equation, applies. Shock measurements give only values of p_x at which various events occur, including the onset of transformation. Mean pressure $\bar{p}$ is obtained from Eq. (3)

$$\bar{p} = p_x - \tfrac{4}{3}\tau,$$

where τ is maximum resolved shear stress. In this paper, τ is computed from measured values of the HEL and appropriate values of elastic constants; it is often ignored entirely. Measurement of τ is desirable, but measurement of a second component of stress in shock experiments is not simple. If a phase transition occurs at higher pressure than the HEL, τ may be expected to change from its value at the HEL because of stress relaxation, work hardening, temperature increase, and density increase, so that its exact value at the transition point is not determinate without additional stress measurements. A more detailed discussion of difficulties experienced in correcting for shear strength is given by Duvall (1976).

Jones and Graham (1971) have reviewed the shock literature for experimental evidence of the effects of shear stress on phase transitions. They find mean shock pressure for bismuth, corrected for the HEL, in close agreement with statically determined values, but in that case the HEL is small. For germanium the shear correction to p_x is about 15%, and $\bar{p}$, corrected for the HEL, is within the range of static measurements, though the spread in both cases is rather large. On the basis of one experiment each with CdS and InSb, the value of $\bar{p}^{TL}$, corrected for the HEL, for the shock transition is lower than the static transition pressure.[4]

The only systematic experimental study of effects of τ on transition pressure has been in iron. The HEL of iron was varied from 0.7 to 1.9 GPa by varying heat treatment and carbon content (Minshall, 1961; Loree *et al.*, 1966a; Jones and Graham, 1971). Their data suggest that the transition is occurring at constant $\bar{p}$, independent of the resolved shear stress. Supporting evidence is provided by Forbes (1976), who finds $\bar{p}^{TL}$ to be constant in Armco iron when specimen thickness is varied, whereas p_x^{TL} varies as the HEL.

A more extreme case than the one just described exists in heterogeneous rocks and minerals. It has been observed that some brittle materials lose a substantial portion of their shear strength under shock loading (Fowles, 1962; Wackerle, 1962; Graham and Brooks, 1971; Graham, 1974). Grady *et al.* (1975) have recently proposed that this results from heterogeneous melting associated with the yield process (cf. Sec. VI.C). In such a case, correction for strength based on the HEL is totally inappropriate.

On the basis of investigations conducted to this date, there is evidence that in a number of cases the macroscopic shear stress has no effect on the shock initiation pressure of transformation other than the addition of $4\tau/3$ to $\bar{p}$, as in Eq. (3). Nevertheless, there are some possible exceptions to be noted in Sec. IV, and it appears necessary to give careful consideration to the effects of shear stress on each of the materials under study. A tabulation of HEL is given by Jones and Graham (1971).

F. Finite transformation rates

Time available for a phase transition to occur in a mass element compressed by shock may be only a few nanoseconds and does not normally exceed a few microseconds. If the required time for transition is longer, the transition will not be detected in the usual shock experiment because of sample size limitations. This contrasts so dramatically with time scale in static experi-

[4]Superscript (or subscript) *TL* denotes the pressure of transition determined in compressive loading. *TU* denotes a value obtained in unloading experiments; *T* denotes equilibrium transition values.

ments that validity of comparisons between shock-induced and statically measured transitions has quite properly been questioned (Roy, 1969; Bridgeman, 1956; Bethe, 1942). It is fortunate that experimental manifestations of transition kinetics are quite direct and readily detected in shock experiments, provided the rate lies within a rather broad range defined by geometry of the experiment. Roughly speaking, if the time required to effect a significant fraction of the transition is less than $d/3U_s$ and greater than about 10^{-8} s, the transition rate can be measured in a shock experiment. Here d is diameter of the experimental sample and U_s is shock propagation velocity. For a 90 mm diameter target and a shock speed of 5 km/s, the upper limit is about 6×10^{-6} s. With large explosive systems it is possible to increase this limit several fold (Walsh and Rice, 1957). The lower limit of about 10^{-8} s is determined by electronic response times and inaccuracies of mechanical assembly and impact (Hayes, 1972). Kormer *et al.* (1966) have suggested that index of refraction measurements can detect transformation times as short as 10^{-11} s. (The kinetics of phase transformations in shock-loaded solids has recently been reviewed by Hayes, 1977.)

The amount of material which must be transformed in order to effect a two-wave structure is defined implicitly by the requirement that the effective R–H curve must lie below the Rayleigh line passing through the transition point. This varies with amplitude of the Plastic I wave and relates to detector resolution (Forbes, 1976).

If a transition has been detected, or is thought to have been detected, identification of the new phase is difficult. The new phase may be metastable or it may be a different stable phase than observed statically (Hayes, 1974). In principle it may be possible to make flash x-ray diffraction measurements of the high-pressure phase (Johnson and Mitchell, 1972). The equation of state of the new phase can be estimated by the procedures described in Sec. II.G, but identification of the new phase is normally accomplished through close comparison of shock and complementary static pressure measurements.

Effects of finite transformation rate on shock-wave structure can be described by incorporating a rate function

$$d\alpha/dt = \psi(V, T, \alpha) \tag{40}$$

in a simple model of constitutive relations to be used with the flow equations, Eqs. (5), (6), and (8), where α is mass fraction of the second phase. Solution of these equations for some simple problems suggests experimental procedures to be followed in measuring reaction rates.

Recall that each phase in a two-phase system is represented by a surface in $P-V-T$ space, and that the surfaces do not intersect ("system" here refers to a small mass element). In equilibrium the space between surfaces is bridged by a cylindrical surface with generatrix parallel to the V axis. When the transition is out of equilibrium, the entire range of both surfaces and the entire space between them must be considered momentarily accessible to the system. The exact state path is determined by interactions of the changing stress and temperature fields and the rate law, Eq. (40). These interactions are calculated by combining constitutive relations of the material with the flow equations. In the simplest case, constitutive relations of the two individual phases are their equations of state. For the mixed phase, they consist of an appropriate mixture of equations of state of the two phases and the transition rate law. Mass exchange then becomes an irreversible process.

Assume that the following conditions apply in a partially transformed state:

1. Shear stresses are negligible.
2. Pressure is common to both phases.
3. Temperature is common to both phases.
4. Particle velocity, U_p, is common to both phases.
5. Interface energy is negligible.

Conditions (2), (3), and (5) are to some extent incompatible since (2) and (3) require the presence of many small islands of the second phase dispersed in the first, whereas this condition is just the one which tends to make interface energy important. Because of the complexity, this difficulty is ignored for the present, but it must be kept in mind for future consideration. Condition (4) is reasonable for solid–solid transitions, perhaps somewhat less reasonable for liquid–solid, and unreasonable for liquid–vapor transitions, which are not considered here.

With the above assumptions, state variables at each point in the continuum are unique. From assumption (5),

$$E(P, T) = (1-\alpha)E_1(P, T) + \alpha E_2(P, T) \tag{41}$$

and

$$V(P, T) = (1-\alpha)V_1(P, T) + \alpha V_2(P, T). \tag{42}$$

Subscripts "1" and "2" refer to first and second phases, respectively. Differentiating Eqs. (41) and (42) yields, within the mixed phase region,

$$dV = (1-\alpha)dV_1 + \alpha dV_2 + (V_2 - V_1)d\alpha, \tag{43}$$

$$dE = (1-\alpha)dE_1 + \alpha dE_2 + (E_2 - E_1)d\alpha. \tag{44}$$

Equations of state in the two phases are taken in the form

$$V_i = V_i(P, T), \tag{45}$$

$$E_i = E_i(P, T), \tag{46}$$

$$i = 1, 2.$$

Equations (43) and (44) and the differentials of (45) and (46) contain nine variables: dV, dE, dV_1, dV_2, dE_1, dE_2, $d\alpha$, dP, and dT. When these six equations are combined with the first law in the form

$$dE = -PdV \tag{47}$$

the resulting set of equations can be solved for dP and dT in terms of dV and $d\alpha$ (Horie and Duvall, 1968a, 1968b; Andrews, 1973; Hayes, 1975).

$$dP = a_{11}dV + a_{12}d\alpha, \tag{48}$$

$$dT = a_{21}dV + a_{22}d\alpha, \tag{49}$$

where the a_{ij}'s are functions of α, P, and T.

If the transition occurs under equilibrium conditions, the Clausius–Clapeyron relation with latent heat of transformation, L, applies:

$$dP/dT = \Delta S/\Delta V = f(P) = L/T\Delta V, \tag{50}$$

where $f(P)$ is a known function. Divide Eq. (48) by (49), set the ratio equal to $f(P)$, and solve for $d\alpha$. This yields

$$d\alpha = (a_{21}f - a_{11})dV/(a_{12} - a_{22}f). \tag{51}$$

Substitution of Eq. (51) into (48) and (49) yields for the *equilibrium transition*

$$dP = (a_{12}a_{21} - a_{11}a_{22})f\,dV/(a_{12} - a_{22}f) \tag{52}$$

and

$$dT = dP/f(P). \tag{53}$$

Equations (43)–(46) and (51)–(53) comprise the constitutive relations for the mixed phase region when the transformation occurs under equilibrium conditions. For the irreversible case, Eqs. (43)–(46), (48), (49), and (40) comprise the constitutive relations. To use them, divide all differentials by dt to form convective derivatives. These are then combined with the flow equations to form a complete set. Specification of initial and boundary values specifies a problem.

For the equilibrium transition, Eq. (52), the effect of a step increase in pressure at the sample surface is to produce a double shock wave like that shown in Fig. 6; amplitude of the first shock is the transition pressure p_x^{TL}.

For the irreversible case, where Eq. (40) applies, application of a step P_2 at the sample surface produces a shock wave in which the initial step in pressure decays toward the transition pressure as it propagates into the sample. This is illustrated in Fig. 13. The wave progresses toward the equilibrium form of Fig. 6 at a rate determined by Eq. (40). The simplest procedure for estimating transition rate is to measure the amplitude of the first wave for different specimen thicknesses and compare with calculated decay curves.

If the problem is drastically simplified by assuming that the first shock is a discontinuity propagating *at sound velocity* (Duvall, 1964), with $\Delta V = \text{const}$, $C_{p1} = C_{p2}$, $V_1(P, T)$ independent of T, $dV_1/dP = \text{const}$, and if Eq. (40) is approximated by

$$d\alpha/dt = -(\alpha - \alpha_{eq})/t_0 \tag{54}$$

with t_0 constant and α_{eq} defined by Eq. (42) in the mixed phase region, then it follows that amplitude P_1 of the first shock varies with propagation distance as (Horie and Duvall, 1968b)

$$P_1 = P_2 - (x\Delta V/2U_s^{(1)}t_0)dP/dV_1 \quad V_1 \leq V_{TL} + \Delta V$$
$$= P^{TL} + (P_2 - P^{TL})\exp(-x/2U_s^{(1)}t_0)$$
$$\times V_{TL} + \Delta V \leq V_1 \leq V_A, \tag{55}$$

where $U_s^{(1)}$ is propagation speed of the first shock and (P^{TL}, V_{TL}) is the point at which the R–H curve in phase 1 intersects the mixed phase boundary.

Equation (54) is an oversimplified form of the law for irreversible transformation. An improved form has been given by Andrews (1970, 1971), and an elegant formulation of the entire problem has recently been given by Hayes (1975).

There has been little study of transformation rate effects in shock-induced transitions. Some authors have reported effects of driving pressure on transition pressure (Loree *et al.*, 1966a). According to Eq. (55), this may be a manifestation of finite transformation rate. Novikov *et al.* (1965) have interpreted rise time in the third shock in iron (the Plastic II wave) in terms of reaction rate; but other rate-dependent effects, including viscosity, may enter here, as does also the effective equilibrium R–H curve in the mixed phase region (cf. Sec. II.D). Specific attention to transformation rates has been given by Warnes (1967) for antimony, Hayes (1974) for KCl, Barker and Hollenbach (1974) and Forbes and Duvall (1975) for iron. Their results, discussed in Sec. IV, show that transition kinetics can be significant and can be measured at the boundary of the mixed phase region. This is accomplished by the simple expedient of measuring the rate of decay of the Plastic I wave and deducing the initial transformation rate, from Eq. (55) or some equivalent. Limitations on the technique are provided by time resolution of the measurement and by size of the shock assembly. This measurement does not directly give information about transition rate in the mixed phase region. That must be obtained from comparisons of measured and calculated wave profiles and from the steady profile of the Plastic II wave (Novikov *et al.*, 1965).

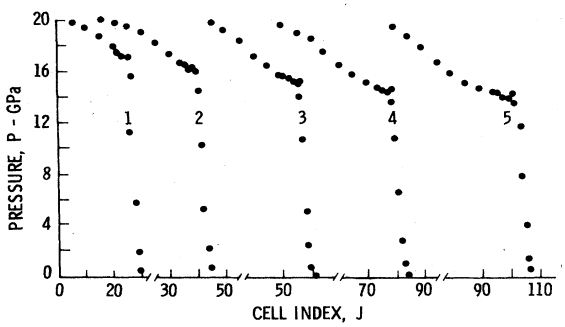

FIG. 13. Pressure profiles for a 20.0 GPa shock wave in iron with rate-dependent phase transition: $t_0 = 1/3$ μs, 1. $t = 0.526$ μs, 2. $t = 0.812$ μs, 3. $t = 1.105$ μs, 4. $t = 1.554$ μs, $\Delta V = -0.004$ cm³/g (Horie and Duvall, 1968a). "Cell index" is a space coordinate in the direction of propagation.

G. Properties of the high-density phase from shock data

The problem is indicated in Fig. 14. The point H has been determined experimentally, so P^T and V_1^T are measured directly; internal energy E_1^T is calculated from the Rankine–Hugoniot relation. The equation of state of phase 1 is presumed known, so temperature T^T and entropy S_1^T can be calculated. A portion of the measured R–H curve, LM, has been identified as lying in phase 2. The Clausius–Clapeyron coefficient dP/dT is presumed known. We wish to determine the parameters V_2^T and S_2^T and the equation of state of the high-density phase.

On LM, P_2, V_2, and E_2 are known from the jump conditions. The information required to extend our know-

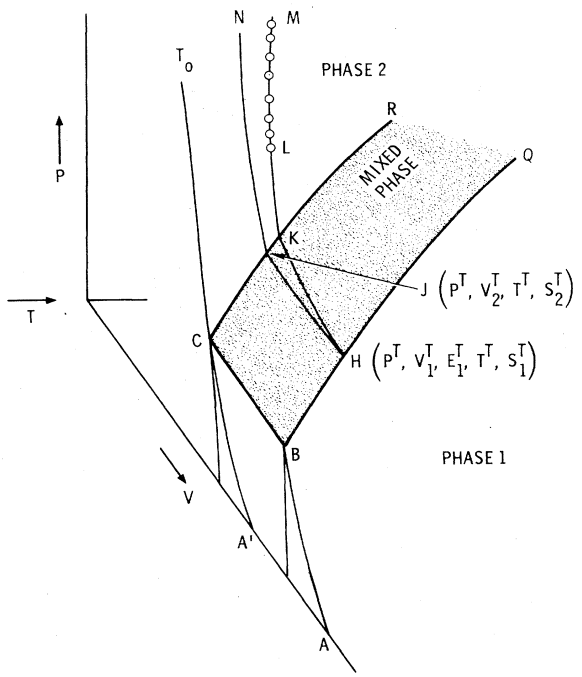

FIG. 14. *ABCD* is isotherm at temperature T_0; $A'C$ is a metastable extrapolation of the phase 2 isotherm at T_0; H is the intersection of the R–H curve in phase 1 with the mixed phase boundary, BQ; HJN is an isotherm through H; $HKLM$ is the R–H curve in the mixed phase and phase 2; LM is a section of the R–H curve in phase 2 determined by measurements.

ledge of these parameters into adjacent regions is defined by the thermodynamic differentials

$$dE = (-P + T\Gamma\rho C_V)dV + C_V dT, \tag{56}$$

$$dP = -(K/V)\,dV + \Gamma\rho C_V dT, \tag{57}$$

$$dS = \Gamma\rho C_V dV + C_V dT/T, \tag{58}$$

where K is the isothermal bulk modulus, Γ is the Gruneisen parameter, C_V is the specific heat at constant volume, and $\rho = 1/V$. If K, Γ, and C_V are assumed to be known functions of V and T, Eqs. (56)–(58) can, in principle, be integrated, assuming E, P, V, S, and T to be known at some reference point, say L on the R–H curve LM. Of these five parameters, only two, S_L and T_L, are unknown. The result of the integration is three functions:

$$E = E(V, T; S_L, T_L), \tag{59}$$

$$P = P(V, T; S_L, T_L), \tag{60}$$

$$S = S(V, T; S_L, T_L). \tag{61}$$

With attention fixed on the isotherm $T = T^T$, set $P = P^T$, $S = S_2^T$, $V = V_2^T$, $E = E_2^T$, and invoke the two additional conditions of equilibrium, assuming the phase change to be first order:

(i) Clausius–Clapeyron equation:

$$S_2^T - S_1^T = (V_2^T - V_1^T)dP/dT. \tag{62}$$

(ii) Equality of the Gibbs functions at the phase boundaries:

$$E_2^T - E_1^T = -P^T(V_2^T - V_1^T) + T^T(S_2^T - S_1^T). \tag{63}$$

Also, from Eq. (60),

$$P(V_2^T, T^T; S_L, T_L) = P^T. \tag{64}$$

Equations (62)–(64) can then, in principle, be solved for the three unknown parameters S_L, T_L, V_2^T, where E_2^T and S_2^T have been replaced by the functions on the right-hand sides of Eqs. (59) and (61). With V_2^T determined, the volume change in transition is given by

$$\Delta V = V_2^T - V_1^T.$$

Of the functions K, Γ, and C_V, the first is dominant in determining V_2^T. The measured section, LM, of the R–H curve provides information about K. It can be used in the following way. Variations in entropy along the R–H curve are given by the equation (Duvall and Fowles, 1963)

$$2TDS = (V_0 - V)DP + (P - P_0)DV, \tag{65}$$

where capital "D" denotes variation along the R–H curve, and (P_0, V_0) is the point at which the R–H curve is centered. Eliminating DS between Eqs. (58) and (65) yields

$$\frac{DT}{DV} + \Gamma\rho T = \frac{V_0 - V}{2C_V}\frac{DP}{DV} + \frac{P - P_0}{2C_V} \equiv f(V). \tag{66}$$

Combining Eqs. (57) and (66) yields an expression for K/V

$$\frac{K}{V} = \left[\frac{\rho\Gamma(V_0 - V)}{2} - 1\right]\frac{DP}{DV} + \Gamma\rho\left(\frac{P - P_0}{2} - \Gamma\rho C_V T\right). \tag{67}$$

If Γ is known, Eq. (66) can be integrated to give an expression for $T(V)$, along the R–H curve, which contains the reference temperature T_L. Except for this constant, Eq. (67) then gives the volume dependence of K along the R–H curve. Its temperature dependence is made explicit by assuming a formula for C_V.

Several writers have considered the construction of complete equations of state for use in shock applications (Cowperthwaite, 1966; McQueen *et al.*, 1967; Andrews, 1970, 1973; Hayes, 1972, 1974; Johnson *et al.*, 1974). A particularly simple form is obtained if $\Gamma\rho$ and C_V are assumed constant. Then the Helmholtz energy A has the form

$$\begin{aligned} A(V, T) = {} & E_L - P_L(V - V_L) - S_L T - f(V; V_L) \\ & - \Gamma\rho C_V(V - V_L)(T - T_L) \\ & - C_V T \ln(T/T_L) + C_V(T - T_L). \end{aligned} \tag{68}$$

The internal energy is

$$\begin{aligned} E(V, T) = {} & E_L - P_L(V - V_L) - f(V; V_L) \\ & + \Gamma\rho C_V T_L(V - V_L) + C_V(T - T_L). \end{aligned} \tag{69}$$

Pressure and entropy are

$$P(V, T) = P_L + f'(V; V_L) + \Gamma\rho C_V(T - T_L), \tag{70}$$

$$S(V, T) = S_L + C_V \ln(T/T_L) + \Gamma\rho C_V(V - V_L). \tag{71}$$

Substitution of these equations into Eqs. (62)–(64) yields the following set to be solved for T_L, S_L, and V_2^T:

$$f'(V_2^T; V_L) + \Gamma\rho C_V(T^T - T_L) = P^T - P_L \tag{72}$$

$$S_L - S_1^T + C_V \ln(T^T/T_L) + \Gamma\rho C_V(V - V_L) = (V_2^T - V_1^T)dP/dT, \tag{73}$$

$$E_L - E_1^T - P_L(V_2^T - V_L) - f(V_2^T; V_L) + \Gamma\rho C_V T_L(V - V_L) + C_V(T^T - T_L) = (V_2^T - V_1^T)(-P^T + T^T\, dP/dT). \tag{74}$$

The above procedures for determining ΔV and the equation of state of the second phase are simple to describe, but it is not evident that they are easy to use. McQueen *et al.* (1967, 1970) and Carter (1973a) have made extensive second-phase calculations. McQueen *et al.* choose the reference point to be at ambient temperature and pressure in the metastable region of phase 2. The reference curve of compression is assumed to be the R–H curve through this ambient point, characterized by a linear $U_s - U_p$ relation:

$$U_s = C_0 + s U_p . \tag{75}$$

Density at the ambient point, C_0 and s are then adjusted by trial and error until the observed R–H curve in phase 2 is reproduced. They have shown that changes in initial density translate the recalculated R–H curve in the $U_s - U_p$ plane, changes in C_0 rotate it, and changes in s influence its curvature. The entire calculation is carried out numerically and its use is simple when computer programs have been established.

These procedures for estimating equation of state of the second phase produce uncertainties arising from estimates made for C_V and Γ. There are additional unassessed errors because of the difference between p_x, which is measured, and P, which is used in the theory, as indicated earlier in Sec. II. Other errors result from the difference between transition pressure measured in shock compression, p_x^{TL} or $\bar{p}^{TL}$, and equilibrium transition pressure $\bar{p}^T$, to be discussed in Sec. IV.

III. EXPERIMENTAL TECHNIQUE

A. Introduction

Theory of the mechanics, thermodynamics, and finite transformation rates associated with shock-induced polymorphic phase transformations can be used to predict basic features of the phenomena and as a framework for interpretation of experimental results. Nevertheless, the assumptions underlying present theory are expected to lead to oversimplified descriptions of real material behavior, and experimental observations must play a leading role in the development of improved understanding of shock-induced transformations. This section contains a summary of experimental techniques that have been used to probe the characteristics of transformations. No attempt will be made to provide a comprehensive picture of shock loading techniques. More comprehensive reviews of techniques (Graham and Asay, 1977; Fowles, 1973) or individual research papers may be consulted for experimental details, which are often important to the interpretation of measurements. Loading methods and measurement techniques will be briefly described after some general underlying considerations are presented.

The determination of characteristics of a transformation is impeded by very-high-pressure transient characteristics of the experiment. The chaos perceived by the naked eye and ear is avoided in shock loading experiments that are designed to be completed in the few nanoseconds or microseconds of time for which a sample is subjected to well-controlled uniaxial strain produced by plane loading over a large area. This limited time scale, the need for uniaxial configurations, and the destructive nature of the experiment prohibit or severely limit measurements that are commonplace at atmospheric pressure or in static high-pressure studies. Development of a measurement technique is often a lengthy and involved process; as a result, shock probes, although sophisticated, are not yet able to use many tools of modern solid-state physics. In spite of these difficulties, the ability to readily achieve very high pressures and the ease with which pairs of stress-volume states can be determined have stimulated numerous experimental investigations of shock-induced transformations.

Most of our knowledge about shock-induced transformations is derived from measurements of shock and particle velocities produced by well-controlled loading. These quantities are sensitive to stress-volume states of the sample material since they are direct manifestations of inertial reaction to the loading. Their interpretation is complicated by plastic deformation and by temperature increases which accompany shock compression.

Electrical measurements have been successfully used to indicate the onset of transitions under static high pressure. Similar measurements under shock compression have been of limited value owing to complications of the environment. For example, interpretation of electrical resistance measurement under shock loading is complicated by difficulties of achieving *in situ* measurements and by plastic deformation. Since resistivity is sensitive to defects, the massive and varied defects produced by shock loading are hard to untangle from other effects. Magnetization change, on the other hand, is less sensitive to defects, but measurements have been limited to a few ferromagnetic alloys. Although there is promise for improvement in electrical probes of shock-induced transformations, their contributions to date have been minimal and most experimental results have been obtained from detection and analysis of stress profiles resulting from well-controlled loading.

B. Loading methods

Shock-wave loading systems are designed to apply loads over large plane areas of samples so that the sample is maintained in a state of uniaxial strain for sufficient time for measurements to be completed. As high-pressure loading waves interact with lateral boundaries, lateral release waves propagate inward and reduce pressures as they arrive at interior locations. This means that samples must have large diameter-to-thickness ratios, with diameters which typically range from 25 to 300 mm. Observations are then limited to central regions of the sample. Total durations of experiments are typically 1 μs; hence loads must be applied simultaneously over a sample surface within times

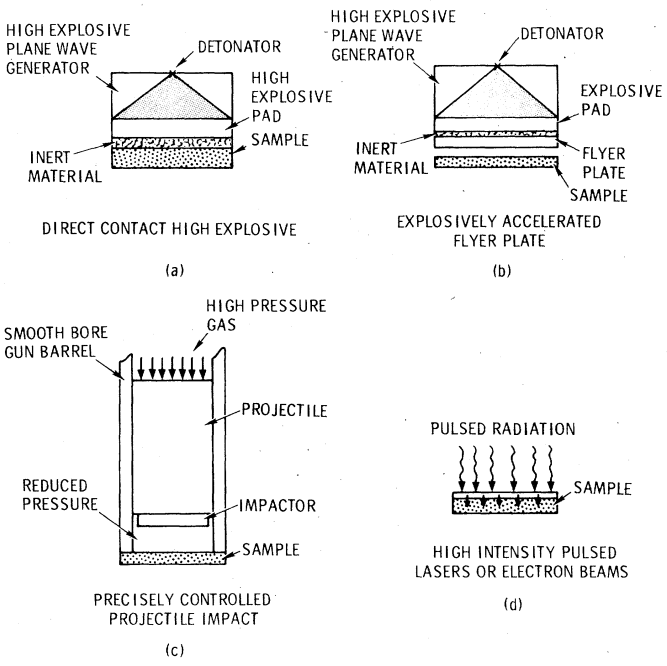

FIG. 15. The methods most commonly used to apply shock loading to samples are shown. In all cases the loading methods introduce waves into samples over diameters from 25 to 300 mm with simultaneity of about 10 ns.

of about 10 ns. It is also desirable that the loading system maintain a constant pressure input whose amplitude can be easily changed from experiment to experiment and whose duration can be easily controlled.

Loading methods in widespread use are shown in Fig. 15; each will be briefly described in turn. Less attention will be directed toward explosive loading since it has been described in recent reviews (Fowles, 1973; McQueen *et al.*, 1970). Actual input pressure values and profiles in a sample depend explicitly on sample properties; values quoted are representative only.

1. Contact explosives [Fig. 15(a)]

The first quantitative scientific shock loading experiments were made possible by fabrication of high explosive lenses that produce plane shock waves over diameters up to about 300 mm (see the comprehensive treatment of data obtained with these systems in Rice *et al.*, 1958). These plane-wave generators, with various explosive pads, produce pressures in aluminum samples in the range 10 to 40 GPa under relatively routine conditions. Pressure imparted to a sample depends upon the particular explosive material and mechanical impedance of the sample. Typical pressures in aluminum are 17 GPa with Baratol, 24 GPa with TNT, 35 GPa with Composition B, and 40 GPa with Octol (Deal, 1962; Los Alamos, 1969). Special nitroguanidine lenses have been developed to produce pressures of 4 GPa in aluminum (Benedick, 1965). The contact explosive loading method has been widely and successfully used but several disadvantages have led to development of other techniques.

Direct contact explosives have limited capacity to produce pressures less than 10 GPa and more than about 40 GPa in materials with impedances like aluminum. Accordingly, projectile impact techniques were developed for lower input stresses, and explosively accelerated flying plates were developed for higher-pressure experiments. Other disadvantages of direct contact explosives relate to the difficulty of varying input pressure in small increments and lack of control on pressure release. Furthermore, the ability to fabricate explosive lenses is limited to a few laboratories, and the large amount of explosive material detonated in an experiment requires special experimental ranges.

2. Explosively accelerated flyer plates [Fig. 15(b)]

To achieve higher pressures, plane-wave generators are used with explosive pads to accelerate flyer plates to high velocities as shown in Fig. 15(b). Separation of the explosive from the flyer plate by a thin plastic insert or a thin air space reduces peak pressure in the flyer plate and damage to and heating of the plate are minimized. In order to maintain planarity and integrity of the plate, the free run distance to impact is typically a few centimeters, i.e., a small fraction of its diameter. Typical impact velocities range from 1 to 7 km/s and produce pressures in aluminum from 10 to 100 GPa. For materials of higher impedance, such as iron, pressures of several hundred GPa are achieved. Systems of this type are described by McQueen *et al.* (1970). The flyer plate velocity can be measured near the plane of impact, providing an additional measured experimental parameter.

3. Projectile impact [Fig. 15(c)]

During the past ten years, impact loading with precisely controlled projectiles accelerated in smooth-bore guns has become a widely used method of shock-wave loading. Originally developed for research at low pressures, guns have now been developed to achieve the same maximum pressures produced by explosive loading (Isbell *et al.*, 1968).

A precisely dimensioned projectile is faced with the desired impacting material, smoothly accelerated in vacuum through a distance of many projectile lengths, and allowed to strike its target in a plane impact with precise alignment of impacting surfaces. For given impactor and target materials the stress produced at impact increases monotonically with impact velocity. If impactor and target are of the same material, the impact is called "symmetric." Then particle velocity imparted to the sample is exactly one-half the projectile velocity. Since projectile velocity may easily be measured with an accuracy of 0.1%, the symmetric impact experiment provides the most precisely known input conditions of any shock-wave loading experiment.

The principal problem in impact experiments is maintenance of alignment of the impacting surfaces. Limits on allowed misalignment, called "tilt," vary with impact velocity, but tilt values of 500 μrad are normally acceptable for projectile velocity of about 1 km/s.

Compressed gases or propellants are used to accelerate projectiles to the desired velocity. Compressed gas has been more widely used because it is cleaner,

subject to closer control, and more convenient for a conventional laboratory operation. Projectile velocity is varied continuously by varying gas pressure or powder charge and projectile mass.

All guns are custom made (Thunborg *et al.*, 1964; Taylor and Rice, 1963; Halpin *et al.*, 1963; Barker and Hollenbach, 1964; Linde and Schmidt, 1966; Fowles *et al.*, 1970), but bore diameters of 63.5 and 102 mm are common. Bore diameter determines maximum sample size; hence larger bores are used when thicker samples and longer observation times are essential. Barrel lengths range from 3 to 24 m.

Projectile velocities range from 30 m/s to 1.5 km/s with compressed gas guns, up to 2.3 km/s with guns driven by chemical propellants, and up to 8 km/s with two-stage light gas guns (Jones *et al.*, 1966). A recently developed drop weight impactor has produced precisely controlled impacts from 0.9 to 3.5 m/s with tilt at impact of 10 μrad (Flinn *et al.*, 1975).

In an impact experiment the input pulse duration is controlled by thickness of the impactor. If the impactor surface opposite the impact face is backed with air or a low impedance material, the shock wave from the impact surface reflects, reduces pressure, and propagates back through the impactor into the sample. Such unloading wave experiments are becoming increasingly important for probing sample response in high-pressure states.

4. Pulsed radiation [Fig. 15(d)]

Pulsed radiation has not been widely used to investigate shock-induced phase transformations, but the intense radiation pulses from lasers and electron beams have been used effectively in other material property studies. Deposition times may be short enough that absorption of radiation occurs under conditions of essentially constant volume, producing large stresses and high temperatures (see, for example, Gauster *et al.*, 1973).

5. Special loading configurations

The impedance match (McQueen *et al.*, 1970) and quartz gauge impactor (Ingram and Graham, 1970) configurations are special variations in loading methods which are widely used. The impedance match method is based upon determination of shock velocity, particle velocity, and compression characteristics of standard materials. Some standard materials are 2024 aluminum alloy, 921-T aluminum alloy, copper, iron, and a uranium–molybdenum alloy (McQueen *et al.*, 1970). Loading is applied to the standard material, and measurement of shock velocities in the standard and the sample is sufficient to establish pressure and particle velocity in the sample. Use of the standard material eliminates the need to measure particle velocity, which is the more difficult measurement.

Use of a quartz gauge mounted on a projectile as an impactor makes it possible to directly determine stress and particle velocity histories at the impact interface, provided impact stress in the gauge does not exceed 4.0 GPa. A facing of sapphire on the quartz permits measurements to 8.0 GPa, and a facing of tungsten carbide permits measurements to 15 GPa. The technique is especially useful for study of materials that propagate complex wave profiles, for experiments at elevated temperatures, or for materials with time-dependent responses. The quartz impactor may be combined with more conventional rear surface measurement of propagated wave profiles to provide detailed knowledge of both input and propagated stress profiles.

C. Measurement techniques

In a typical shock experiment the sample is loaded in uniaxial strain to the desired input pressure and response of the sample is determined with detectors whose response characteristics have been determined beforehand. Most measurements are directed toward determination of pairs of shock-wave velocity and particle velocity values at critical locations on wave profiles. Detailed descriptions of the various detectors are unnecessary here; but technique is still a crucial element in establishing our knowledge of properties under shock loading conditions, and major features of the detectors are noted. A summary of detectors which have been used for phase transition studies is given in Table I.

Shock velocity is determined by detecting times of arrival of the wave at two or more stations at known locations. This is conceptually simple, but large errors are easily introduced if, for example, care is not taken to control or determine tilt of the wave in the plane of the detectors and to determine response times of detectors. In many experiments, arrival times must be determined within a few nanoseconds to achieve suitable accuracy in the derived shock velocity. As indicated in Table I, methods for discrete determination of arrival time include charged pins and argon flash gaps that luminesce when shocked to high pressure.

These same discrete arrival time detectors can be used to determine particle velocity in experiments in which the wave is reflected from a free surface and arrival time of the free surface is measured as it moves outward and contacts detectors at discrete locations. Since total free surface displacement is usually much smaller than sample thickness, free surface measurements are more difficult than shock velocity measurements. Free surface velocities are obtained by differentiation of the displacement versus time data, and particle velocity may be taken as one-half the free surface velocity; corrections to this approximation are made as required (Walsh and Christian, 1955). More accurate determination of particle velocity is obtained if detectors are used to determine impact velocity in a symmetric impact configuration.

An example of U_s vs U_p data obtained with flash gaps in the impedance match configuration is shown in Fig. 16. A phase transformation in NaCl should be characterized by a horizontal line, under ideal conditions, since flash gaps detect only the arrival time of the first wave (cf. Sec. II.D). Transition pressure and volume are computed from the $U_s - U_p$ point where there is a substantial break in the behavior. Such a break is fairly clearly indicated for [111] data; the situation for [100] data is uncertain.

If a single shock wave of constant amplitude is to be

TABLE I. Experimental techniques used for detection of shock-induced phase transformations.[a]

Displacement versus time—discrete measurements	
1. Electrically charged pins	Minshall, 1955b
2. Flash gaps	McQueen *et al.*, 1970
3. Optical time of arrival	Coleburn, 1964
Displacement versus time—continuous measurements	
4. Inclined optical mirror	Doran, 1963a
5. Optical image	Davis and Craig, 1961
6. Inclined prism	Eden and Wright, 1965
7. Displacement capacitor	Hughes *et al.*, 1961
Time-resolved velocity or stress	
8. Quartz gauge	Graham *et al.*, 1965; Graham, 1975
9. VISAR (optical interferometer)	Barker and Hollenbach, 1972
10. Electromagnetic velocity gauge	Dremin *et al.*, 1965
11. Manganin gauge	Keough and Wong, 1970
12. Sapphire gauge	Graham and Ingram, 1968
13. Velocity capacitor	Rice, 1961; Ivanov and Novikov, 1963
Electronic property measurement	
14. Electrical resistance	Keeler and Mitchell, 1969
15. Magnetization change	Graham, 1968; Royce, 1968
Postshock sample examination	
16. Metallurgical	Fowler *et al.*, 1961; Johnson *et al.*, 1962
17. X-ray diffraction	Coleburn and Forbes, 1968
18. Petrographic analysis	Chao, 1967
19. Other conventional probes	...
Others	
20. Flash radiograph	Breed and Venable, 1968
21. Flash x-ray diffraction	Johnson *et al.*, 1972

[a] For a more complete description of these and other measurement techniques, see Graham and Asay (1977) and Fowles (1973).

measured, discrete displacement-versus-time measurements are sufficient to determine shock and particle velocity values with good accuracy. If, however, material response is not ideal and there is structure in the wave profile, discrete displacement time detectors may not provide a good measure of changes in structure.

When free surface displacement is continuously recorded, the presence of multiple shock fronts is detected, and data interpretation is more precise than when flash gaps are used. Closely spaced pin measurements of surface displacement provide an approximation to the required data; three optical methods, the inclined mirror, the inclined prism, and the optical image, provide better approximations (Table I). One edge of the inclined mirror is in contact with the sample free surface, and shock arrival and free surface displacement are detected by monitoring reflected light with a high-speed streak camera. The optical image technique monitors position of a wire and its image in a polished free surface. Continuous optical and pin techniques are more productive than the flash gap technique since they provide data on the second, higher-pressure shock wave, which can be used to determine thermodynamic properties of the high-pressure phase.

Even continuous measurements of displacement cannot follow fine detail, since measured data are differentiated to obtain free surface velocities. Direct time-resolved measurement of stress or particle velocity can be accomplished with quartz gauges or optical interferometers or other devices with more limited time resolution (Table I).

The quartz gauge is an x-cut quartz disk affixed to the surface at which stress is to be measured. When a shock wave crosses the interface between sample and gauge, a piezoelectric current is produced that is nearly proportional to the normal stress component at the interface. Its time resolution is limited by circuit response and wave tilt at the interface. Its useful recording time is propagation time of a dilatation wave through the disk. The greatest pressure it can reliably report is about 4.0 GPa. Under favorable planar impact conditions it has a time resolution of a few nanoseconds. Other piezoelectric gauges have been studied. One which is useful to about 1.0 GPa is lithium niobate (Graham and Jacobson, 1973; Graham and Asay, 1977).

The VISAR, an acronym for Velocity Interferometer System for Any Reflector, has a time resolution of about 3 ns. It is a modification of the Michelson interferometer in which fringe shift is made proportional to velocity instead of displacement. It can be used to monitor velocity of a free surface or of an interface between sample and a transparent buffer. Its maximum pressure measurement capability is limited only by the integrity of solid surfaces and it can be used on diffusely reflecting surfaces (Barker and Hollenbach, 1974).

The remainder of the techniques in Table I will not be discussed in detail. The difficulty of interpreting resistance measurements under shock compression was

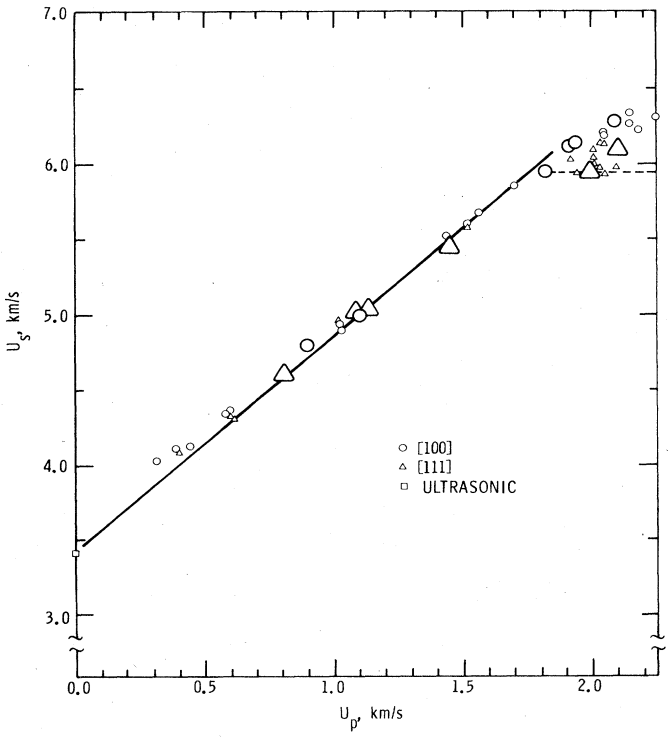

FIG. 16. The observed shock velocity versus particle velocity for NaCl, as reported by Fritz *et al.* (1971). The larger symbols indicate more than one datum point. The ultrasonic bulk sound speed determined by Haussühl (1960) is shown at the lower extension of the shock data. The data in the vicinity of $U_s = 6$ km/s indicate that a phase transition is occurring. However, the behavior is different from that expected in the idealized case, for which a horizontal line in the U_s vs U_p relation would be observed.

mentioned earlier. The post mortem technique of metallurgical examination has provided surprisingly good information in several instances. Of particular note is the work of Johnson *et al.* (1962) which provided the first experimental evidence for a triple point in iron at 11.5 GPa and 775 K by metallurgical examination.

Of the other detectors, the electromagnetic gauge, the Manganin gauge, and the sapphire gauge are capable of wave profile measurements. The first two of these have been used extensively. The flash radiograph provides measurement of locations of shocks at various times and has been used to observe kinetic effects in the antimony transition in a configuration of steady two-dimensional plane flow.

X-ray diffraction measurements under static high pressure are valuable for determining characteristics of high-pressure polymorphic phase transitions (Banus, 1969). X-ray diffraction measurements are a recent addition to the probes available for shock-induced phase transition measurements. The success so far enjoyed by these measurements is the result of a substantial effort and it is not clear how widely applicable the technique will be. Nevertheless the measurements have shown that shock-loaded crystals retain order at the microscopic level in spite of gross plastic deformation (Johnson *et al.*, 1970, 1971, 1972). The technique has been successfully used to identify a high-pressure BN phase (Johnson and Mitchell, 1972). A similar flash x-ray device has been constructed in Japan (Kondo *et al.* 1975). For further descriptions of the technique see Mitchell *et al.* (1973a, 1973b).

IV. EXPERIMENTAL OBSERVATIONS OF POLYMORPHIC PHASE TRANSITIONS

A. Summary of shock-induced polymorphic phase transition measurements

Results of a comprehensive search to document measurements of shock-induced polymorphic phase transformations are shown in Table AI in the Appendix. The summary is too extensive to fully discuss in the text; however, Table AI gives considerable information on each measurement and a reference to the original article. Except in special cases no attempt has been made to document measurements on geologic materials since this work has been reviewed by Ahrens *et al.* (1969) and Ahrens (1972). Second-order and melt transitions are not included in Table AI. They are treated separately in Sec. V and VI, respectively.

Entries in the table give a description of the sample and its original condition and give observed values of p_x^{TL} and η_{TL} for the transition.[5] The table also includes information on loading method and measurement technique and special remarks. If kinetic effects are associated with the transition, sample thickness is an important variable; hence, thickness or range of thicknesses is included under remarks.

Examination of the entries in Table AI shows that iron is the most extensively investigated material. The transition stresses of iron alloys have also been widely investigated but are typically single measurements. Of the measurements on elements, the antimony results are especially interesting because of large kinetic effects. Bismuth has been well investigated and its importance to static pressure calibrations makes the work of particular importance. Germanium and silicon are interesting because of their large HEL values. The graphite-to-diamond transition has been investigated by a number of authors. Among the alkali halides, NaCl is of interest and KCl has shown interesting crystallographic orientation effects. Among the oxides both vitreous silica and crystalline quartz show features not found in other solids.

In the remainder of this section individual materials will be separately discussed in an attempt to bring the observations into perspective.

B. The $\alpha \rightleftarrows \epsilon$ transformation in iron

The 13 GPa $\alpha \rightharpoonup \epsilon$ transformation in iron is the most widely studied shock-induced phase transition. Progress from a newly discovered transition to a well-characterized $\alpha \rightleftharpoons \epsilon$ transition illustrates the important role that various static high-pressure and shock loading techniques can play in characterizing a transition. Further-

[5] p_x^{TL} is transition pressure observed in shock loading; $\eta_{TL} = 1 - V_{TL}/V_0$ is the corresponding volume compression.

more, the shock investigations cover a period of 20 years and afford an opportunity to check consistency of measurements and to assess the roles of different instrumentation.

Minshall reported results from shock measurements on iron at the Berkeley meeting of the American Physical Society in 1954 (Minshall, 1955a). His pin technique records of free surface motion showed the arrival of three distinct shocks, which he identified as an elastic wave of 0.67 GPa amplitude, a Plastic I wave, commensurate with a phase transformation at 13.0 GPa, and a Plastic II wave representing driving pressure. This information was incorporated with other measurements and reported by Bancroft *et al.* (1956). Following this discovery, considerable effort was directed toward reconciling shock and static loading experiments and identifying the high-pressure phase. In 1956 Bridgman attempted, without success, to detect the transition with resistance measurements in static high-pressure experiments. Subsequent measurements of the well-known Bi I→Bi II transition by Duff and Minshall (1957) gave confidence in comparisons of shock and static experiments. Katz *et al.* (1959) and Curran *et al.* (1959), with oblique shock measurements, found qualitative agreement with the observations of Bancroft *et al.* The gross difference between static and shock measurements was finally reconciled by resistance measurements of Balchan and Drickamer (1961), who observed the transition in static experiments. This measurement at 13 GPa emphasized that Bridgman's failure to observe the transition was the result of an incorrect calibration for the high-pressure scale with the Bridgman anvil apparatus.

The new high-pressure phase was first thought to be the fcc (γ) phase. Claussen (1961) determined the $\alpha \rightarrow \gamma$ phase boundary with a high-pressure belt apparatus to about 8 GPa. [The original data were corrected for the new pressure scale by Kaufman (1961).] Kennedy and Newton (1963) used a piston–cylinder apparatus for similar studies to 5 GPa. When Kaufman (1961) extended his $\alpha \rightarrow \gamma$ phase stability calculations to 17 GPa, disagreement between static experiments, calculations, and shock observations was apparent. Minshall (1961) reported further studies of the shock-induced transition in iron and in low carbon steels, including some in which the initial temperature of the sample was varied, and determined that the slope of the phase boundary in the vicinity of the 13 GPa transition was in substantial disagreement with Kaufman's calculations.

The gross discrepancy between shock measurements and combined results of thermodynamics and static measurements on the $\alpha \rightarrow \gamma$ transitions was resolved by experiments of Johnson *et al.* (1962), who used a shock loading technique with samples at temperatures from 78 to 1158 K to suggest the existence of a triple point at 775 K and 11.5 GPa. It is significant that these measurements, which were crude by shock loading standards, were instrumental in establishing correct overall features of the phase diagram and have not been greatly altered to date. It is likely, however, that important quantititive features determined by Johnson *et al.*, such as the location of the triple point, are in error due to the experimental method. Their experiments did not use plane-wave loading. Transition pressures were determined from observations of the locations of dark-etching zones within sectioned samples, earlier identified as transformed regions by Smith (1958) and Katz (1955). Locations of zone boundaries were correlated with transformation pressure by reference to Bancroft *et al.* (1956) at room temperature and calibration of the pressure field using a pellet momentum technique de-

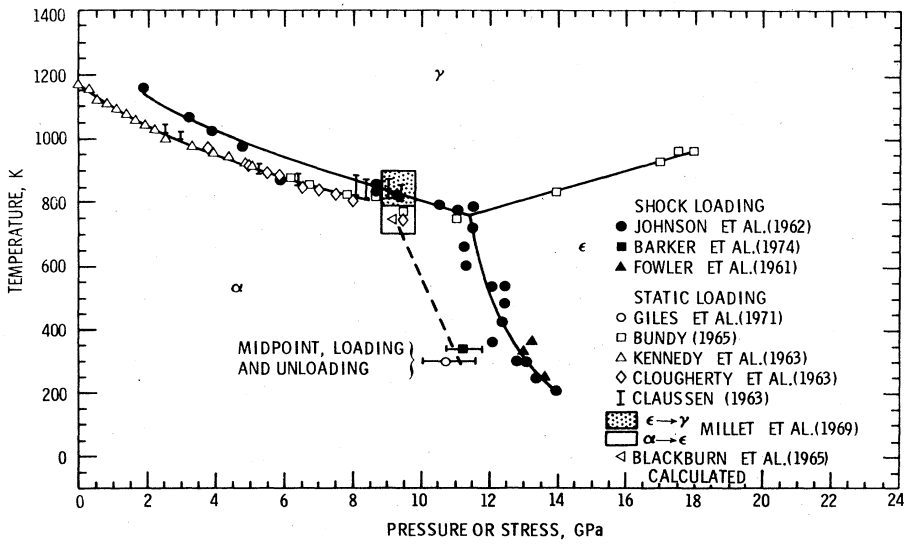

FIG. 17. The temperature–pressure phase diagram of iron as determined by shock and static loading experiments and calculation of the triple point. The shock loading data do not include a shear strength correction. The data of Barker *et al.* (1974) include the temperature increase due to shock loading, while the other shock data are plotted at the initial sample temperature. Data on the α–γ phase line by Leger *et al.* (1971) under static loading agree with the other static loading investigations but are not shown owing to a lack of space. The dotted line connects the calculated triple point of Blackburn *et al.* (1965) to the equilibrium stress or pressure determined as the mean value between loading and unloading in both static and shock loading investigations.

TABLE II. Critical transformation conditions for iron in the vicinity of 300 K.[a]

	$\alpha \rightarrow \epsilon$ (loading)				$\epsilon \rightarrow \alpha$ (unloading)		average	
	p_x^{TL} GPa	$\bar{p}^T$ GPa	P^{TL} GPa	η_{TL} %	p_x^{TU} GPa	P^{TU} GPa	P_e^T or $p_x^T \eta_T$ GPa	%
Shock loading								
Bancroft *et al.* (1956)	13.0[b]	···	···	6.4	···	···	···	···
Loree *et al.* (1966a)	12.9	12.5	···	6.4	···	···	···	···
Barker *et al.* (1974)	12.8	12.4	···	6.3	9.8 ± 0.4	···	11.3 ± 0.5[c]	10.0
Static loading								
Giles *et al.* (1971)	···	···	13.3	6.6	···	8.1	10.7 ± 0.8	10.3
Mao *et al.* (1967)	···	···	13	6.8	···	···	···	···
Drickamer (1970)	···	···	11–12	···	···	···	···	···
Bundy (1975)	···	···	11.2	···	···	···	···	···

[a] p_x^T is the observed value of p_x at the transition; $\bar{p}^T$ is the mean pressure calculated from $\bar{p}^T = p_x^{TL} - (2/3)(1-2\nu)/(1-\nu)$(HEL); ν = Poisson's ratio = 0.28, P^T is the pressure at the initiation of the transition under quasihydrostatic conditions, $\eta_T = 1 - V_{TL}/V_0$, where V_{TL} is the specific volume at the initiation of the transition and V_0 is the initial specific volume (= 1.27 $\times 10^{-4}$ m^3/kg); P_e^T is taken as the mean of P^{TL} and P^{TU}.

[b] Based on lowest pressure input, thickest sample.

[c] Uncorrected for shear strength effects.

scribed earlier by Rinehart and Pearson (1954).

Identification of the high-pressure phase as hcp (ϵ) was suggested from static high-pressure x-ray diffraction measurements of Jamieson and Lawson (1962) and Jamieson (1963a) on the basis of a single diffraction line. Confirmation of the ϵ phase resulted from full x-ray diffraction patterns obtained by Takahashi and Bassett (1964) and Clendenen and Drickamer (1964). Bundy (1965) confirmed general features of the phase diagram with static resistance measurements of the $\alpha \rightarrow \epsilon$ and $\epsilon \rightarrow \gamma$ phase boundaries to 18 GPa. These he connected directly to the Johnson *et al.* (1962) triple point. The temperature–pressure phase diagram indicated by present measurements and theory is summarized in Fig. 17.

X-ray diffraction studies of α and ϵ phases at high pressure have been used to determine compressibility of both phases and volume change at the transition. Recent work by Mao *et al.* (1967) and Giles *et al.* (1971) shows different results from earlier work by Clendenen and Drickamer (1964).

Evidence that the $\alpha \rightarrow \epsilon$ transition pressure measured on static loading is not an equilibrium value has been obtained from x-ray diffraction measurements. (Similar nonequilibrium behavior under shock loading will be noted later.) Giles *et al.* (1971) established an equilibrium pressure of 11.0 GPa for the transition, based on the mean of $\alpha \rightarrow \epsilon$ and $\epsilon \rightarrow \alpha$ transition pressures observed in a static loading–unloading cycle. This mean pressure is in better agreement with the triple point at 9.2 GPa and 750 K calculated by Blackburn *et al.* (1965) and the high-pressure Mössbauer effect measurements of Millet and Decker (1969) than are the loading measurements. Furthermore, the recent measurement of 5.4% for volume change at the transition (Giles *et al.*, 1971) appears to be in good agreement with thermodynamic conditions at the triple point proposed by Blackburn *et al.* (1965).

Barker and Hollenbach (1974) have recently reported an unusually complete study of wave profiles in impact-loaded iron using projectile impact loading and the VISAR interferometer system. They were able to examine both loading and unloading profiles. Critical values characterizing the transition obtained by Barker and Hollenbach are compared with other shock and static compression measurements in Table II.

Several different features of the various measurements shown in Table II are of interest. Among shock data there is remarkable consistency concerning transition stress and volume. This is especially notable when the difference between early and recent experiments is considered. Early experiments used plane-wave explosive loading while recent ones used projectile impact loading. Early experimenters detected wave arrivals with pins, and recent ones used the VISAR to record surface velocities continuously. Although the measurements of Barker and Hollenbach show considerable detail not observed by Bancroft *et al.*, the best assignments of transition pressure and volume are in excellent agreement. This produces confidence that the value of loading stress at transition is close to 12.8 GPa, which, after a correction for shear strength effects, corresponds to a mean loading pressure of 12.4 GPa.[6]

Shear strength corrections are somewhat uncertain because of our lack of knowledge of modeling plastic deformation in shock-loaded metals, as described in Sec. II.E. However, the correction for iron is carefully considered on the basis of experimental observations of a common volume compression at the transition, independent of the various HEL values observed in low carbon steels (Jones and Graham, 1971). Nevertheless, unloading measurements of Barker and Hollenbach (1974) at stresses below the transition provide evidence that the 0.4 GPa shear strength correction may be too large.

[6] This excellent agreement among shock loading investigators was recently broken by a report of the transition at 15 GPa by Anan'in *et al.* (1973), as determined with an *in situ* Manganin gauge. Because of reported difficulties with calibration of such gauges the measurements are open to some question. Vereshchagin *et al.* (1969b) have also reported the transition at 15.3 GPa in static loading experiments.

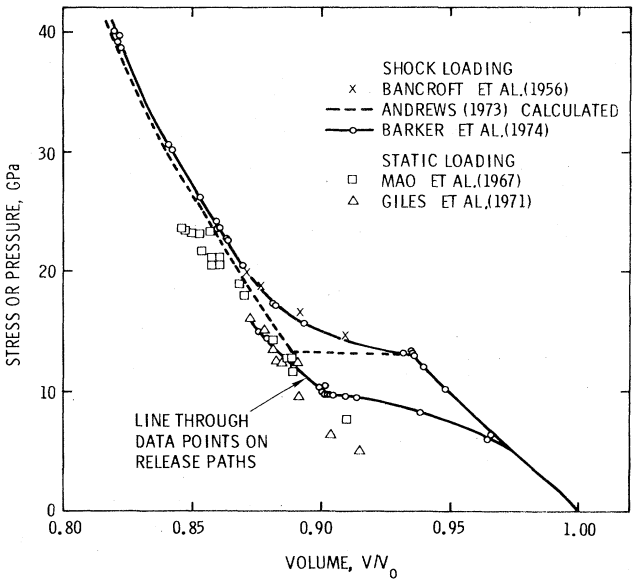

FIG. 18. The stress or pressure versus relative volume for iron is shown as determined by shock and static loading investigations. The dashed line represents the calculated equilibrium curve for shock loading. Shock loading data in mixed phase region between 13 and 20 GPa show a significantly lower compressibility than expected for equilibrium thermodynamic conditions.

The value of the mean pressure of 12.5 GPa is in reasonable agreement with the loading pressure of 13.3 GPa obtained from x-ray diffraction studies [especially when the pressure distribution problems of *in situ* static pressure markers are considered (Jamieson and Olinger, 1971)]; however, the difference between resistance measurements of Drickamer (1970) and Bundy (1975) and shock data are possibly outside experimental errors.

Barker and Hollenbach (1974) measured wave profiles resulting from controlled release of pressure. From these measurements a pressure–volume curve for release of pressure was determined. Their data, shown for loading and unloading in Fig. 18 along with the data of Giles *et al.* (1971), establish the $\epsilon \rightarrow \alpha$ reversal pressure as 9.8 ± 0.4 GPa. This value is in remarkably good agreement with the observations of Giles *et al.* and appears to confirm the concept of a martensitic transition with different forward and reverse pressures as proposed by Giles *et al.* The equilibrium pressure, taken as the mean of loading and unloading transition pressures, is 10.7 ± 0.8 GPa from static x-ray diffraction measurements and is 11.3 ± 0.5 GPa based on shock loading measurements. Measurements of Barker and Hollenbach show complete reversion to α at 5.5 GPa, compared to 4.9 GPa for the static experiments. Thus shock and static data on reversion of $\epsilon \rightarrow \alpha$ on release of pressure are in good agreement. Equilibrium pressure established by Giles *et al.* and by Barker and Hollenbach are in reasonable accord with the calculated triple point of Blackburn *et al.* (1965), as shown in Fig. 17.

Finite transformation rates associated with the iron transition have been recognized for some time. Duvall and Horie (1965) used observed compressibilities in the mixed phase region to calculate equilibrium values of the slopes of phase lines and found poor agreement. Horie and Duvall (1968a) developed a finite transformation rate model (described in Sec. II.F) to calculate wave profiles for iron shocked above the transition pressure. Their calculations indicated need for more detailed wave profile measurements and for further calculations to define appropriate relaxation times. Novikov *et al.* (1965) indicated the need for finite transformation rates to explain their wave profile measurements in iron.

Based on Eq. (55) the most apparent manifestation of finite transformation rate are p_x^{TL} values which depend on sample thickness and input pressure. Loree *et al.* (1966a) recognized "overdrive pressure" and sample thickness effects and reported an equilibrium value of p_x^{TL} based on thick samples and input pressures not far above 13 GPa. Input pressure and sample thickness effects are also apparent in the work of Bancroft *et al.* (1956) and Minshall (1961). Forbes and Duvall (1975) observed thickness effects in samples varying in thickness from 1 to 25 mm.

Barker and Hollenbach (1974) also obtained data to test the dependence of p_x^{TL} on input pressure and sample thickness. Their data, shown in Fig. 19, can be well fitted by Eq. (55) with $t_0 = 0.18$ μs. Although this agreement between the simple transformation rate model and experiments is gratifying, the relaxation time obtained apparently does not correctly predict rise time of the Plastic II wave, P_{II}, nor does it correctly predict change in time of arrival of p_x^{TL} with input pressure. Barker and Hollenbach concluded that a fixed transformation rate model may be too simple to fully describe all data for iron; it is, nevertheless, remarkably successful in describing thickness and input pressure effects.

Barker and Hollenbach also observed that the $\epsilon \rightarrow \alpha$ reversal is at least as fast as the $\alpha \rightarrow \epsilon$ transition. They found no evidence for relaxation in stress behind the Plastic I wave as observed by Novikov *et al.* (1965). Rise times of P_{II} waves were about the same in both investigations.

Further evidence for thermodynamic nonequilibrium in iron shock-loaded into the mixed phase region between 13 and 22.5 GPa is obtained from the difference between the observed pressure-volume curve in Fig. 18 and the calculated Hugoniot of Andrews (1973) based on self-consistent equations of state for α and ϵ iron. As previously indicated, hysteresis on static loading and unloading indicates similar nonequilibrium behavior. The observation of thermodynamic nonequilibrium under shock loading in the mixed phase region will be noted for other shock-induced transitions.

Electrical resistance and demagnetization measurements associated with the shock-induced 13 GPa transition have been used to probe the transition. Fuller and Price (1962) measured resistance of iron wires shock-loaded below and above the transition and found an increase in resistance by a factor of about 2.5 in the vicinity of 15 GPa. Wong *et al.* (1968) made similar measurements on iron and interpreted irregularities in the observed resistance below the transition as evidence for partial transformation below 13 GPa. Above 13 GPa their data agreed with those of Fuller and Price. The

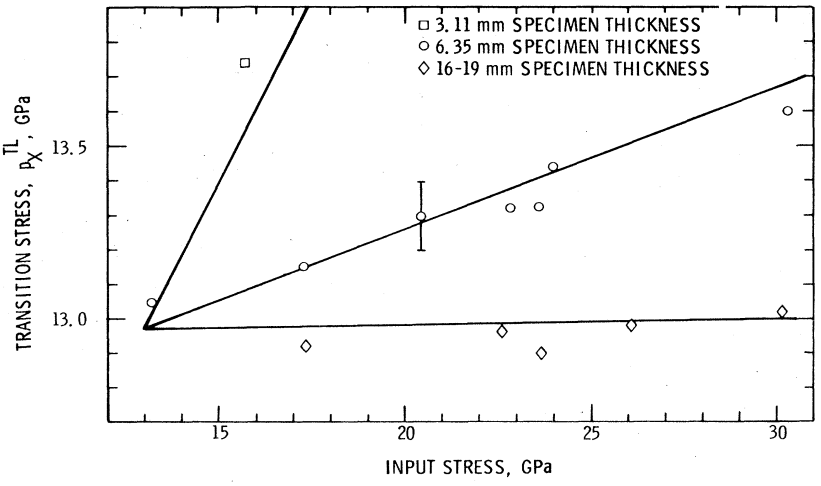

FIG. 19. Transition stress versus input stress for iron of different thickness, as reported by Barker *et al.* (1974). The solid lines fit to the data are characterized by a relaxation time of 0.18 μs for the $\alpha-\epsilon$ phase transition.

observed irregularities below the transition appear to be well within the reproducibility of the measurements and do not provide convincing evidence of the postulated low stress partial transformation. Based on eddy current decay times, Royce (1968) and Keeler and Mitchell (1969) showed smooth change in resistance with stress below 8.0 GPa and an increase of resistance at 17.5 GPa. The importance of shock-induced defects in changing the resistance of shock-loaded iron is evident in the large discrepancy between static data of Balchan and Drickamer (1961) and shock loading data below 13 GPa. The strong influence of deformation details on resistance of shock-loaded metals is apparent in the extensive work on Manganin under shock loading (Graham and Asay, 1977) and in shock measurements on silver (Dick and Styris, 1975).

Although resistance measurements under shock loading clearly show a large increase in resistance associated with the 13 GPa transition, they have not been performed at sufficiently small stress increments to accurately determine a value for transformation pressure. Projectile impact experiments appear to be well suited for such a determination should further work of this kind be undertaken.

Shock-induced magnetization changes are less sensitive to details of plastic deformation than are changes in resistance and are subject to more direct interpretation. Royce (1968) has made shock demagnetization measurements at 17, 22, and 32 GPa and at higher pressures. They indicate that iron is nonferromagnetic above 32 GPa and show substantial decreases in magnetization at 18 and 22 GPa. These observations are in agreement with the nonferromagnetic character of ϵ iron deduced from Mössbauer effect measurements of Pipkorn *et al.* (1964). The shock demagnetization measurements were made using explosive loading techniques with large input pressure increments, and measurements of the pressure to complete the transition were not made. A similar measurement by Graham (1968) on 3% SiFe with projectile impact loading provides detail on critical pressures. A more detailed review of electronic property measurements with impact loading techniques is given by Graham (1967).

Wong (1969), from results of a double shock loading experiment, inferred that magnetization change in iron is complete at 16 GPa. This result disagrees with measurements of the R–H curve and with demagnetization measurements of Royce (1968). Keeler and Mitchell (1969) also showed substantial demagnetization at 17.5 GPa. They reported apparent demagnetization signals at 8 GPa which they interpreted as due to a partial transformation, having failed to recognize that such effects can easily result from stress-induced magnetic anisotropy and do not require the proposed transformation at low stress. Recently, Novikov and Mineev (1974) have reported shock demagnetization measurements in an iron–bakelite mixture that minimizes eddy currents, and they found no evidence for a lower-pressure transition.

Even though several authors have proposed partial transformation below 13 GPa based on electronic property measurements, the data are fragmentary and incompletely analyzed and give no compelling evidence for transformation at low pressure.

Other works on the iron transition that are of less direct interest include the prediction of a rarefaction shock (Drummond, 1957), observation of smooth spalls in iron as a result of the rarefaction (Erkman, 1961; Lethaby and Skidmore, 1959; Ivanov *et al.*, 1962), and observation of the rarefaction shock by flash radiography (Balchan, 1963). Low-pressure R–H curve measurements have been performed by Taylor and Rice (1963) and Barker (1975). Pressure–volume measurements to 170 GPa were obtained by McQueen and Marsh (1960), to 900 GPa by Al'tshuler *et al.* (1962) and Krupnikov *et al.* (1963), and to 3.4 TPa by Al'tshuler *et al.* (1968a). Curran (1971) has reported a small effect of magnetic field on transition stress in disagreement with theory and with later observations of Barker and Hollenbach (1974). Al'tshuler (1965) has reviewed other shock compression measurements on iron in the Soviet Union.

C. bcc iron base alloys

As previously mentioned, early attempts to identify the low-temperature, high-pressure phase of iron were directed toward the hypothesis that the high-pressure

phase was fcc. Accordingly, shock loading investigations of the effect of alloying on the transition stress were initiated in hope that trends established might help in the identification. Although the alloy studies did not accomplish that goal, the investigations were extensive and established well-defined trends that are largely uninterpreted to date. Quantitative interpretation of the effect of alloying on the 13 GPa transition remains one of the significant unsolved problems in high-pressure metallurgy.

Alloys investigated included Fe–Si, Fe–Ni, Fe–Co, Fe–V, Fe–Cr, Fe–Mo, Fe–Mn, Fe–C, and various ternary Fe–Ni–Cr combinations. All alloys were in the bcc phase at 1 atm and 300 K. It is noteworthy that there has never been a pressure-induced polymorphic transition detected for an fcc iron alloy. However, certain of the fcc iron alloys undergo pressure-induced, second-order phase transitions due to strongly pressure-dependent magnetic properties, as will be described in Sec. V.

One particular alloy, a low carbon 28.4 at.% (atomic percent) NiFe alloy, which is metastable in the martensitic, bcc phase, has been carefully investigated in static and shock loading experiments and is worthy of special note. The Fe–Mn alloy system has also been investigated under static and shock loading and gives an interesting test of Kaufman's method (Kaufman, 1969; Kaufman and Bernstein, 1970) of calculating effects of alloying on transition pressure.

Experimental determination of p_x^{TL} values for iron alloys were first reported by Fowler *et al.* (1961) for Fe–Ni, Fe–Cr, and Fe–Ni–Cr alloys. Zukas *et al.* (1963) studied transitions in Fe–Si alloys up to 6.8 wt% (weight percent) Si and in single crystals of 2.9 wt% Si along two different crystallographic directions. Loree *et al.* (1966a, 1966b) extended the alloy studies to Fe–V, Fe–Mo, Fe–Co, Fe–C, Fe–Ni, and Fe–Mn. All of these authors used direct contact high explosive loading and detected transition stresses with the pin technique. Fowler *et al.* (1961) used metallurgical examination of recovered samples to determine Hugoniot curves at pressures above the transitions. These data give some limited information on the effect of alloying on volume change at the transition. Zukas *et al.* (1963) used similar techniques and concluded that volume change at transition decreased as silicon content was increased; they found no difference between transition stresses observed in single crystals of two orientations and a polycrystalline sample of the same composition. At input pressures in the single shock region Loree *et al.* (1966a) found that R–H curves for the Fe–V alloys were the same, even though transition stresses increased significantly with vanadium concentration. Similar results were noted for the Fe–Co alloys.

A summary of effects of various solutes on transition pressure is shown in Fig. 20: addition of nickel and manganese substantially lowers it; addition of vanadium and cobalt substantially increases it. Transition pressures for vanadium concentrations greater than 11 wt% were not accurately determined, but p_x^{TL} values as high as about 58 GPa were observed at 40 wt% V. Work by Loree *et al.* (1966a) for iron–carbon is not shown in Fig. 20 since the observed strong effects of heat treatment

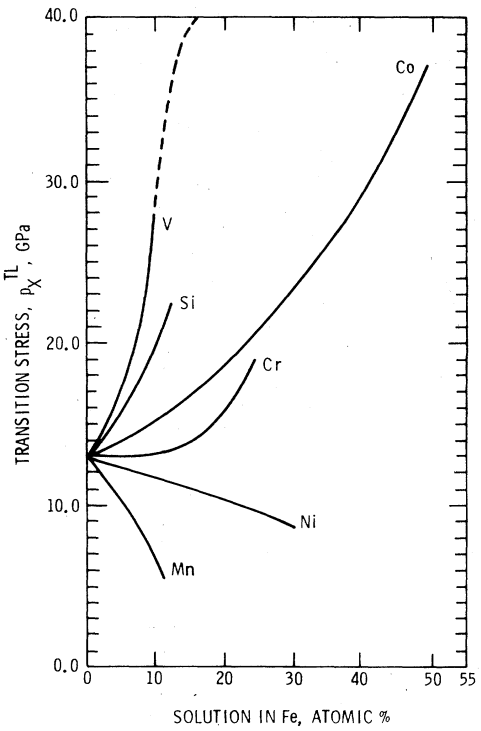

FIG. 20. Transition stresses observed for iron alloys under shock loading. The data on vanadium and cobalt alloys are from Loree *et al.* (1966a). The data on silicon alloys are from Zukas *et al.* (1963). The data on chromium alloys are from Fowler *et al.* (1961). Data from Gust and Royce (1970) on chromium alloys are similar to those of Fowler *et al.* (1961). The data on manganese alloys are from Loree *et al.* (1966b). The data on nickel alloys are from Fowler *et al.* (1961) and Loree *et al.* (1966b). Loree *et al.* (1966a) report estimates of transition stresses as high as 58 GPa for 28 at.% vanadium alloys. Data on molybdenum alloys from Loree *et al.* (1966a) are not shown.

indicate that shear strength effects were significant. Data they obtained for Mo concentrations greater than 14 wt% are not shown because the samples were initially in a mixed phase condition.

Bundy (1967) observed transitions in Fe–V and Fe–Co alloys with static high-pressure resistance measurements. He found substantially higher transition pressures than those observed in shock experiments. This discrepancy is apparently resolved in later work by Bundy (1975), whose new measurements show excellent agreement between static and shock loading work in two Fe–Co alloys.

Trends in transition stress with alloy content are well defined. None of the alloy systems show discontinuous behavior as solute content is changed. Except for a few special cases, the effects of alloy composition on transition pressure have not been studied to determine their implications for phase stability at high pressure. The continuous changes in p_x^{TL} with solute indicate that high-pressure phases are hcp.

Giles and Marder (1971) studied transitions in Fe–Mn alloys under static pressure with their high-pressure x-ray diffraction apparatus. X-ray patterns on loading and unloading indicate a large hysteresis similar to that

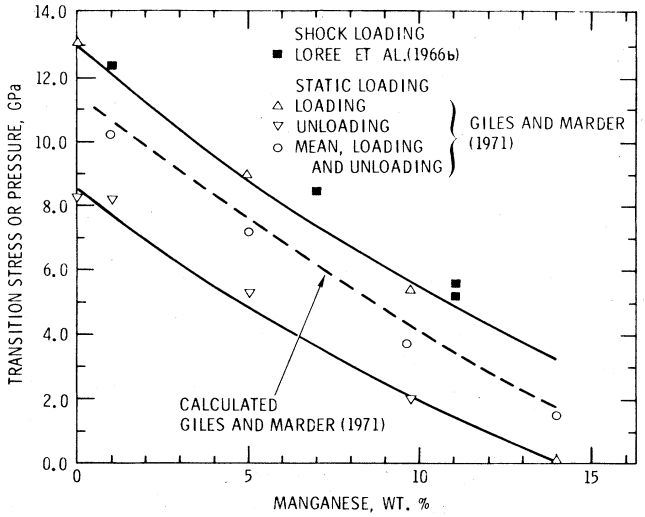

FIG. 21. The effect of alloying iron with manganese is to lower the transition stress or pressure as indicated from static and shock loading measurements. For static loading, the pressure for the reverse transition on unloading is significantly lower than for loading, while the equilibrium pressure taken as the mean of loading and unloading is found to be in good agreement with equilibrium thermodynamic calculations. After Giles and Marder (1971).

found for iron (Giles and Marder, 1971). Their results are compared with shock data (Loree *et al.*, 1966b) in Fig. 21. Agreement between static and shock transition pressures on loading is reasonably good and would be improved if a correction for shear were applied. (An HEL measurement on 10 wt% Mn alloy by Graham with a quartz gauge shows an HEL of 1.0 GPa.) The calculated mean between loading and unloading pressure is shown to agree well with equilibrium pressures calculated by Kaufman's thermodynamic theory. The agreement between calculation and experiment indicates that thermodynamic calculations may prove useful in identifying other pressure-induced iron alloy transitions.

Shock-induced transition measurements in ternary Fe–Ni–Cr alloys are reported by Fowler *et al.* (1961) and by Gust and Royce (1970). Static high-pressure x-ray diffraction measurements on this alloy system are reported by Giles and Marder (1971) and Jamieson (1963a).

Shock demagnetization measurements on a 3.25 wt% SiFe commercial alloy, Silectron, have revealed considerable detail on initiation of the transition, the mixed phase region, and the input pressure at which a single shock wave is formed (Graham, 1968). The detail derived from these measurements results from use of a projectile impact technique to apply input pressures in small increments over a wide range of pressure. The shock-induced demagnetization is shown in Fig. 22. At high pressure the material is in a nonferromagnetic state. Onset of transition stress is at 14.5± 0.5 GPa and transition is complete at 22.5± 1 GPa. Other data indicated that a single shock wave is formed at input pressures greater than 37.5 GPa. According to data in Fig. 22 the transformation does not proceed linearly with pressure in the mixed phase region; initial increments of pressure above 14.5 GPa appear to produce larger amounts of the nonferromagnetic phase than higher pressures. Completion of the mixed phase region at 22.5 GPa is in good agreement with the pressure–volume (R–H) data of Zukas *et al.* (1963). Changes in magnetization below the transition are due to stress-induced magnetic anisotropy (inverse magnetostriction) and pressure dependence of magnetization of the bcc phase.

Christou and Brown (1971) have examined Fe–Mn alloys recovered after shock loading for evidences of retained high-pressure phases. Interpretations by Christou (1972) of the role of defects, determined from annealing studies of shock-loaded Fe–Mn alloys, have been criticized by Schumann (1973).

Investigations of the pressure-induced martensite-to-austenite transition in a low carbon 28.4% Ni–Fe alloy have provided an unusually complete test of the use of thermodynamic data taken at atmospheric pressure to predict a pressure-induced transition. A well-annealed sample of this alloy is stable in the fcc, austenitic, phase at room temperature and atmospheric pressure. Cooling the sample to liquid nitrogen temperatures for many hours transforms it to a metastable, mostly martensite (bcc) phase that is retained indefinitely when temperature is subsequently raised to room temperature. Thus an alloy of fixed chemical composition is available for study in both the bcc and fcc phases, and thermodynamic properties can be determined for both phases. Furthermore, the transition from bcc to fcc in the vicinity of 675 K is accessible for study in a purely hydrostatic apparatus. The transition can also be readily studied with quartz gauge under impact loading in both fcc and bcc phases. Time-resolved wave profile measurements provide information for detailed pressure–volume de-

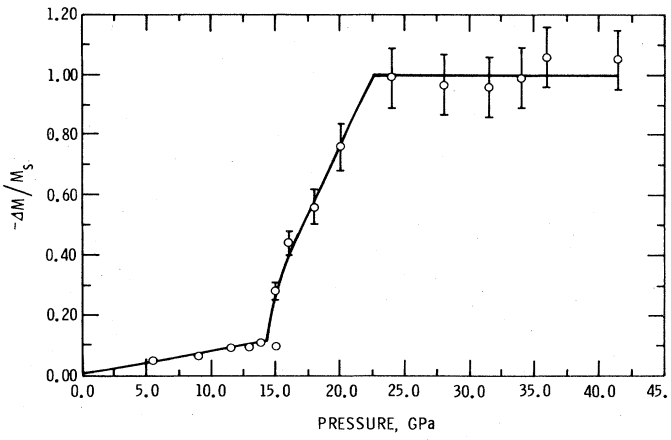

FIG. 22. The indicated relative change in magnetization, M_s, for various shock loading pressures for Fe–3.25 wt % Si shows a phase transition to a nonferromagnetic phase beginning at about 14 GPa. The data indicate that the transition is complete at 22.5 GPa. The apparent magnetization change below the transition is that expected from stress-induced magnetic anisotropy and the change in magnetization with pressure for the bcc phase. The figure illustrates how experiments conducted at closely spaced input pressure can provide independent data on details of ferromagnetic to nonferromagnetic transitions. From Graham (1968).

terminations. These happy circumstances have led to an opportunity to predict and study details of a pressure-induced transition under both static and shock loading.

Stress wave profiles in an impact-loaded bcc 28.4% Ni–Fe alloy measured by Graham *et al.* (1967) showed a region of unusual compressibility from a few hundred MPa to 2.0 GPa. Subsequent investigations of shock-loaded samples by Rohde *et al.* (1968) showed that shear stress resulting from the shear strength was responsible for partial transformation to the fcc phase. Measurements of pressure dependence of the austenite start temperature A_s (the temperature at which bcc martensite begins to revert to fcc austenite under increasing temperature) under static loading by Rohde and Graham (1969) to 2.0 GPa show a large decrease in A_s with pressure. The observed decrease in A_s agrees well with predictions from a simple isothermal model in which transition pressure is determined by free energy and volume differences between the two phases. Predictions from an adiabatic model were not significantly different from the isothermal model. Rohde (1970) extended the investigation on this same alloy to impact loading at temperatures between 298 and 663 K to test the thermodynamic model to higher pressure. His data are shown in Fig. 23. When a correction is made for partial transformation caused by shear strength at low pressure, shock and static loading data are found to be in good agreement. At higher pressures the shock data are found to accurately coincide with the adiabatic model of the transition. Rohde and Albright (1971) quantitatively determined the effect of shear stress on this same alloy in uniaxial tension experiments and found excellent agreement with the theory. Since predictions of thermodynamic theory for behavior at high pressure are based on independently determined thermodynamic constants, agreement between theory and experiment at high pressure is remarkable confirmation of the validity of the models.

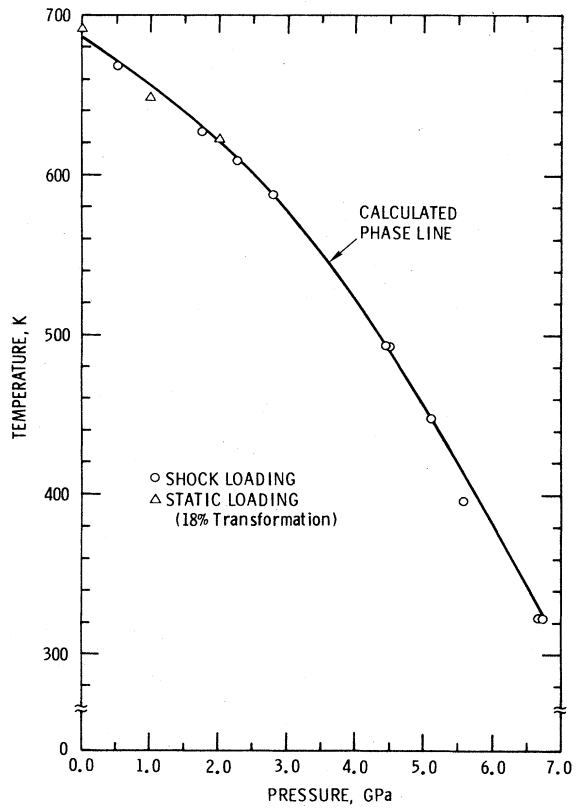

FIG. 23. The calculated and observed phase line for a low carbon Fe–28.4 at.% Ni alloy whose thermodynamic properties can be studied in both the bcc and fcc phases. The behavior under both static and shock loading is found to be in excellent agreement with the phase line calculated from the thermodynamic properties of the two phases. After Rohde (1970).

Pope and Edwards (1973) repeated measurements of Rohde and Graham (1969) with measurements under static high pressure on an alloy of similar composition and found an anomalously large decrease in A_s with pressure up to 200 MPa. This effect was found to result from shear on the interfaces between the two phases (Pope and Warren, 1974). The appreciable effects of shear stresses on the transformation can apparently be modeled well enough under shock loading that accurate predictions of transition pressures can be made from thermodynamic data.

Later work on Fe–Ni alloys by Christou (1973) was found to disagree with previous experimental observations and with previous thermodynamic predictions. A critique of this work has been given by Rohde and Graham (1973).

D. Antimony

Duff and Minshall (1957) referred to shock loading experiments on antimony which showed a transition characterized by an unusually pronounced decay of p_x^{TL} with sample thickness. [The detailed data are reported by McQueen (1964).] Katz *et al.* (1959) confirmed the existence of a multiple wave structure in antimony. A detailed study of the transition was reported by Warnes (1967), whose p_x^{TL} values measured at different sample thickness are shown in Fig. 24. Transition pressure decreases strongly with sample thickness to 20 mm, then decreases more slowly to 50 mm. Based on an extrapolation to thicker samples, Warnes assigned an equilibrium p_x^{TL} of 8.8 GPa. This value is probably a few hundred MPa high, since it is based on average shock velocity determinations. Application of a shear strength correction yields a mean pressure lower by about 100 MPa.

Static high-pressure data indicate a rhombohedral to simple cubic transition completed in the vicinity of 7.0 GPa (Vereshchagin and Kabalkina, 1965), followed by a cubic to hcp transition in the vicinity of 8.3 to 8.8 GPa (Vereshchagin and Kabalkina, 1965; Bridgman, 1942). More recent work by McDonald *et al.* (1965) and Kabalkina *et al.* (1970) indicates that the high-pressure phase is not hcp. Considering the errors in both shock and static loading experiments, the observed transition pressures are in good agreement.

The lower-pressure transition apparently involves little or no volume change (Kabalkina *et al.*, 1970), and Warnes saw no evidence of it in the wave profile. The R–H curve below the transition showed softening which

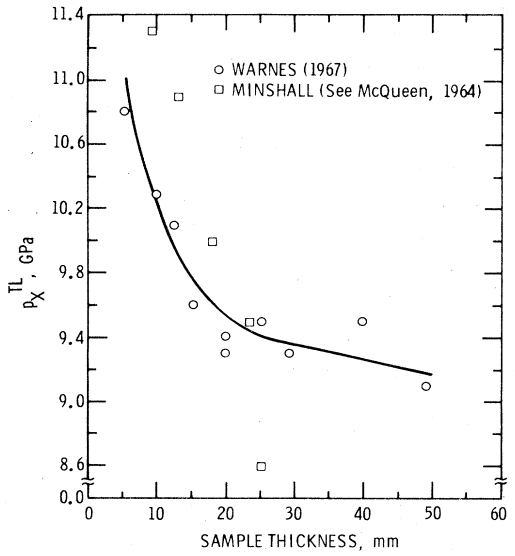

FIG. 24. The transition stress for antimony observed under shock loading has been found to exhibit an unusually slow transformation rate. The slow rate is manifested as a strong dependence of the observed transition stress on sample thickness.

is consistent with the static observations.

Thickness variations of p_x^{TL} observed by Warnes for thicknesses less than 20 mm are well fitted by a relaxation time $t_0 = 3$ μs in Eq. (55). This relaxation time is at least an order of magnitude larger than that for thin samples of iron (Forbes, 1976). A single transformation rate cannot explain the behavior indicated by measurements at thicknesses less than and greater than 20 mm.

Further evidence for nonequilibrium thermodynamic behavior in the shock-induced transition is contained in the data of Warnes in the mixed phase region about 8.8 GPa, where the Hugoniot curve is observed to lie above the equilibrium curve.

A flash x-ray profile of shocks in antimony in two-dimensional steady flow was later reported by Breed and Venable (1968). Figure 2 of their paper was an overlay of a flash radiograph of a wave pattern in two-dimensional flow produced by detonation of the high explosive, baratol, in contact with antimony. The figure showed profiles of a Plastic I wave associated with the phase transition and a Plastic II wave corresponding to the input pressure produced in antimony. They directed particular attention to the curvature of the Plastic II wave front, which indicates that the wave starts at a very low velocity and accelerates rather rapidly to its final velocity, which differs but slightly from the velocity of the Plastic I wave.

This curvature is a rational consequence of the finite transition rate and Plastic I decay noted by Warnes. From the jump conditions, Eqs. (9) and (10), with U_1, V_0, P_0, P, V replaced by $U_{p1}, V_1, P_1, P_2, V_2$, respectively, velocity of the second shock is

$$U_{s2} = U_{p1} + V_1[(P_2 - P_1)/(V_1 - V_2)]^{1/2}.$$

With P_2 and V_2 fixed and P_1 and ρ_1 decreasing, the second shock accelerates. With a relatively simple transformation this result can be applied to the Breed and Venable radiograph. The Plastic II profile so calculated is shown as OB in Fig. 25. Measurements by Breed and Venable (1968) are indicated by curve OB'. The calculated profile reproduces essential features of the observation, though differences remain (Duvall, 1973).

Hayes (1972), using a formalism slightly different from that in Sec. II.F, has inferred from the thin-sample data of Fig. 24 a transformation time of 2.3 μs. This time is in reasonable agreement with the observed value of 2–3 μs for the time delay of formation of the Plastic II wave reported by Breed and Venable (1968). Forbes (1976) shows relations among the various formalisms which have been used.

E. Bismuth

The temperature–pressure phase diagram of bismuth has been the subject of much study, which will undoubtedly continue. Its many polymorphic transitions are especially important because of their use as fixed-point calibrations. The Bi I→ Bi II and melting transitions are of particular interest under shock loading since they afford an excellent opportunity to develop our understanding of transitions based on carefully characterized static high-pressure studies. A recent summary of the Bi phase diagram is given by Liu *et al.* (1973).

The investigation of bismuth under shock loading by Duff and Minshall (1957) is one of the classic papers of shock-wave physics. Measurements of the solid I → solid II and the solid I→ liquid transitions were attempted. The solid I→ solid II transition was apparently detected, but pressure of the transition was about 250 MPa higher than would be expected from static measurements. Transformation rates were apparently very rapid since values for p_x^{TL} were found to be independent of sample thickness. In experiments at elevated temperature, Duff and Minshall failed to observe evidence for melting in the wave profiles, even though pressure and temperature were in the equilibrium liquid region as determined by static pressure measurements. Because of the importance of these transitions, the disagreement between static and shock loading results raised serious questions about the nature of shock-induced transitions. Further experiments by Hughes *et al.* (1961) under shock loading were inconclusive in resolv-

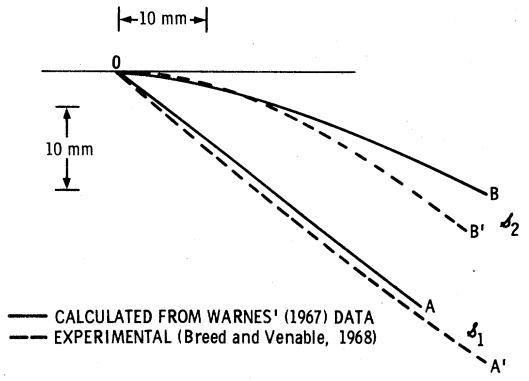

FIG. 25. Observed and calculated Plastic I and Plastic II wave fronts in antimony in two-dimensional steady flow.

TABLE III. Bi I→ Bi II transition[a] (normalized to 295 K).

Author	p_x^{TL} GPa	$\bar{p}^{TL}$ GPa	P^T GPa	η_{TL} %
Shock loading				
Duff and Minshall, 1957[b]	2.69–2.75	···	···	6.5–6.7
Larson, 1967[c]	2.46–2.56	2.43–2.57	···	5.8–6.1
Asay, 1974[d]	2.50–2.53	2.55±0.03	···	5.8
Static loading				
Heydemann, 1967a, 1967b	···	···	2.55	···
Giardini and Samara, 1965	···	···	···	6.4

[a] p_x^{TL} is the stress observed under shock loading which is associated with the transition; η_{TL} is the volume compression from atmospheric pressure to the onset of the transition; $\bar{p}^{TL}$ is the mean pressure calculated from p_x^{TL}. The value shown is corrected by +90 MPa to account for a 20 K shock-induced temperature rise. P^T is the transition pressure measured in a hydrostatic environment.

[b] The range shown corresponds to values observed on four samples with 3 mm grain size.

[c] The range shown corresponds to values observed on samples: 21 cast, 7 pressed, and 7 single-crystal.

[d] The range shown corresponds to values observed in four pressed samples with 30μm grain size.

ing the questions raised by the work of Duff and Minshall.

Larson (1967) investigated the solid I→ solid II transition under shock loading, using wave profile measurements made with the quartz gauge. Thirty-five different samples were shocked, including cast and pressed polycrystalline and single-crystal samples. With his improved time resolution, compared with that available to Duff and Minshall, Larson measured the HEL and showed that the transition wave has considerable structure. When a correction is made for shear strength and for a +90 MPa difference in pressure due to a 20 K shock-induced temperature rise, his data are found to be in excellent agreement with the static pressure determination. Larson's and other shock measurements are shown in Table III and compared with static data.

Asay (1974) used projectile impact loading and detected wave profiles with the VISAR to study both the solid I→ solid II and solid I→ liquid transition. (His melting transition measurements are described in Sec. VI.B.) Since the VISAR is insensitive to wave front tilt, even better wave profile resolution was obtained than that reported by Larson. As shown in Table III, Asay's measurements of p_x^{TL} are in good agreement with Larson's values and with the static measurements.

Some of the differences between measurements by Duff and Minshall and those by Larson and Asay may have been due to material differences since the former investigators used polycrystalline samples with large grains. However, improved resolution in the pressure–time profiles obtained by Asay shows the Plastic I wave to be characterized by a rapid increase in particle velocity followed by a region of slowly increasing amplitude in the (p_x, t) plane. The relatively poor time resolution available to Duff and Minshall would have caused them to miss the initial break in slope and to overestimate the pressure of the Plastic I wave by an amount approximately equal to their reported error, as pointed out by Asay. This illustrates a point that must always be kept in mind when assessing numerical results of shock wave experiments: there is frequently an arbitrary element in the interpretation of experimental records which may result from instrumental deficiencies or may reflect attempts to oversimplify the records. This arbitrariness produces, in turn, some uncertainty in the numerical results. There are exceptional situations where interpretation is unambiguous, but, in general, the significance of agreement between static and shock loading results should be assessed with careful analysis of the characteristics of the instrumentation and the uncertainty associated with kinetic and shear strength effects.

By shock loading into the melt region, Asay determined the pressure of the solid I–solid II–liquid triple point. His pressure determination, which is the mean of nine different measurements, is shown in Table IV. Again, there is good agreement between static and shock loading results.

The lower-pressure phase diagram shown in Fig. 26 indicates that shock and static loading data at various temperatures are in good agreement. Thus, the more modern wave profile measurements show that static and shock loading measurements in bismuth are in good agreement. It does not appear that more accurate determinations will be achieved in bismuth under shock

TABLE IV. Triple point determinations Bi I→ liquid→ Bi II.

Author	p_x^{TL} GPa	Temperature K
Shock loading		
Asay, 1974	$1.70^{+0.08}_{-0.05}$[a]	···
Static loading		
Bridgman, 1935	1.70	456
Bundy, 1958	1.52	453
Panova *et al.*, 1961	1.72	457
Klement *et al.*, 1963	1.67	464

[a] ± indicates range of values determined for different samples and under different initial temperatures. No attempt has been made to apply a strength correction.

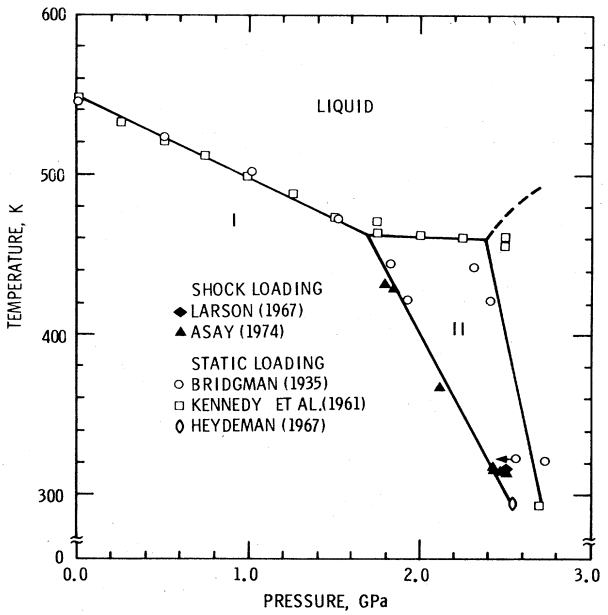

FIG. 26. Determinations of the phase diagram of bismuth I, bismuth II, and liquid by static and shock loading are found to be in good agreement. Earlier discrepancies reported by Duff and Minshall (1957) were apparently caused by a lack of time resolution of their detectors.

loading because there is uncertainty in the correct assignment of transition stress for wave profiles in which pressure changes slowly with time.

As is the case with transitions in other solids, lack of thermodynamic equilibrium in the mixed phase region is indicated in the measurements of Duff and Minshall by the differences between the calculated and observed Hugoniot curve in the mixed phase region above the solid I→ solid II transition pressure.

Johnson *et al.* (1974) have reported a complete solid I–solid II–liquid equation of state for bismuth from which equilibrium calculations can be readily made. Differences between calculated and observed rise times indicate that equilibrium calculations do not correctly describe details of the material response. This work was extended to a more complete and elegant treatment incorporating transformation rates by Hayes (1975). This work is described in more detail in Sec. VI.B.

F. Graphite-to-diamond transformation

Parsons (1920) subjected graphite to explosive shock waves and produced what he believed to be diamond in the recovered residue, but positive identification was not possible at that time. Riabinin (1956) attempted unsuccessfully to identify diamond in graphite recovered from shock loading experiments. DeCarli and Jamieson (1961) subjected shock-loaded graphite to chemical separation, followed by x-ray diffraction analysis, and produced positive evidence of the existence of diamond particles in the residue. Alder and Christian (1961) reported an abrupt change in slope of the R–H curve for graphite of 95% theoretical density at about 40 GPa; this they identified with formation of the diamond phase. This result was confirmed by Pavlovskii and Drakin (1966) and by Trunin *et al.* (1969). An apparent second transformation reported by Alder and Christian at about 60 GPa was attributed to experimental error by Pavlovskii and Drakin and Trunin *et al.*

Doran (1963b) reported measurements of the R–H curve for pyrolytic graphite to about 30 GPa, and Coleburn (1964) reported measurements to 49 GPa. Both authors found compressibility decreasing substantially above about 10 GPa, in contrast with measurements mentioned in the preceding paragraph; in those cases compressibility was essentially constant below 40 GPa. Coleburn found no evidence for a transition at 40 GPa. McQueen (1964) and McQueen and Marsh (1968) reported a multitude of measurements on diamond and graphite of various densities for pressures between 2.4 and 90 GPa. Their data on pyrolytic graphite agree with the Doran and Coleburn values in the same pressure ranges and show a break in slope of the $U_s - U_p$ curve at 40 GPa which they interpreted as the transition to diamond. Their measurements show no evidence of a transition above 40 GPa, in agreement with Trunin *et al.* (1969). Pavlovskii (1971) has reported shock compression data on single-crystal diamond between 50 and 580 GPa and finds no evidence for a high-pressure phase transition. McQueen and Marsh (1968) also reported data on pressed powder diamonds between 43 and 128 GPa and found no evidence for a transition.

McQueen and Marsh fitted their $U_s - U_p$ data on pyrolytic graphite below 40 GPa with two straight lines having a break in slope at about 6 GPa. They attribute this break to a second-order phase transition associated with buckling of basal planes. They were able to fit R–H curves for all the various graphite densities by assuming them to respond to pressure according to the equation of state of pyrolytic graphite above 6 GPa with a Gruneisen parameter, Γ chosen so that $\Gamma\rho = \text{const}$.

Both Dremin and Pershin (1968) and McQueen and Marsh (1968) found that graphites of densities lower than 2.2 Mg/m^3 exhibit a break in their P–V curves around 23 GPa. These observations indicate that the graphite-to-diamond transition is lowered in samples of lower initial density.

It appears fairly certain that graphite does indeed transform to diamond at a shock pressure of the order of 40 GPa with a mixed phase region extending to 60 GPa. It is equally certain that there is no metallic transition of the kind reported by Alder and Christian for $P < 300$ GPa (Trunin *et al.*, 1969). The second-order transition at 6 GPa in pyrolytic graphite suggested by McQueen and Marsh (1968) is speculative. To place it on firmer ground appears to be a formidable task. Increasing porosity appears to decrease the transition pressure possibly due to the effect of temperature.

Alder and Christian (1961), Pavlovskii and Drakin (1966), and Dremin and Pershin (1968) reported that measurements below 40 GPa were sensitive to sample thickness. This observation is consistent with a finite transformation rate for the transition to diamond. McQueen and Marsh (1968) did not see thickness effects, but the possibility does not appear to be excluded by their data.

In related work on recovered samples, Trueb (1968,

1970) has identified both hexagonal and cubic forms of carbon and has identified a "hard" graphite, which apparently resulted from conversion of diamond formed during shock loading. Only the cubic form of diamond is found in recovered shock-loaded graphite in a copper matrix (Trueb, 1971). In examination of Madagascar graphite compressed to a density of 2.05 Mg/m^3 and shock loaded to 45 GPa for a duration of 300 ns, Pujols and Boisard (1970) found a well-defined region within the sample which had apparently transformed to diamond and reverted to graphite on unloading. Fournier and Oberlin (1971) have examined recovered samples of shock-loaded graphite with an electron microscope and found diamond as well as other disordered forms of graphite.

Commerical shock processes presently being used for production of commerical diamond yield crystallites ranging from 500 Å to 30 μm in size (DeCarli, 1966; Trueb, 1971).

DeCarli (1967, 1976) has identified diamonds in graphite shock-loaded to pressures less than 15 and as great as 150 GPa, using more porous samples at the lower pressures. He attributes diamond formation to nucleation and growth processes, followed by immediate quenching in heterogeneously heated samples. It has also been suggested that diamond is formed by direct compression of rhombohedral graphite, but this seems unlikely since amounts of recovered diamond appear to be independent of starting material (DeCarli, 1967).

Diamonds found in meteorites are believed to result from shocks produced in terrestrial or extraterrestrial impact (Lipschutz, 1964; DeCarli, 1967), and the presence of diamonds in certain minerals is considered as evidence of meteoritic origin (Lipschutz, 1968). Vdovykin *et al.* (1973) have shock-loaded samples of carbonaceous matter from two meteorites and produced diamonds.

G. Germanium and silicon

Germanium and silicon exhibit particularly interesting transitions because their HEL values are a substantial fraction of their transition pressures. For example, [111] orientation Ge crystals have HELs of about 4.5 GPa compared to the transition pressure of about 14 GPa, and [111] orientation Si crystals have HELs of about 5.0 GPa compared to transition pressure of about 10 GPa. Thus, these crystals offer an excellent test of the equivalence of shock and static loading transition pressure measurements in the presence of large shear stresses resulting from shear strength.

Minomura and Drickamer (1962) reported a decrease in resistance of six orders of magnitude in Ge at static high pressures between 12.0 and 12.5 GPa; the large change in resistance and other considerations indicated that the transition was to a metallic phase. With x-ray diffraction techniques, Jamieson (1963a) determined that both Si and Ge go to the white Sn phase when pressure is increasing; both revert to a still different structure when pressure is subsequently decreased (Kasper and Richards, 1964). Jamieson also measured volume compression required to initiate the transition and volume change between the two phases.

In the first shock loading work on Ge, McQueen (1964) reported a multiple wave structure with an HEL of about 4.0 GPa and a transition stress of about 12.5 GPa. Graham *et al.* (1966) used resistance measurements of impact-loaded [111] Ge to give a measure of the HEL and the transition pressure. Pavlovskii (1968) used the electromagnetic gauge in explosive loading experiments to measure wave profiles in [111] samples. He derived values for the HEL and p_x^{TL} that were in good agreement with Graham *et al.*; however, measured particle velocity and shock velocity values show considerable disagreement with other measurements and with the shock velocity predicted from ultrasonic measurements. Hence, Pavlovskii's measurements apparently contain two compensating errors and raise questions about problems with the electromagnetic gauge technique.

Jacquesson *et al.* (1970) reported thermoelectric emf measurements on [111] Ge which confirmed shock velocity measurements of Graham *et al.* for the elastic and transition waves. Gust and Royce (1972) reported wave profile measurements on [111], [100], and [110] Ge and determined HEL and transition pressure values. Their p_x^{TL} values are somewhat lower than the value reported by Graham *et al.*, but the stated errors appear to bring the measurements into agreement within experimental error.

A comparison of shock and static loading transition values in Table V shows reasonable agreement, after shear strength correction, between shock and static pressures and between volume compressions required to initiate the transition. No significant discrepancies are indicated between shock and static loading measurements even though shock loading pressures are subject to large shear stress corrections.

In the mixed phase region above the transition, Graham *et al.* reported a value of compressibility in agreement with that calculated from the equilibrium phase line, whereas the more numerous measurements of Gust and Royce disagree with the equilibrium calculation. Since the investigation of Graham *et al.* included only a single measurement in that region, it is likely that their result is incorrect because of misinterpretation of the resistance record. If this is true, the mixed phase region of shock-loaded Ge exhibits nonequilibrium behavior, as do other materials which have been examined.

The situation with silicon is less well-defined than with germanium. Minomura and Drickamer (1962) reported a five to six order-of-magnitude change in the resistance of silicon samples between 19.5 and 20 GPa when shear stresses were low. A resistance drop was observed between 13.5 and 15 GPa when shear stresses were high, even though there was no indication of intermediate transitions when shear stresses in their apparatus were low. Jamieson's (1963a) x-ray diffraction measurements in an apparatus with large shear stress showed the transition at a volume compression of 9.2%, which corresponds to approximately 16 GPa. Thus Jamieson's measurements confirm the sensitivity of the transition to shear. Wentorf and Kasper (1963) found the transition to be sensitive to shear, temperature, and time of pressure and found a bcc structure from samples recovered after release of pressure.

TABLE V. Critical transformation conditions for germanium in the vicinity of 300 K.[a]

Author	p_x^{TL} GPa	$\bar{p}^{TL}$ GPa	P^T GPa	η_{TL} %
Shock loading				
McQueen, 1964	12.5±0.7	...	...	...
Graham *et al.*, 1966	13.6–14.2	11.4–12.2	...	12–13
Pavlovskii, 1968	14.3	12.0	...	...
Gust and Royce, 1972	12.5±1.5[b]	c	...	11.6[b]
Static loading				
Minomura and Drickamer, 1962	...	...	12.0–12.5	...
Jamieson, 1963a	...	...	...	12.5

[a] p_x^{TL} is the observed stress associated with the transition; $\bar{p}^{TL}$ is the mean pressure computed from p_x^{TL} and a shear strength correction based on the HEL; P^T is the transition pressure measured in a hydrostatic environment; and η_{TL} is the volume compression to initiate the transition.

[b] The value shown is that observed for [111] orientation samples. Measurements on [110] and [100] showed the same result within the stated errors.

[c] No strength correction was attempted on these data due to the large stated errors in both p_x^{TL} and the HEL values.

In 1964, McQueen reported wave profile measurements obtained by Wackerle on shock-loaded silicon. No transition was identified since the wave profiles showed slowly rising plastic waves with inflections which were not consistent under different loading conditions. Pavlovskii (1968) reported similar measurements and was able to determine a value of 4.0 GPa for the HEL and 11.2 GPa for the suspected phase transition. As indicated previously, however, there are questions about his experiment since his elastic wave velocities differ considerably from those predicted from elastic constants.

Gust and Royce (1971) performed a thorough investigation of Si with explosive loading applied in [111], [110], and [100] directions. In addition to the HEL values, which varied from 9.2 to 5.4 GPa, they observed, in most cases, two successive apparent phase transitions at 10 and 14 GPa. (In the [100] orientation, only the higher-pressure transition was observed.) Volume compression to initiate the second transition, 10.3%, corresponds reasonably well with Jamieson's measurements. Gust and Royce did not observe higher-pressure transitions, even though their work extended to much higher pressure.

Electrical measurements of emf generated during shock compression of Si do not appear to give any new insights into the nature of the transition (Coleburn *et al.*, 1972; Mineev *et al.*, 1971).

Thus neither static nor shock loading investigations give a clear picture of the pressure-induced transitions in silicon. Since the transition or transitions are sensitive to shear, the relation between static and shock observations is confused. Certainly, one or both of the shock transitions may well be to metastable phases.

H. Alkali halides–KBr, NaCl, and KCl

Transition pressure measurements in several alkali halides have been of considerable interest under both static and shock loading. NaCl plays a crucial role as an internal standard for high-pressure x-ray diffraction studies based on the work of Decker (1971) and shock loading investigations of Fritz *et al.* (1971); hence, several reports of low-pressure phase transitions have been of concern. The thermodynamics of solid solutions of KCl–RbCl, KCl–KBr, KCl–KF, and KCl–NaCl systems at elevated temperatures under static high pressure have been extensively studied by Darnel and McCollum (1970, 1971). Transition pressure measurements under shock loading are of particular interest since the alkali halides exhibit very low HEL values and shear strength corrections should be minor if not negligible. Furthermore, the transitions in crystals such as KCl, KBr, and RbCl are at sufficiently low pressure that the quartz gauge can be used to provide accurate time-resolved wave profile or impact surface measurements. Work in the Soviet Union on alkali halides under shock loading is summarized by Al'tshuler (1965).

Christian (1957) inferred from shock measurements at high pressures that transitions had occurred in KF, KCl, KBr, KI, RbCl, RbBr, and RbI, but his measurements provided neither irrefutable evidence of transition nor values of transition pressures. He also found that NaCl crystals with [111] orientation experienced lower pressures than those with [100] orientation, at approximately 27 GPa, using the same driver system. He suggested that this might be evidence for transition to the CsCl structure, since such a transition should occur more easily in the [111] than in the [100] orientation.

The transition pressure in KBr under shock loading was first measured by Al'tshuler *et al.* (1963). The transition pressure in crystalline KBr observed at 1.85 ± 0.08 GPa (Larson, 1965) with the quartz gauge under shock loading is in excellent agreement with the transition pressure of 1.80 GPa determined for static loading (Darrel and McCollum, 1970). Shock loading measurements on porous polycrystalline samples showed no dependence of p_x^{TL} on sample thickness, but the transition pressure of 2.38 GPa obtained from wave profile measurements with the electromagnetic gauge seems unaccountably high (Dremin *et al.*, 1965). A more recent

measurement by the same group, Adadurov *et al.* (1970), on pressed powder shows the transition at 2.05 GPa.

Static high-pressure x-ray diffraction measurements on NaCl have shown evidence for a phase transformation near 1.7 GPa (Evdokimova and Vereshchagin, 1963a, 1963b; Pistorius, 1964), and a transition at 2.9 GPa under shock loading has also been reported (Larson, 1965; Larson *et al.*, 1966). Johnson (1966) reexamined the static x-ray diffraction experiments, found no transition, and concluded that earlier reports of a transition were due to a lithium impurity. Furthermore, Samara and Chrisman (1971) and Corll and Samara (1966) found no evidence for a phase transition in dielectric and elastic constant measurements to 2.6 GPa. White *et al.* (1968) reexamined the shock transition and traced the reported transition in powdered samples to a problem in the loading system. The presence of secondary yielding was a possible explanation for the small anomaly in single-crystal shock experiments (Royce, 1969). Weidner and Royce (1970), however, in their last examination of the problem, concluded that there is a residual disturbance in pressure–time profiles of shocked single-crystal NaCl between 2 and 3 GPa which resists explanation as either experimental error or secondary yield. It seems unlikely that a phase transition exists in this region, but the case cannot yet be considered closed.

High-pressure phase transitions have been observed in NaCl under shock loading (Hauver, 1966a; Hauver and Melani, 1970; Fritz *et al.*, 1971) and under static loading (Bassett *et al.*, 1968). The flash gap data from which the transition conditions are derived under shock loading (Fig. 16) indicate a difference in behavior between [111] and [100] crystals. The shock transition pressure for the [111] orientation is about 23 GPa at a volume compression of 31.7% and calculated temperature of 1120 K. The static pressure transition is observed at a volume compression of 35.7%, which corresponds to a pressure of 30 GPa according to the isotherm derived by Fritz *et al.* The Hauver and Melani data are in essential agreement with those of Fritz *et al.*, though they contain a suggestion of a higher-pressure transition. The substantial difference between static and shock pressures indicates that two different transitions may be involved, or that error may exist in the static pressure calibration. Brazhnik *et al.* (1969) have examined shock-loaded NaCl samples subjected to a range of conditions and found evidence for material that had transformed to a high-pressure phase and "recrystallized" to the low-pressure phase.

Al'tshuler *et al.* (1963) first reported a phase transition in potassium chloride under shock loading in the vicinity of 2 GPa. Hayes (1974) has reported a very complete study of the 2.0 GPa transition in potassium chloride (NaCl to CsCl structure) under impact loading. Unlike previous shock loading investigations, Hayes utilized direct measurements of the stress and particle velocity at the impact surface provided by quartz gauges in projectile impact experiments. This technique provides a time-resolved record of the stress and particle velocity at the impact face, from which a direct measure of relaxation from initial to final states and an accurate measure of the transition conditions can be obtained. Hayes observed a very fast transformation, complete in less than 10^{-8} s, to a metastable state in both [111] and [100] crystals, followed by slower transformations at rates that depended upon crystallographic orientation.

TABLE VI. Critical transformation conditions for KCl in the vicinity of 300 K.[a]

Author	p_x^{TL} GPa	$\bar{p}^{TL}$ GPa	P^T GPa	η_{TL} %
Shock loading				
Hayes, 1974	2.12	2.08	···	8.6
Al'tshuler *et al.*, 1967	1.9	···	···	8.0
Dremin *et al.*, 1965[b]	1.89	···	···	9.8
Static loading				
Darnel and McCollum, 1970	···	···	1.96	···
Samara and Chrisman, 1971	···	···	2.13	···

[a] p_x^{TL} is the observed stress associated with the transition; $\bar{p}^{TL}$ is the mean pressure computed from p_x^{TL} and a shear strength correction based on the HEL; P^T is the transition pressure measured in a hydrostatic environment; and η_{TL} is the observed volume compression to initiate the transition.

[b] The porosity of this pressed polycrystalline sample was 5%.

Hayes' measurements are compared to other shock and static loading measurements in Table VI. Excellent agreement exists between Hayes' and static measurements. Transition pressure values of Al'tshuler *et al.* (1967) and Dremin *et al.* (1965), obtained from wave profile measurements with the electromagnetic gauge, are somewhat lower than Hayes' values. An extension of Hayes' work for [110] orientations and for initial temperatures of 318 K is reported by Gupta and Duvall

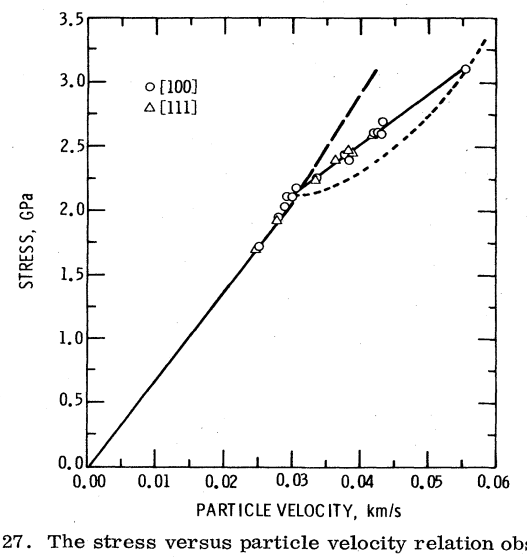

FIG. 27. The stress versus particle velocity relation observed in impact surface measurements on KCl by Hayes (1974) indicates a transition at a stress of 2.12 GPa. In the mixed phase region above the transition the compressibility is much smaller than indicated by the equilibrium thermodynamic calculations (dashed line). The calculated line that fits in the mixed phase region was characterized by a nonequilibrium high-pressure phase with an excess entropy of 3.9×10^2 m^2/s^{2}K.

(1975). From index of refraction measurements on shock-loaded KCl and KBr, Kormer *et al.* (1966) have inferred that the transitions are complete in 10^{-11} s.

Al'tshuler *et al.* observed a reverse transition under unloading at about 1.0 GPa lower pressure than the loading transition. Samara and Chrisman (1971) report for the case of static loading a hysterisis of 500 MPa between loading and unloading.

Pressure–particle velocity states at the impact surface in Hayes' experiments are shown in Fig. 27. Although the transition occurs at the correct pressure, a rapid transformation to a metastable state more energetic than the equilibrium state is indicated in the mixed phase region above the transition. Hayes computed the excess entropy of this state and suggested that it is associated with the nucleation of many small nuclei. Other sources of excess entropy may be production of point defects, large interfacial areas, and internal strains. Podurets and Trunin (1974) have considered effects of interfacial area associated with many small nuclei.

I. III-V and II-VI compounds–CdS, InSb, and BN

Cadmium sulfide and indium antimonide undergo transitions within their elastic compression ranges under shock loading; hence the relative contribution of shear stress is especially large. Boron nitride is of particular interest because shock loading has been found to cause an irreversible transition to a high-pressure phase. Furthermore, in a monumental achievement, x-ray diffraction measurements have been accomplished on the high-pressure phase of BN in the shocked state.

Jones and Graham (1971) summarize the data of Kennedy and Benedick (1966) on CdS and unpublished data of Kennedy and Benedick on InSb (1965). Both of these crystals apparently undergo phase transitions with large, about 20%, volume changes which are consistent with static observations of the wurtzite-to-rock salt structure for CdS (Kabalkina and Troitskaya, 1964) and the zinc blende-to-white tin structure (Hanneman *et al.*, 1964) or an orthorhombic structure for InSb (Kasper and Brandhorst, 1964). Kennedy and Benedick (1966) also reported large decreases in resistance in CdS shock-loaded above the transition in a manner consistent with that observed by Samara and Drickamer (1962) under static loading. (Static high-pressure work on these materials has been reviewed by Rooymans, 1969.)

Under shock loading both transitions are observed at mean pressures and volume compressions significantly less than static values. Hence, even though the volume change between high- and low-pressure phases is about the same as is determined statically, the shock transitions may be strongly influenced by shear. The possibility of a metastable state cannot be ignored.

Although high-pressure phases of shock-compressed solids are rarely recovered after the loading, dense boron nitride is apparently easy to recover since many different groups have recovered dense phases of BN, albeit with somewhat different results. Bundy and Wentorf (1963) reported a direct transformation of hexagonal BN to wurtzite under static loading at 13 GPa at temperatures around 300 K and a preference to form a cubic, zinc blende form at temperatures between 2500 and 4000 K. Frequently, both forms appeared together. Shock wave loading experiments have shown the presence of a transition between 12 and 12.8 GPa (Adadurov *et al.*, 1967; Al'tshuler *et al.*, 1967; Coleburn and Forbes, 1968), in agreement with static loading measurements. Kuleshova (1969) has reported a significant increase in resistance of shock-loaded BN at 13.5 GPa.

Batsanov *et al.* (1965) reported recovery of an unidentified dense form of BN after shock loading. Adadurov *et al.* (1967) recovered wurtzite crystallites after shock loading above 12 GPa. Dulin *et al.* (1969) reported recovery of both wurtzite and diamond structure crystallites with wurtzite predominating under shock loading from 12 to 50 GPa at initial temperatures between 120 and 800 K. Loading pressure did not appear to influence the yield of dense phases; however, increase in initial temperature and reduction of initial density reduced the yield. Coleburn and Forbes (1968) recovered micron-size cubic zinc blende crystallites with traces of wurtzite. Soma *et al.* (1975) have also reported recovering the wurtzite form of BN from shock loading. These observations indicate that although dense phases are always recovered for hexagonal BN shock-loaded above 12 GPa, the yield and structure of the dense phase apparently depends upon details of shock loading and characteristics of the starting material.

With their flash x-ray diffraction apparatus, Johnson and Mitchell (1972) obtained diffraction records for BN in the shocked state at 24.5 GPa, a pressure sufficiently large to produce a single shock in the high-pressure phase. Their records showed a diffraction line corresponding to the 100 line of the wurtzite phase, narrower and more intense than those obtained from recovered samples after shock loading. It was inferred from this that the crystal in its shocked state retains its crystalline form in large measure and that the micron-sized particles found in recovered samples are produced by extensive inelastic deformation and/or microfracturing that follows the initial shock. The single 100 line is not sufficient for complete identification of the high-pressure phase, but the determination that the transition produces large, uniformly oriented crystallites that attain significant sizes in times of a few tens of nanoseconds is a significant result. Ritter (1973) has discussed lattice deformation mechanisms consistent with the observations of Johnson and Mitchell (1972).

J. Quartz

Quartz is a material with properties much admired and widely utilized at atmospheric pressure. Under shock loading, its properties are complex, and for that reason quartz may be the most interesting of materials included in this review. Much of the interest stems from shock loading created in nature by the impact of meteorites on the earth, which creates dense polymorphs of quartz and other perplexing changes in the properties of quartz rocks. High-pressure polymorphs of quartz are possible candidates for earth mantle material and are consequently of considerable interest in geophysics (see the review by Ahrens *et al.*, 1969). Further interest in quartz under shock loading follows from the wide use of quartz gauges in shock loading research.

Crystalline quartz is also of interest because it exhibits the largest purely elastic strain of any solid yet investigated and, when the stress of the HEL is exceeded, quartz exhibits an apparent catastrophic and substantial loss of shear strength, unlike most solids. With these incentives for research, it is not surprising that shock loading investigations of quartz are of relatively long standing and continue to the present. This section considers shock loading investigations of quartz not because they are typical of work on other materials or are comparable to static pressure investigations, but because of the unique behavior of quartz, which in many respects has no counterpart in static high-pressure investigations.

In 1962, Neilson *et al.* described impressive luminosity and piezoelectric effects that indicated unusual mechanical properties in shock-loaded quartz. These observations led Wackerle (1962) to carry out an investigation of the stress–volume behavior of quartz under shock loading from 4 to 70 GPa. Wackerle's classic paper reported a thorough, comprehensive investigation of both fused quartz (vitreous silica) and crystalline quartz which exposed a number of unusual effects. Further investigation of these effects are the source of much of the subsequent work on quartz. Adadurov *et al.* (1962) published a less extensive investigation at the same time as Wackerle. Contemporary work by Fowles (1962) was published at a later date (Fowles, 1967).

Wackerle observed the following effects:

1. In crystalline quartz, HELs varied from 4.5 to 14.5 GPa and depended upon the crystallographic orientation and particulars of the experiment.
2. In crystalline quartz, a substantial reduction of shear strength is observed for stresses immediately above the HEL, unlike the behavior of most solids which are believed to maintain an approximately constant level of shear strength above the HEL.
3. An apparent phase change in crystalline quartz at 14.4 GPa.
4. A mixed phase region in crystalline quartz which extended from 14.4 to 38 GPa (the compressibility in this region was unusually small and the cusp in the R–H curve at 14.4 GPa did not lead to a multiple wave structure).
5. A well-defined high-pressure R–H curve that was common for both fused and crystalline quartz.
6. An anomalous low-stress compressibility for fused quartz (as expected from ultrasonic third-order elastic constant measurements and from earlier static measurements by Bridgman), finally changing to a compressibility that decreases with stress in the normal manner.
7. Recovery of amorphous quartz from crystalline quartz shock loaded to 50 GPa.
8. Recovery of compacted fused quartz from fused quartz shock loaded at 25 GPa, and normal fused quartz from samples loaded at 50 GPa.

Wackerle's stress–volume curve for crystalline quartz, shown in Fig. 28, demonstrates many of these unusual properties.

Discovery of the shock transition at 14.4 GPa and an approximate temperature of 475 K occurred almost simultaneously with the discovery of a dense polymorph of quartz with a density of about 4.28 Mg/m^3 and rutile structure by Stishov and Popova (1961). This dense phase, called stishovite in this country and stipovorite in the Soviet Union, was synthesized at a pressure of about 16 GPa and a temperature of 1473 K. Previously, Coes (1953) had synthesized a hexagonal dense phase of quartz, now known as coesite, at 3.5 GPa and 1023 K.

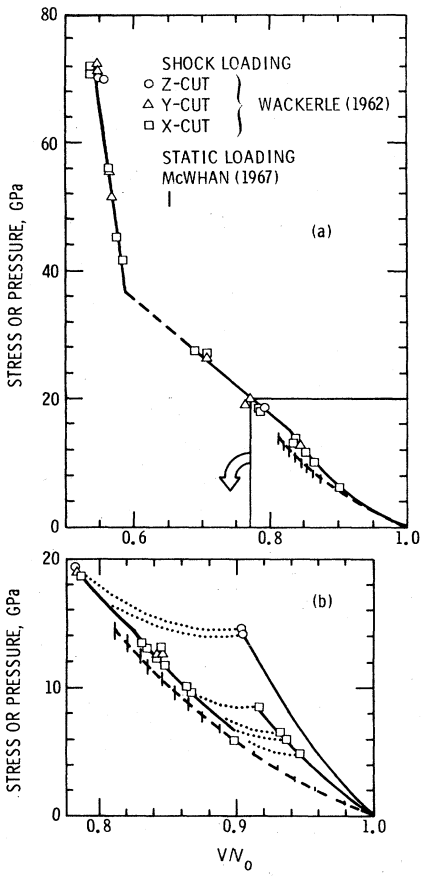

FIG. 28. The stress–volume relation for quartz determined by Wackerle (1962). The upper portion of the figure, a, emphasizes the data above the transition at 14.5 GPa. A mixed phase region extends from 14.5 to 39 GPa. Properties of the high-pressure phase, which has properties similar to stishovite, can be determined from the data above 39 GPa. The lower portion of the figure, b, emphasizes the elastic compressional properties of quartz with unusually large HEL values. For stresses above the HEL the material loses a substantial portion of its shear strength and approaches hydrostatic compressions. This loss of shear strength is apparently associated with heterogeneous melting described in Sec. VI.C.

Wackerle's investigation of the high-pressure phase was extended to 260 GPa by Al'tshuler *et al.* (1965). Ahrens and Rosenberg (1968) obtained loading and unloading data in the mixed phase region. High-pressure investigations by Trunin *et al.* (1971a) extended to 650 GPa, and Trunin *et al.* (1971b) studied porous samples with densities of 1.15, 1.35, 1.55, 1.75, and 2.2 Mg/m^3. Except for porous solids, in which temperatures are very high, the high-pressure phase above 38 GPa has properties close to those expected for stishovite. Trunin *et al.* (1971b) found differences in the R–H

curves in certain of their porous samples which were more nearly consistent with the properties of coesite.

An equation of state for stishovite was first constructed from Wackerle's data by McQueen *et al.* (1963). These authors felt that the high-pressure phase was probably a dense silica glass whose short-range order was stishovite. Other authors, Anderson and Kanamori (1968), Ahrens *et al.* (1969), and Ahrens *et al.* (1970), have constructed different equations of state for stishovite based on alternative formulations or on newer thermodynamic data. The various shock loading, static loading, and thermodynamic data on stishovite are summarized by Davies (1972), who constructed a new equation of state for both stishovite and the "coesite-like" phase observed by Trunin *et al.* (1971b). All equations of state rely heavily on the shock compression data; there are unresolved differences among the various treatments and the measured thermodynamic constants of stishovite.

High-pressure x-ray diffraction studies on stishovite and coesite by Bassett and Barnett (1970) showed a bulk modulus for stishovite which was in significant disagreement with that derived from the shock data, constrained to an initial density of 4.29 Mg/m^3. They suggested that the high-pressure shock-loaded material might be a mixture of small stishovite crystallites and a short-range order glass. Consideration of heterogeneous melting for quartz just above the HEL, discussed in Sec. VI.C, lends credence to this view and raises questions as to whether the high-pressure phase obtained under shock loading is a pure solid stishovite phase. Primak (1975) has expressed the opinion that the high-pressure phase is not stishovite, but is most likely a dense ordered array of oxygen atoms with disordered silicon atoms.

Finite transformation rates for the 14.4 GPa transition are indicated in the sample thickness dependence measurements of Al'tshuler *et al.* (1965) and the unusually small compressibility in the mixed phase region. Podurets and Trunin (1971) have given qualitative consideration to reaction rates to account for Wackerle's data in the mixed phase region. Podurets and Trunin (1974) have used the data in the mixed phase region to calculate nuclei sizes. Calculations of this sort are clouded by the heterogeneous melting upon yielding described in Sec. VI.C.

Attempts by DeCarli and Jamieson (1959) to recover dense quartz from shock-loaded single crystals were unsuccessful; however, they did recover amorphous quartz. DeCarli and Milton (1965) successfully recovered stishovite but no coesite from shock-loaded crystalline quartz. Deribas *et al.* (1968) have recovered both stishovite and quartz in shock-loaded porous quartz samples. Stishovite is apparently easier to recover than coesite under shock loading. It is noteworthy that the opposite is true of dense quartz recovered from meteorite craters. German *et al.* (1973) have recently reported recovery of a dense orthorhombic form of quartz from samples shock-loaded between 35 and 90 GPa.

Both coesite and stishovite have been recovered from meteorite craters. The discovery of naturally occurring coesite by Chao *et al.* (1960) and of naturally occurring stishovite by Chao *et al.* (1962) was in Meteor Crater, Arizona. A summary of coesite and stishovite recovered from meteorite craters is given by Stoffler (1971). Coesite has been found in seven craters, whereas stishovite is found in only two. Coesite is also found to be more abundant than stishovite. The broader area of changes in quartz rocks in meteorite craters is summarized by Chao (1967) and in a very comprehensive review by Stoffler (1972).

Wackerle's observation of compacted fused quartz recovered after shock loading to 25 GPa is similar to that observed by Roy and Cohen (1961), who observed permanent densification of fused quartz above hydrostatic pressures of 2 GPa. A comprehensive treatment of compaction phenomena in fused quartz is given by Primak (1975).

Evidence for a low-pressure transition in fused quartz is reported by Graham (1971), who determined second-, third-, and fourth-order longitudinal elastic constants from shock loading experiments of Barker and Hollenbach (1970). Above a compression of 6% the elastic constants were found to increase with stress in the normal manner. Similar behavior has been observed by Bridgman (1948). This is apparently a higher-order transition.

The $\alpha \rightarrow \beta$ quartz transition under shock loading has been investigated by Gauster *et al.* (1973), who used stress pulse measurements in crystalline quartz samples, pulse heated in 50 ns with a high-energy electron beam machine. Their observations between 250 MPa and 2 GPa at temperatures from 495 to 1635 K are consistent with the high-pressure phase measurements of Cohen and Klement (1967).

K. Hydrogen

The possibility of producing metallic hydrogen at very high pressures has long been a subject of interest and speculation. Wigner and Huntington (1935) appear to have been the first to suggest that such a transition might occur; they estimated the pressure of transition to be not less than 25 GPa. When 100 GPa pressures began to be achieved in shock waves, there was some hope that they might provide a means for direct observation of the metallic state. In order to achieve the required pressures in a shock wave, it is necessary to precompress the hydrogen to a substantial density. Even so, it turns out that the heating that accompanies shock compression is so great as to eliminate any possibility of producing the required transition. This difficulty has in turn led to consideration of implosion techniques for isentropic compression (Hawke, *et al.*, 1972; Hawke, 1977; Lubkin, 1976; Grigor'ev *et al.*, 1972). Shock compression experiments have helped to improve theoretical estimates of the transition pressure, but there still exists no definitive answer to the question of metallic transition. Shock experiments and their interpretation have been summarized by Ross (1974), Van Thiel *et al.* (1974), and Ross *et al.* (1975). In the meanwhile Vereshchagin *et al.* (1975) has reported observations of a conducting phase in hydrogen under static compression to about 100 GPa.

V. SECOND-ORDER PHASE TRANSITIONS

In contrast to first-order phase transitions, which are characterized by discontinuities in volume and entropy, second-order phase transitions involve phases for which volume and entropy are continuous, but higher derivatives of energy, specific heat, compressibility, and thermal expansion are discontinuous. The Ehrenfest relations, which interrelate the variables changing at the transition, are

$$\Delta\beta_T = \Delta\alpha(dT_C/dP),$$
$$\Delta C_p = TV\Delta\alpha(dT_C/dP)^{-1}, \tag{76}$$

where β_T is isothermal compressibility, α is volume thermal expansion coefficient, T_C is critical temperature, P is pressure, C_p is specific heat at constant pressure, T is temperature, V is specific volume, and Δ indicates the change at the critical temperature and pressure.

Based on Eqs. (76), the most apparent manifestation of a second-order phase transition in a shock-loaded solid will be a pronounced change in compressibility at the critical pressure and temperature. This change in compressibility should be apparent from stress–volume measurements that characterize the compressibility both below and above the transition. In situations where compressibility decreases, the transition should also be indicated with time-resolved detectors by a sudden decrease in rise time of a plastic wave above the critical pressure.

If the transition is to be significant enough to be detected, it is apparent from Eqs. (76) that the critical temperature must be sensitive to pressure. Such behavior is not common, but certain ferromagnetic alloys have Curie temperatures that are highly sensitive to pressure. Figure 29 shows measurements of the pressure derivative of the saturation magnetization of the iron–nickel alloy system. (The change in saturation magnetization with pressure is directly related to the change of Curie temperature with pressure. See Kouvel, 1963.) For compositions less than 28 at.% Ni, the alloys are stable in the bcc phase and are characterized by magnetizations that are insensitive to pressure. From the previous discussions of bcc iron alloys, it is apparent that these alloys would be expected to go through polymorphic phase transitions at pressures much less than the Curie point transition. On the other hand, alloys with Ni content greater than 28 at.% Ni are stable in the fcc phase and, in the vicinity of 28 at.% Ni, show unusually large sensitivity of magnetization to pressure. Accordingly, fcc Fe–Ni alloys with compositions in the vicinity of 28 at.% Ni are the most likely candidates to undergo pressure-induced, second-order phase transitions.

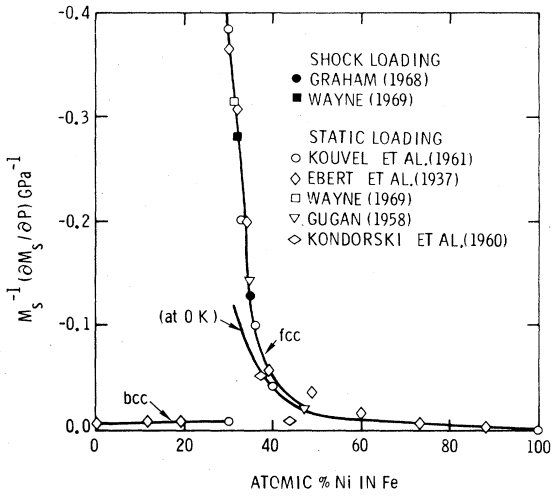

FIG. 29. The relative change in saturation magnetization with pressure is a strong function of composition for the iron–nickel alloy system. Alloys with nickel contents less than about 28 at.% are stable in the bcc phase and have magnetizations that are insensitive to pressure. Alloys with nickel contents greater than about 28 at.% are stable in the fcc phase, and for compositions between 28 and 40 at.% Ni the magnetizations are very sensitive to pressure. A similar effect is noted for the pressure dependence of the Curie temperature. Pressure sensitive magnetic properties lead to higher-order phase transitions, which have been observed under shock and static loading.

Curran (1961) considered the possibility of second-order phase transitions in iron and in Invar, a 36 wt.% Ni–Fe alloy. His analysis was directed toward the possibility that a multiple shock wave structure would be produced by the transition. His experiments on Invar under explosive loading did not show a multiple wave structure; however, the stress–volume curve showed a gradual decrease in compressibility as the stress was increased. The experiments did not positively identify a second-order phase transition.

Graham *et al.* (1967) reported an investigation of the stress–volume relation of a 28.4 at.% Ni–Fe alloy under impact loading. This alloy was chosen for study because the Curie temperature is highly sensitive to pressure and the expected transition at 2.5 GPa is well within the stress range for which the quartz gauge can provide accurate, time-resolved wave profile measurements. Furthermore, with projectile impact loading, data could be obtained in the immediate vicinity of the transition.

The stress–volume curve obtained by Graham *et al.* is shown in Fig. 30. A pronounced decrease in compressibility is observed at 2.5 GPa. Furthermore, the decrease in compressibility is manifested by a dramatic decrease in rise time of the plastic wave for input stresses just above 2.5 GPa. After a correction for shear strength at the HEL, the computed value for dT_C/dP from the shock loading investigation is in excellent agreement with static compression measurements. Thus, this study provides quantitative identification of the pressure-induced, second-order, ferromagnetic-to-paramagnetic transition in this fcc iron alloy and provides thermodynamic data on the change in variables at the transition. Given these data on 28.4 at.% Ni, it is apparent that the behavior of Invar observed by Curran was a consequence of a similar ferromagnetic-to-paramagnetic transition. For some unknown reason, the change in compressibility in that alloy is more gradual.

To further investigate the behavior of Invar, Graham (1968) measured the magnetization change under impact loading from 3 to 20 GPa. The measured coefficient is

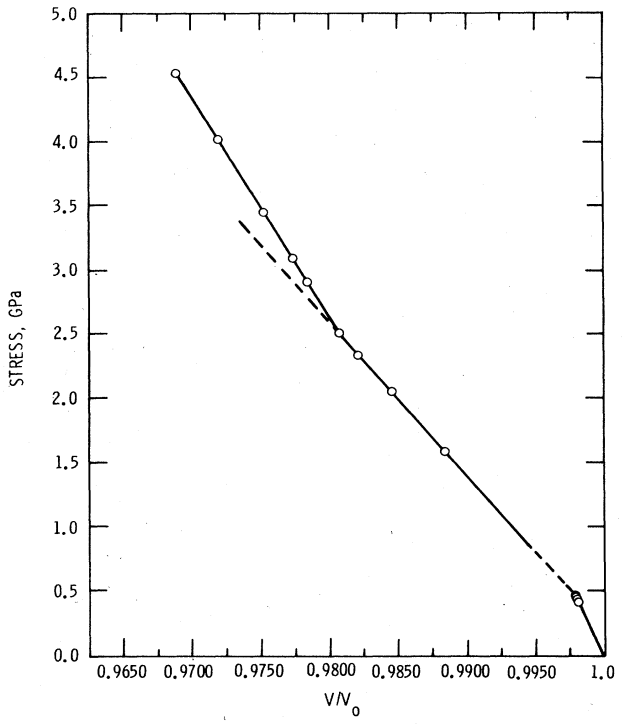

FIG. 30. The stress versus volume relation for a low carbon 28.4 at.% Ni–Fe alloy in the fcc phase shows a second-order phase transition indicated by a large decrease in compressibility at stress of 2.50 GPa. The dashed line indicates an extension of the compressibility of the lower stress data. When a correction for shear strength is applied to the shock data to account for the 0.45 GPa Hugoniot elastic limit, excellent agreement is noted between shock and static loading determinations of the dependence of Curie temperature on pressure. After Graham *et al.* (1967).

shown in Fig. 29 along with the other static pressure measurements. The measured shock loading coefficient is found to be in excellent agreement with static pressure measurements. Wayne (1969) performed static and shock loading measurements of the change in magnetization with pressure or stress in a 31.4 at.% alloy and found reasonable agreement between the two measurements. His data are also shown in Fig. 29.

Theories of the pressure dependence of Curie temperature and static pressure experiments have been extended to ternary iron alloys by Edwards and Bartel (1974). Edwards (1976) has performed shock loading experiments similar to those above on the change in magnetization on several cobalt substituted alloys, $Fe_{0.65}(Ni_{1-x}Co_x)_{0.35}$ with $x = 0.06$ and 0.08, and finds good agreement between static and shock loading results.

Results of this work indicate that static and shock loading measurements of changes in Curie temperature and magnetization with pressure are comparable insofar as their effect on magnetization is concerned. It appears that theory and static pressure experiments provide a basis for quantitative prediction of details of second-order ferromagnetic-to-paramagnetic transitions in ferromagnetic solids under shock loading. The shock loading experiments may in turn be used to provide additional information on changes in compressibility accompanying these transitions.

VI. SHOCK-INDUCED MELTING AND FREEZING

Melting is a first-order transition for which $\Delta V = V_{liq} - V_{solid}$ is normally positive, ΔS is normally positive, and therefore $dP/dT > 0$. Transitions are known for which $\Delta V < 0$ and $dP/dT < 0$. Melting of bismuth is an example of this type which is discussed in the latter part of this section.

A hypothetical P–V–T surface for a normal liquid and solid is shown in Fig. 31. Solid and liquid surfaces are labeled and the mixed phase region is the cylindrical surface $NMPR$. The dotted line QW is the projection of this surface on the P–T plane. FGH is an isotherm originating in the liquid, passing into the mixed phase region and then into the solid. Two cases can be distinguished which depend upon the magnitude of dP/dT:

1. A pressure–volume R–H curve, starting at a point, say A, in the solid, intersects the phase boundary MR at B. It may then proceed through it into the liquid, as shown by the curve $ABCD$, stay within the mixed phase region, or return to the solid. The essential point is that it intersects the boundary.
2. The R–H curve may stay within the solid, in which case no shock-induced melting is possible.

In the second case it may be possible to freeze the liquid by initiating a shock in the liquid phase. Such a case is discussed at the end of this section.

If $dP/dT < 0$, $\Delta V_1 > 0$, $\Delta S < 0$, which seems unlikely, the R–H curve originating in the solid will always intersect the phase boundary. A detailed discussion of the geometry of melting thermodynamics as it relates to shock waves is given by Horie (1967).

The possibility of shock-induced melting has often been questioned because of the short times involved. If

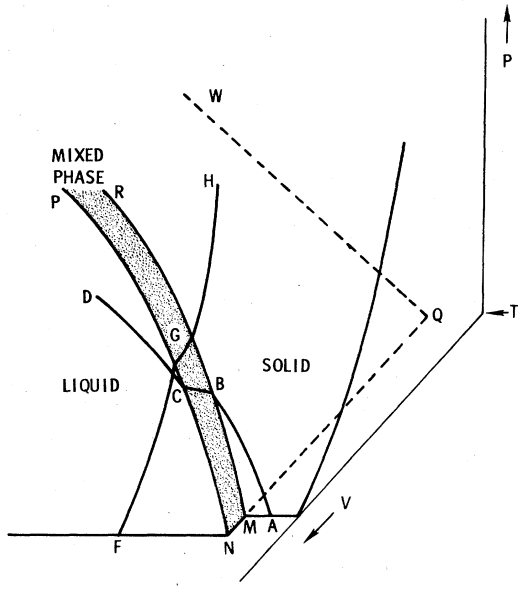

FIG. 31. P–V–T surface for a normal liquid and solid. The mixed phase region is bounded by $RPNM$.

melting did not occur in the time available in a shock experiment, the R–H curve, AB of Fig. 31, would continue on the metastable surface of the solid lying behind the liquid surface and, on release of pressure, would once again return to the stability field of the solid state unless irreversible shock heating were great enough to produce a terminal liquid state at zero pressure. No significant attempt has been made to answer this question theoretically, and there have been persistent efforts to determine melting in shock experiments. The first of these was by Duff and Minshall (1957), who failed to find evidence of melting when shock pressure extended into the liquid region.

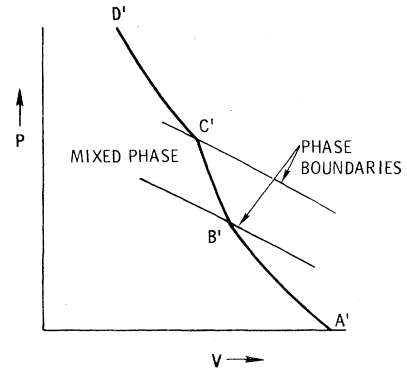

FIG. 32. Projection of phase boundaries and R–H curves of Fig. 31 onto the pressure–volume plane.

A. Homogeneous melting of normal materials

In a report of shock measurements at pressures up to 200 GPa, McQueen and Marsh (1960) expressed the opinion that materials, such as lead and thallium, with low melting points had probably melted in some of their experiments. This belief was based on the observation that thermodynamic paths of the shocked material intersected the melt region in such cases. In such cases, also, it was sometimes observed that the $U_s - U_p$ graph showed a discontinuity in slope at the calculated melting point.

That such a slope discontinuity might result from melting is readily seen from Eq. (33). At point B of the R–H curve of Fig. 31, its slope changes discontinuously. This is shown more clearly in Fig. 32, where phase boundaries and the R–H curve starting at A are projected onto the P–V plane. The points labeled $A'B'C'D'$ are projections of $ABCD$ in Fig. 31. Since dP/dV changes discontinuously at B' and C', R of Eq. (33) also changes discontinuously, producing a discontinuity in dU_s/dU_p. Whether the total change is large enough to be detected in a $U_s - U_p$ plot cannot be determined in advance.

The most extensive investigation of this possibility has been reported by Carter (1973a), who has constructed complete equations of state for a number of materials, mapped the P–T phase planes, which sometimes include several polymorphic transformations, and shown that the calculated melting curves for Pb, Gd, Eu, Er, and Ce intersect R–H curves close to the point at which a break in the $U_s - U_p$ curves occur. His results are listed in Table VII. Although there is a substantial amount of speculation in this work, it is hard to label the results coincidental, and it must be taken as substantive evidence that equilibrium melting can occur in the short time available in shock experiments.

Kormer *et al.* (1965a), in experiments with KCl and KBr, reported discontinuities in dU_s/dU_p as indicating melting. Hauver and Melani (1964) found breaks in $U_s - U_p$ slope for Plexiglas and polystyrene which may be related to melting. Abrupt changes in the character of polarization signals were also found in the pressure ranges of transition. McQueen *et al.* (1971) have reported solid–liquid phase line calculations in Cu and experiments in porous Cu in which melting is thought to occur.

TABLE VII. Table of melting pressures in shock waves.

Material	P^T, GPa	T(est.)	Method	References
Sulfur[b]	6–10		Resistance change, break in U_s–U_p curve	Berger *et al.* (1960, 1962)
KCl	33–48[a]		Radiation temperature	Kormer *et al.* (1965b)
KBr			Break in U_s–U_p curve	Kormer *et al.* (1965a)
KCl			Break in U_s–U_p curve	Kormer *et al.* (1965a)
NaCl	54–70[a]		Radiation temperature, break in U_s–U_p curve	Kormer *et al.* (1965b, 1965a)
Pb	~22		Crater shape	Belyakov *et al.* (1965)
	23–25		Impact ejecta, spall, $\Delta t = 3 \times 10^{-7}$ s	Belyakov *et al.* (1967)
	41–124		Viscosity measurement	Mineev and Savinov (1967)
	28	1210 K	$\Delta V > 0$, break in U_s–U_p curve	Carter (1973a)
Cd	~31		Crater shape	Belyakov *et al.* (1965)
Zn	~44		Crater shape	Belyakov *et al.* (1965)
Sn	~28		Crater shape	Belyakov *et al.* (1965)
Plexiglas	28		Break in U_s–U_p curve	Hauver (1966b)
Al	105–202		Break in U_s–U_p curve	Mineev and Savinov (1967)
Gd	70	3500 K	$\Delta V > 0$, break in U_s–U_p curve	Carter (1973a)
Eu	11	950 K	< 0, break in U_s–U_p curve	Carter (1973a)
Erb	44	2070 K	~ 0, break in U_s–U_p curve	Carter (1973a)
Cerium	43	3600 K	> 0	Carter (1973a)
Fe	>184			Hord (1975)

[a] Melting region extends from first to second temperature.
[b] David and Hamman (1958) suggested that this pressure is transformation to a metallic solid.

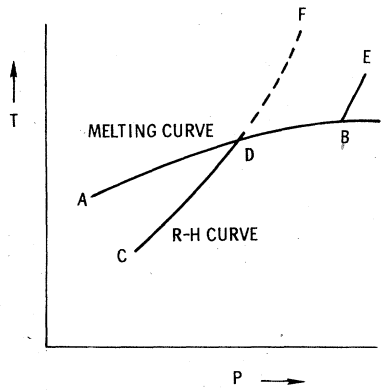

FIG. 33. Temperature–pressure phase diagram and R–H curve.

More direct evidence of melting in shock was sought by Kormer *et al.* (1965b). They constructed melting curves for NaCl and KCl based on a Simon equation and R–H curves from shock data and theoretical equations of state, Fig. 33. For no melting, the calculated R–H curve is *CDF*. For equilibrium melting, the R–H curve is *CDBE*. Temperature was inferred from radiation measurements and was found to follow the equilibrium curve, not the metastable one. They inferred from this that melting occurred under equilibrium conditions. Other workers, e.g., Urtiew and Grover (1971, 1974) and Grover and Urtiew (1974), have encountered serious difficulties in attempting to measure temperature from radiation, so some caution must be exercised in accepting these conclusions as irrefutable.

The discontinuity in dU_s/dU_p reported by Kormer *et al.* (1965a) occurred at a pressure corresponding to point *D* in Fig. 33. No break in slope was found in NaCl. Some further confirmation was provided by Mineev and Savinov (1967), who measured viscosity of Al, Pb, and NaCl as a function of shock pressure by a shock perturbation method. They found that beyond a certain pressure for each material the viscosity decreased quite rapidly. By assuming this to be due to melting, they obtained estimates of the melting pressure. Their values for NaCl fell within the range determined by Kormer *et al.* (1965b).

Belyakov *et al.* (1965, 1967) inferred the existence of shock-induced melting from mechanical effects. While measuring craters produced in lead by flat aluminum disks striking a thick target, they observed that above a critical impact speed the crater changed from a hemispherical to a conical cavity. Assuming this to result from melting, they used the critical impact speed in the shock equations and calculated a melting pressure of approximately 22 GPa. Similar experiments in tin, cadmium, and zinc gave the pressures in Table VII.

In later experiments they used flash x rays of copper cylinders striking lead sheet. The x rays showed the character of the ejecta from the rear of the sheet to change discontinuously at impact speed corresponding to shock pressure of 23 to 25 GPa. A similar experiment with thin foils enabled them to estimate the characteristic melting time. In Fig. 34 *OACE* is an equilibrium R–H curve entering the mixed liquid–solid phase region at *A* and leaving it at *C*. *AB* is the metastable extension of the solid phase Hugoniot. If the shock carries the material to a point *B* in the metastable solid phase, and if the pressure is maintained long enough, the state point of the material will eventually relax back to an equilibrium state, say *D*. If the total shock profile is unchanging in time (which is not possible, but may not be a bad approximation), it will relax along the Rayleigh line, *OBD*, as shown. The resulting shock wave profile will have the general character shown in Fig. 34(b): the pressure will drop from P_B to P_D in a distance Δx or time $\Delta x/U_s$. This time is a measure of the time required to melt under shock conditions. By measuring velocities given to a set of foils by the shock of Fig. 34(b), it is possible to infer the slope of the shock profile (O'Brien and Davis, 1961). Belyakov *et al.* (1967) did this using lead foils and flash x-ray to measure foil motion. They found $\Delta t \simeq 3\times10^{-7}$ s. Many details of their experiment are not given, but it is an interesting experiment and result, to be compared with theory or other experiments in the future.

It is possible to measure sonic velocity in the shocked state. A shock or rarefaction can be made to follow the primary shock in a flyer plate experiment by making the plate thin and backing it with a material of higher or lower impedance. Reflection from this rear surface sends the required wave into previously shocked material (see, for example, Barker and Hollenbach, 1974). If shocked material is in an elastic–plastic state, a second shock should travel at bulk wave velocity $(\sqrt{k/\rho})$, whereas a rarefaction should have elastic wave speed $\sqrt{(k+\frac{4}{3}\mu)/\rho}$. An alternative is to produce a disturbance in the shock wave which spreads laterally across the shock front. By measuring its progress in a known time, lateral rarefaction velocity can be determined (Al'tshuler *et al.*, 1960). Comparison of measured values with predictions from equations of state provides a clue to the state of shocked material. If rarefaction velocities appear to be bulk rather than elastic, the liquid state is suggested. Hord (1975) has measured lateral rarefaction velocities in shock-loaded iron at 180 GPa. He concludes that it has not melted at this pressure.

Asay and Hayes (1975) measured velocity of an overtaking rarefaction in initially porous aluminum for shock pressures between 0.6 and 11 GPa. The temperature

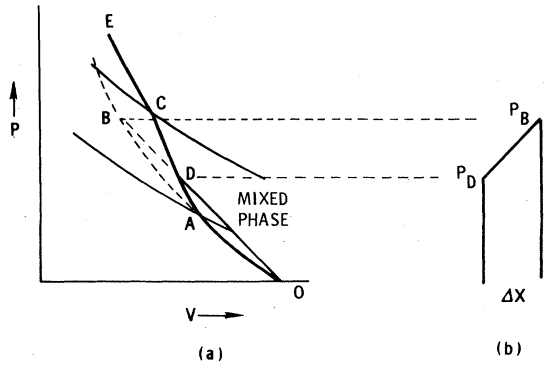

FIG. 34. (a) R–H curves in the mixed phase region. (b) Wave profile from metastable melting.

produced in a shock wave of given pressure is increased in an initially porous material, relative to the solid, so that melting may be expected at a lower pressure. In Asay's experiments, melting was estimated from equation of state calculations to occur at 7.5 GPa. A discontinuity in rarefaction velocity was found at 7.0 GPa, and this was taken as evidence of the onset of melting. The work of Grady *et al.* (1975) suggests that the change would have been observed even if partial melting occurred. This might result from inhomogeneity of temperature distribution in the porous material.

B. Bismuth

The phase diagram of bismuth (Fig. 26) has been mapped out in static measurements and some aspects of it are controversial. Nevertheless, the Bi I–II and I–liquid boundaries are well established. A shock wave with initial temperature $T_0 \gtrsim 435$ K crosses the boundary between solid and liquid. Since $V_{\text{liq}} - V_{\text{solid}} < 0$ along this boundary, such a shock wave should be double, like those produced by polymorphic transitions. If such a wave is observed, melting is inferred; otherwise not. Duff and Minshall (1957) did one such experiment on polycrystalline bismuth, using pins to detect free surface motion, observed no double wave at the melting line, and inferred that no melting had occurred. They did find a second shock wave at higher pressures which they assumed to arise from crossing the metastable phase I–phase II boundary.

In a series of three papers, Johnson *et al.* (1974), Asay (1974), and Hayes (1975) have given a detailed analysis of the wave structure to be expected for various initial temperatures and final pressures and have compared these with a careful set of experiments. Expectations can be summarized most easily with reference to Figs. 35 and 36 taken from Johnson *et al.* (1974). These are scale drawings of the P–V–T surface in bismuth showing phases I, II, and liquid. Figure 35 is the equilibrium surface; Fig. 36 is frozen, i.e., it is drawn assuming that melting cannot occur. In Fig. 35 are drawn two R–H curves $oabcdp$ and $\hat{o}\hat{c}\hat{d}\hat{p}\hat{e}$. The lower

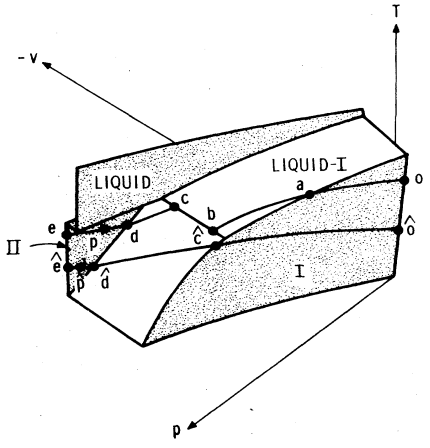

FIG. 35. Equilibrium P–V–T surface in bismuth. After Johnson *et al.* (1974). Two R–H curves for initial temperatures of 400 and 493 K are shown.

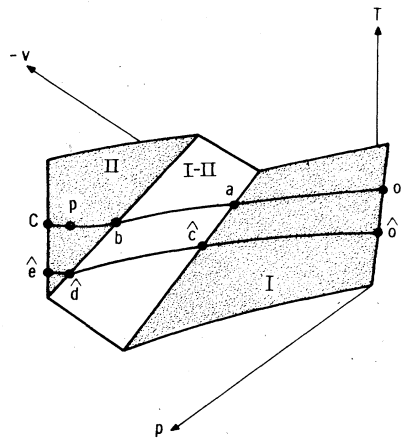

FIG. 36. Metastable P–V–T surface in Bi I→Bi II bismuth in the absence of melting. After Johnson *et al.* (1974). Two R–H curves for initial temperature of 400 and 493 K are shown.

one is for an initial temperature of 400 K. Compression from zero pressure at $\hat{o}$ to $\hat{p}$ in phase II would occur in two shocks: the first from $\hat{o}$ to $\hat{c}$, the second from $\hat{c}$ to $\hat{p}$. The upper R–H curve is for an initial temperature of 493 K. Compression to p in phase II would be via a shock from o to a, a compression fan from a to b, since the R–H curve is convex upward there (Duvall, 1962), and a final shock from b to p. The line segment between I–II and the liquid–I region represents the triple point. If melting were not to occur, Fig. 36 applies, and for both initial temperatures a double shock occurs. These two compression processes are illustrated in the wave profile calculations shown in Fig. 37 for a final compression of about 2.1 GPa. The experimentally observed wave profile is shown in Fig. 37 by the dotted curve, which fits neither calculated curve. The experimental record terminated before the final pressure was reached. It was inferred from the leveling off of the

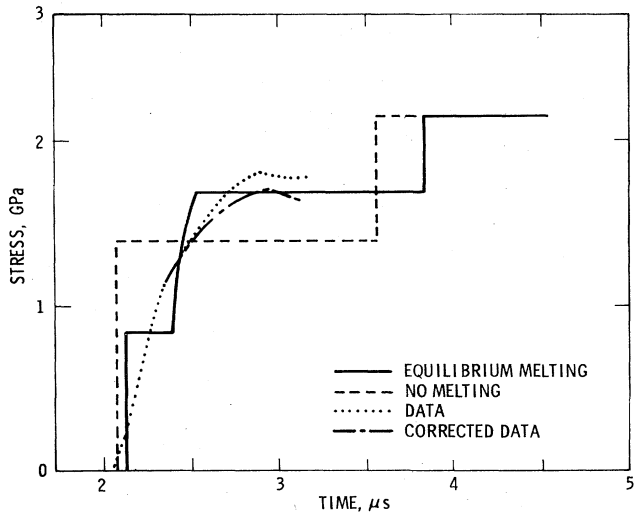

FIG. 37. Calculated and experimentally observed wave profiles for bismuth shock loaded at 2.1 GPa, at an initial temperature of 493 K. After Johnson *et al.* (1974).

stress record at the triple point, about 1.7 GPa, that melting had indeed occurred.

Asay (1974) undertook a more extensive experimental program in which both initial temperature and final pressure were varied, the former to 523 K, which is only 21 K below the melting temperature. His measurements confirmed the Johnson *et al.* (1974) results. Moreover, since the transition (triple point) pressure did not vary with propagation distance between two and six millimeters, he inferred that the rate dependence of melting may be small within the range of his experiments, i.e., the characteristic time for melting is appreciably less than about 10^{-6} s.

Hayes (1975) modified the constitutive relation given by Johnson *et al.* to include a Maxwell-like relation for melting. This was incorporated in one-dimensional wave propagation calculations, and the Asay experiments were simulated for various values of the melting time. His results show that experimental profiles can be reproduced reasonably well for an inverse transformation rate of 2.5×10^{-8} s, which is in accord with Asay's observation that amplitude of the melting shock is independent of propagation distance beyond 2 mm. [Asay (1977) has recently reported additional evidence for melting in bismuth.]

The case thus made for shock-induced melting in bismuth is very strong. The results show that sound and useful work in this field is possible if theory, experiments, and computations are carefully done.

C. Heterogeneous melting

The case for heterogeneous melting upon yielding in shock-loaded quartz has recently been made in three papers which appeared almost simultaneously. Graham (1974) studied the compressibility of x-cut quartz above the HEL and noted a substantial reduction in shear strength and poor agreement with pressure derivatives of bulk modulus determined in other static experiments. Anan'in *et al.* (1974) recovered crystalline quartz samples shock-loaded just above the HEL and found "blocks" of α-quartz surrounded by layers of quartz glass. Grady *et al.* (1975) measured unloading velocities in the mixed phase region of polycrystalline quartz rocks and found a loss of shear strength indicated by bulk wave speeds. The independent interpretation of all three authors associated the loss of shear strength upon yielding with formation of localized regions of planar features in which high temperatures would be expected due to the dissipation of large amounts of energy stored as shear strain. This behavior comes about in material of low thermal conductivity whose shear strength approaches the theoretical strength of the lattice. The large shear strength and apparent loss of shear strength had been observed in quartz by Wackerle (1962) and Fowles (1962, 1967). The latest interpretations associating the loss of shear strength with heterogeneous melting were guided to a large extent by studies of quartz rocks in meteorite craters which show shock-induced planar features and formation of glass [see Chao, (1967) and Stoffler (1972)]. The geophysical literature apparently failed to make the connection between localized planar features of glass and the substantial reduction of shear strength upon yielding.

Grady *et al.* (1975) calculated temperature profiles for heterogeneous melting and pointed out that such inhomogeneities in temperature would be expected to lead to complex conditions far from equilibrium which could lead to melting and formation of dense polymorphs of quartz all within distances of a few microns. The calculations of Walsh (1969) show that the liquid inclusions lead to bulk behavior in solids as indicated by the shock compression data. The combined data on a loss or substantial reduction of shear strength (Wackerle, 1962; Fowles, 1967; Graham, 1974), poor agreement with other measurements on pressure derivatives of bulk modulus (Graham, 1974), recovery of planar quartz glass regions just above the HEL (Anan'in *et al.*, 1974), calculations showing high local temperatures (Grady *et al.*, 1975), and calculations of the effect of liquid inclusions in solids (Walsh, 1969) make a strong case for heterogeneous melting in quartz upon yielding.

Similar reductions of shear strength upon yielding have been observed in crystalline Al_2O_3 (Graham and Brooks, 1971), and behavior such as this is anticipated in quartz and other oxide rocks and minerals. The observations of heterogeneous melting are cause for serious concern that interpretation of data on high-pressure dense phases of rocks and minerals obtained under shock loading may be significantly in error since they are based on assumptions of homogeneous response in thermodynamic equilibrium. Grady (1977) has recently extended the heterogeneous melting model to predict characteristics of transitions in silicates.

D. Freezing

Bridgman noted that pressure-induced freezing occurred in most of the liquids he compressed statically. Speculations about the possibility of shock-induced freezing were natural consequences of this experience. Schardin (1941) fired bullets into CCl_4 and water at speeds varying from 800 to 1800 m/s and photographed them. He found the region surrounding the bullet to be opaque in CCl_4 at 1200 m/s and in water at 1800 m/s, whereas water was transparent at 800 m/s. Snay and Rosenbaum (1952) assembled thermodynamic data on water and calculated R–H curves. For initial conditions at room temperature and atmospheric pressure their R–H curve passed into the mixed phase region between liquid and ice VII at about 2.7 GPa and back into the liquid phase at about 10 GPa. The maximum solid content occurred at about 5 GPa with $\Delta V/V_0 \simeq 0.025$. In a refinement of this calculation using new shock data, Rice and Walsh (1957) found essentially the same result, except that the excursion into the mixed phase region was limited to 3 to 4.5 GPa.

Walsh and Rice (1957) did the first carefully controlled experiments to detect freezing. They used a framing camera to photograph light reflected from a metal plate used to drive a plane shock into the liquid under study. The plate was provided with a contrasting grid and reductions in transparency were equated to freezing. The duration of their experiments was about 20 μsec. They looked at benzene, CCl_4, water, and ethanol with the results shown in Table VIII. Only CCl_4 showed evidence

TABLE VIII. Freezing experiments in liquids.

Material	Pressure range, GPa	Phase transitions Press., GPa	Temp.	Comment	References
Benzene	8–11	···	···	Transparent	Walsh *et al.* (1957)
Benzene	0.48–0.78	···	···	R–H measurement	Cook *et al.* (1963)
Benzene	1.9–43$\Delta V = 17\%$	13.3–19.4	2300 K	Discont. in U_s–U_p; probably not freezing	Dick (1970)
Ethanol	7–10	···	···	Transparent	Walsh *et al.* (1957)
CCl_4	1–17	7–13	···	Increasing opacity with p	Walsh *et al.* (1957)
CCl_4	1.2–12.9	···	···	R–H measurement	Cook *et al.* (1963)
CCl_4	0–1.6	···	···	R–H measurement	Lysne (1971)
CCl_4	8–20	···	···	Brightness measurement	Voskoboinikov *et al.* (1968)
CCl_4	2.7–63.3	16.5	~2500 K	Probably not freezing	Dick (1970)
H_2O	3–10	···	···	Transparent	Walsh *et al.* (1957)
H_2O		11.5	···	Discontinuity in U_s–U_p	Al'tshuler *et al.* (1958)
H_2O	4–30	···	···	Transparent	Zeldovich *et al.* (1961)
H_2O	1.8–11	Double shock		Freezing occurred, see text	Kormer *et al.* (1968)
CS_2	0.4–6.2$\Delta V = 16\%$	···	···	R–H measurement	Cook *et al.* (1963)
CS_2	2.3–52.6	6.2–8.0	···	Discontinuity in U_s–U_p	Dick (1970)
Methanol	9.6–10.7	···	···	R–H measurement	Cook *et al.* (1963)
Liq. N_2	1.9–39.1	13.5	3400 K	Slight discontinuity in U_s–U_p; probably not freezing	Dick (1970)

of transition.

Al'tshuler *et al.* (1958) reported detailed shock measurements in water, including a phase transition at 11.5 GPa. The shock data had a slope discontinuity in the $U_s - U_p$ plane, and there was a change in reflectivity in accompanying optical experiments. Zeldovich *et al.* (1961) explored the region from 4 to 30 GPa using optical transparency measurements and did not find evidence of freezing of water. Kormer *et al.* (1968) reported still more experiments on water. They confirmed the reliability of the Rice and Walsh (1957) equation of state and did reflectivity, index of refraction, and opacity experiments in a system designed to send a double shock into water. They found that if the amplitude of the first shock was between 2 and 3.5 GPa and the second between 4 and 10 GPa, reflection turned to intense diffuse scattering after the second shock entered the water. They interpreted this as formation of ice VII and inferred a time to freeze of the order of 10^{-7} to 10^{-6} s. It seems likely at this time that the Al'tshuler *et al.* (1958) observation was an artifact of their experiment, and that the equation of state of Rice and Walsh (1957) represents a good approximation to the equation of state of water in shock and static loading, provided the requisite time for transformation is available. An interesting sidelight of this is a comment by A. H. Jones (1975) that shock experiments in some water-saturated porous rocks are compatible with the formation of ice VII. In such cases the compression path of the water is apt to be one of multiple shocks, and the results of Kormer *et al.* (1968) accordingly apply.

Following Walsh and Rice's observation that shocked regions in CCl_4 became opaque above about 13.0 GPa, Doran and Ahrens (1963) and Dick (1964) both reported that its electrical conductivity increased rapidly with shock pressure above 12 GPa. Dick (1970), who made shock measurements from 2.7 to 63.3 GPa, also reported a slight bend in the $U_s - U_p$ curve for CCl_4 at 16.5 GPa, corresponding to a weak cusp in the R–H curve. Brightness temperature measurements made by Voskoboinikov and Bogomolov (1968) gave temperatures ranging from 1400 to 2900 K for shocks between 8 and 20 GPa in CCl_4. These were somewhat lower than Dick's calculated temperatures, but of comparable magnitude. Equilibrium calculations show that the R–H curve for CCl_4 from room temperature crosses into the mixed phase region of the solid at about 1 GPa and may reenter the liquid phase at about 16 GPa (Dick, 1970). Lysne (1971) reported shock measurements made below 1.6 GPa at initial temperatures of 254, 264, and 297 K in an attempt to identify this low-pressure phase boundary. There was no positive evidence of freezing in this pressure region, though he notes that calculated temperatures on his R–H curve centered at room temperature are about 40 C greater than those on R–H curves extrapolated from earlier work to low pressures. He suggests that this difference might result from partial freezing, but concludes that none of the experiments on CCl_4 give positive evidence of total freezing or the lack of it. This seems a fair statement. It is unlikely that the 16.5 GPa break noted by Dick is freezing. He suggests, following C. Mader, that it might be due to a chemical reaction

$$2CCl_4 \rightarrow C_2Cl_6 + 2C_2 ,$$

but again there is no positive evidence that this is the case.

Several other liquid measurements are listed in Table VIII, only some of which show evidences of phase change. Dick (1970) notes that the $U_s - U_p$ slope discontinuity in benzene is compatible with similar observations by Warnes (1968) on anthracene, 18 GPa, phenanthrene, 20 GPa, pyrene, 24 GPa. All are hydrocarbons and the pressure of the discontinuity increases with molecular complexity. He suggests that the effect may be due to polymerization.

Dick (1970) also notes that A. Kusobov of Lawrence

Livermore Laboratory has recovered "black fluffy material" from shocked samples of CS_2 and suggests that the 6.2 GPa transformation may be the transformation to a black amorphous solid which occurs statically at about 4 GPa and 390 to 475 K.

The case for freezing in shock is not a strong one, and it is hard to invent any dramatic experiment which will resolve the question, even in principle. It seems more likely that confirmation will come through careful and thorough work with the phase diagrams, as has been done for melting in bismuth. In fact, Asay (1977) has recently reported evidence for refreezing in shock-loaded bismuth based on time-resolved measurements of unloading waves.

VIII. DISCUSSION AND CONCLUSIONS

The experimental observations summarized in previous sections of this review and in Table AI of the Appendix provide quantitative data with which the assumptions underlying theoretical treatments and interpretation of the data can be tested. Although it would be a mistake to generalize, it is possible to come to reasonably specific conclusions regarding interpretation of the shock loading data and directions for future work. Comments concerning specific materials also seem in order.

Perhaps the most important question regarding data obtained describing shock-induced phase transitions is whether they are credible. Do measurements under shock loading lead to determinations of thermodynamic properties of transitions which are as valid as measurements taken under static high-pressure loading? Do the transformations run to completion in the 10^{-6} s or less characteristic of the shock loading experiment? Do experiments under shock loading provide results which are representative of thermodynamic equilibrium?

It is certainly easy to understand how a scientist who has investigated phase transitions under static loading and watched the many minutes sometimes required to complete a transition would be incredulous concerning reports of the same transition running to completion in the eight or nine orders of magnitude shorter time characteristic of shock loading experiments. Nevertheless, the shock loading data speak for themselves and, when the fundamental differences between static and shock loading are considered, radically different reaction rates seem quite credible.

The data indicate that excellent agreement is achieved between the transition pressures established under shock and static loadings for the Bi I→ Bi II transition, the Bi I→ Bi II→ liquid triple point, the KCl transition, the martensite to austenite transition in 28.4 at.% Ni–Fe, and the $\alpha \rightarrow \epsilon$ transitions in Fe–Mn alloys. The comparison is clouded in iron by the different transition pressures obtained by resistance and x-ray diffraction measurements under static loading; the transition pressure determined from shock loading lies between the two. There is good agreement on the germanium transition and excellent agreement on the $\epsilon \rightarrow \alpha$ transition in iron on unloading. Other measurements under shock loading appear credible, but there are insufficient data on which to make a hard comparison between static and shock loading experiments. Notable exceptions to the generally good agreement are the CdS, InSb, and Si transitions under shock loading which do not appear to have counterparts in static experiments. Nevertheless, these differences can in part be anticipated from static observations of sensitivity to shear. Taken as a whole the data indicate that in spite of complications of shear strength, plastic flow, and limited experimental durations, shock loading experiments can provide accurate measurements of transition pressures and transition volumes. This is not to say that all shock loading measurements are equally credible, but the record demonstrates that comprehensive, careful investigations with carefully studied instrumentation and carefully controlled loading will provide credible determinations of thermodynamic characteristics of transitions.

Transformation rates for shock transitions are a matter of prime concern. The various measurements of initial transformation rates under shock loading show that the rates are fast enough to allow the transitions to go to completion in the normal shock experiment, except possibly for antimony. Measurements of the Plastic II wave show that the transformation is indeed completed when driving pressure is great enough. Unfortunately, there are inconsistencies and there is at present no physical basis on which to quantitatively predict reaction rates. Why is it, for example, that the transformation rate for antimony is relatively slow, while the transformation rate for bismuth is fast? In order to develop quantitative physical models for transformation rates, research on nucleation and growth of new phases in shock-loaded solids is of prime importance. If the theory is coordinated with experiments with time-resolved wave profile measurements, it is likely that good progress can be made.

Because of fundamental differences there is little reason to expect similar transformation rates under static and shock loading. Under static loading, rates are dominated by the statistical probability of forming nuclei in a low-defect solid under uniform compression. Under shock loading, the plastic deformation required to achieve the high pressure is a consequence of the creation and motion of copious quantities of defects, which are uniformly swept through the sample by the stress wave. Chief among such defects are dislocations, which are created in large numbers in the Plastic I shock. They are known to be effective nucleation sites for transformation (Christian, 1965), and Johnson (1972) has shown, using conventional numbers for transformation energies and shock-induced dislocation density, that significant numbers of nucleation sites may be created in a fraction of a microsecond. In some materials, twins, formed by plastic deformation, are effective nucleation sites, and German *et al.* (1970b) have suggested that nucleation around twins is responsible for the $\alpha \rightarrow \epsilon$ transition in iron. Forbes (1976) has suggested an alternative mechanism for production of nuclei which is peculiar to shock conditions. He has pointed out that there is an equilibrium distribution of new phase embryos under ambient conditions of temperature and pressure, but that such embryos cannot grow because the parent phase is stable. But when a step in pressure is applied, the driving energy for transformation becomes positive, and some of those embryos which existed ini-

tally have suddenly become growing nuclei under stable conditions for the new phase. Contrast of this suggestion with the conventional view of nucleation illustrates an important need for experiments that distinguish between the roles of shock-produced defects and ambient material state in determining transformation rates under shock conditions. If shock-produced defects control transition rate, then rates which depend upon crystallographic orientation may be manifestations of restrictions imposed by the crystal structure on plastic flow and subsequent growth of crystallites. Then it is important to develop a more detailed fundamental understanding of plastic flow under shock loading. If initial material conditions control transition rate, then a tool may exist for measuring the relative effectiveness of various kinds of nucleation sites. Such a tool would be a valuable aid in furthering our understanding of general processes of transformation.

The problem of measuring equilibrium pressure–volume states is an old one and is not peculiar to shock measurements. Vanfleet and Zeto (1971) describe differences among initiation pressure on loading, initiation pressure on unloading, boundaries of the "region of indifference," and the inferred equilibrium pressure for the Bi I→ Bi II transition. In that case the initiation pressure on loading is about 300 MPa greater than the equilibrium pressure. This difference is reduced by encapsulating the bismuth sample in epoxy, but the pressure excursion in the mixed phase region is increased. It should not be surprising, then, that shock initiation pressure, p_x^{TL}, even when corrected for shear, differs from the equilibrium pressure of transition, nor that the slope $(-dp_x/dV)$ of the R–H curve in the mixed phase region exceeds that calculated for equilibrium, as shown in Fig. 18. Reasons for large values of $(-dp_x/dV)$ are of interest, however. Part of the effect may arise from the presence of shearing stresses not accounted for, as suggested by Vanfleet and Zeto; part may arise from sensitivity of nucleation sites to applied pressure. This latter suggestion is made by Forbes (1976), who shows that the fraction of iron transformed to the ϵ-phase in shock is exponentially related to the difference between Gibbs energies of new and old phases ("driving force"). An analogous relation exists between the amount of α-phase material produced and driving force for athermal martensite transformation in iron. These speculations are stimulating, but do not substitute for good experiments, carefully done. Unloading experiments, like those by Barker and Hollenbach in iron (1974), will aid in establishing equilibrium transition pressures.

Although the flash x-ray diffraction measurements under shock loading are not expected to give complete crystallographic descriptions, the work is of importance in establishing consistency with similar static loading measurements and for assessing general conditions in the shock-loaded state. The work to date has been successful in establishing that inelastic deformation under shock loading does not significantly alter the ordered crystalline nature of solids. In agreement with other transformation rate measurements, the flash x-ray diffraction measurements on boron nitride show that crystallites of significant size are grown in times of a few tens of nanoseconds.

In order for the shock loading experiment to provide full thermodynamic descriptions of transitions, it is necessary to take full advantage of the capability to determine stress and volume. (If there are unknown shear strength effects, the volume at the transition is perhaps a better measure for comparison with static data.) Complete studies include measurements of p_x^T, η_T on loading and unloading, compressibility in the mixed phase region, the HEL, compressibility of the high-pressure phase, and measurement of the dependence of the data on sample thickness and input pressure. These data, with Gruneisen parameter Γ and specific heat C_v, can then be used to determine isothermal compressions. Comprehensive investigations such as these will provide especially useful data characterizing pressure-induced phase transitions.

At this point special comments on specific materials are important to evaluate directions for further work. The calculated triple point in iron appears to be in significant disagreement with the measurements of Johnson *et al.* (1962) and in better agreement with the new equilibrium pressure near 300 K established from loading and unloading measurements. It was pointed out in Sec. IV.C that the measurements of Johnson *et al.* would not be expected to yield accurate values for pressure. In spite of that situation, the static high-pressure work of Bundy (1965) is tied directly to the data of Johnson *et al.*; hence, it appears that a new evaluation of the triple point of iron is urgently needed. If shock loading techniques are employed, plane-wave loading methods that include both loading and unloading should be employed.

Antimony appears to be an especially interesting material to investigate with time-resolved sample response measurements. If roles of the 7 and 8.8 GPa transitions can be separated, the relatively slow transformation rate would be important for more detailed study.

Further studies of the KCl and KBr transitions in the high-pressure phase would be expected to yield more detailed descriptions of the transitions. The low shear strength and simple crystal structures make them excellent candidates for both theoretical and experimental study.

The large apparent shear strength effects in CdS and InSb are significant exceptions to the usual behavior of solids under shock loading, yet the investigations on these materials are incomplete. Detailed studies seem to be in order for these materials. Work on them may provide key information for understanding the role of shear stress in phase transition.

The behavior of quartz under shock loading is the most complex of the materials whose response has been studied in detail. The strong possibility that upon yielding the material develops a heterogeneous structure of α-quartz and localized regions of very high temperature and low viscosity, perhaps melting, greatly complicates analysis of the high-pressure data and raises serious questions concerning interpretation of the data concerning dense phases of quartz and other similar materials. The possibility that local temperatures are thousands of degrees could explain the presence of stishovite under shock loading at average temperatures which were previously thought to be too low compared to the static data. The heterogeneous melting combined with transi-

tions to dense phases could possibly explain the anomalously low compressibility in the mixed phase region above 14.4 GPa. Other materials such as Al_2O_3 have been observed to display yield behavior similar to quartz, and geologic materials are possible candidates for similar behavior. The question of heterogeneous melting and its effect on subsequent high-pressure loading in quartz is a problem of importance that should be pursued with some urgency.

As the different experimental investigations have been summarized, the role of experimental technique has been found to be significant. Better understanding of the bismuth transition involved the use of projectile impact loading techniques and the use of detectors with capabilities for accurate time-resolved sample response measurements. A similar situation is noted for the iron transition. The combination of projectile impact loading and time-resolved measurements appears to be particularly effective for studying shock-induced phase transitions.

Finally, it is perhaps worthwhile to emphasize again that it is a mistake to overgeneralize concerning any aspect of shock-induced phase transitions in either a positive or negative sense. There are many different situations that must be considered on their own merit. It is clear, however, that shock loading experiments can provide credible data concerning pressure-induced transitions. Nevertheless, technique is still critical and it is relatively easy to make errors of interpretation. Comprehensive investigations in the hands of skilled observers, along with critical interpretations of the data, will undoubtedly yield valuable thermodynamic data on phase transitions which may be uniquely obtained under shock loading or may prove to be valuable supplements to static high-pressure data.

Note added in proof: Several references which were inadvertently omitted or have recently come to our attention are the following:

(1) on shock induced vaporization, the paper by Horung and Michel (1972);

(2) on melting in magnesium under shock loading, the paper by Urtieu and Grover (1977);

(3) additional data on transitions in titanium, zirconium, and hafnium are given in McQueen *et al.* (1970);

(4) a thorough study of phase transitions in shock compressed BN is described in Gust and Young (1977); and

(5) the excellent review of optical properties under shock compression by Kormer (1977) summarizes melting curves for alkali halides, and comments upon optical effects associated with polymorphic phase transitions.

ACKNOWLEDGMENT

A Sandia Laboratories internal study group on polymorphic phase transformations, composed of P. C. Lysne, G. A. Samara, L. C. Bartel, and R. A. Graham, provided the initial impetus for the tabular summary of polymorphic phase transformations presented in the Appendix.

APPENDIX A

A summary of polymorphic phase transformations is presented in Table A1.

TABLE A1. Summary of shock-induced polymorphic phase transition observations.[a]

Material	Condition	Transition conditions		Technique	Remarks	References
		Stress (GPa)	Compression (%)			
A. Iron and iron alloys						
Iron						
Armco iron	AR	13.6–13.0	6.69–6.37	E-1	7.2–57 mm	Bancroft *et al.* (1956)
Armco iron	Ann	13.2–12.5	6.41–6.18	E-1	25–57 mm, +	Minshall (1961)
Armco iron	AR	12.8	6.41	E-1	25 mm	Minshall (1961)
Armco iron	CR	13.5	6.57	E-1	25 mm	Minshall (1961)
Armco iron	Ann	13.6	6.49	E-1	25 mm, $T_0 = 222$ K	Minshall (1961)
Armco iron	Ann	13.2	6.26	E-1	25 mm, $T_0 = 330$ K	Minshall (1961)
Armco iron	AR	...	...	P-16	Smooth spall	Erkman (1961)
Armco iron	AR	15.0–1.9	...	D-16	24 T_0 values 78–1158 K, apparent triple point	Johnson *et al.* (1962)
Armco iron	AR	14.5–12.5	6.9–6.2	E	Prism sample, optical lever	Peyre *et al.* (1965)
Armco iron	Ann	12.9 ± 0.1	6.4 ± 0.05	E-1	25 mm, ψ	Loree *et al.* (1966a)
Armco iron	AR	...	...	E-13	Wave structure, *	Novikov *et al.* (1965)
Armco iron	...	15.0	...	P-11	4–17 mm, +	Anan'in *et al.* (1973)
Armco iron	...	14.1–13.1	...	P-4	1–25 mm	Forbes *et al.* (1975)
Armco iron	AR	13.7–12.9	6.3	G-9	3–19 mm, +, ψ, ϕ, γ	Barker *et al.* (1974)
Electrolytic iron	AR	...	...	E-15	Shock demagnetization	Royce (1968)
Iron	AR	...	...	E, G-14	Electrical resistance	Wong *et al.* (1968)
Iron	AR	...	...	E-15	Demagnetization eddy currents	Wong (1969)
Iron	...	...	...	E-14	Electrical resistance	Fuller *et al.* (1962)
Iron	AR	...	...	E-14	Electrical resistance, demagnetization eddy currents	Keeler *et al.* (1969)

TABLE AI. (*Continued*)

Material	Condition	Transition conditions: Stress (GPa)	Transition conditions: Compression (%)	Technique	Remarks	References
Iron (*Continued*)						
Armco iron	AR	···	···	P-20	Double shock and rarefaction shock	Balchan (1963)
Iron	Powder/Bakelite mixture	9.4–11	···	E	Shock demagnetization; $\rho_0 = 5.33$ Mg/m^3	Novikov *et al.* (1974)
Low carbon steels						
Fe 0.05%	Ann	···	···	P-16	Smooth spall for $P > 14.0$ GPa, ASTM grain size 2–3	Banks (1968)
SAE 1020 steel	AR	12.9	6.2	E-1	51 mm	Minshall (1961)
SAE 1020 steel	Ann	13.7–12.8	6.7–6.2	E-1	27–51 mm	Minshall (1961)
SAE 1017 steel	Hot rolled	···	···	E-2	Wedge sample, qualitative	Katz *et al.* (1959)
SAE 1040 steel	Ann	13.6	6.6	E-1	27 mm	Minshall (1961)
SAE 1055 steel	Ann	14.1	6.7	E-1	27 mm	Minshall (1961)
Type St. 3 steel (Soviet Union)	···	15.3	···	P-11	6–20 mm, +	Anan'in *et al.* (1973)
Type Kh VG steel (Soviet Union)	AR	16.0	···	P-11	Also unloading	Anan'in *et al.* (1973)
Type Kh VG steel (Soviet Union)	RC60–62	16.2	···	P-11	Also unloading	Anan'in *et al.* (1973)
Iron–nickel alloys						
Fe–4.1 wt % Ni	AR	12.0	···	E-1	$\rho_0 = 7.848$ Mg/m^3	Fowler *et al.* (1961)
Fe–8.5 wt % Ni	AR	11.8	···	E-1	$\rho_0 = 7.855$ Mg/m^3	Fowler *et al.* (1961)
Fe–9.94 wt % Ni	1273 K, 1 h	12.1	6.75	E-4	$\rho_0 = 7.892$ Mg/m^3, 6.4 mm	Gust *et al.* (1970)
Fe–14.2 wt % Ni	AR	11.0	···	E-1	$\rho_0 = 7.878$ Mg/m^3	Fowler *et al.* (1961)
Fe–20 wt % Ni	AR	10.2	···	E-1	$\rho_0 = 7.910$ Mg/m^3	Fowler *et al.* (1961)
Fe–10 wt % Ni	AR	11.7	···	E-1	···	Fowler *et al.* (1961)
Fe–29 at. % Ni	AR	8.5	4.2	E-1	···	Loree *et al.* (1966a)
Fe–25 at. % Ni	AR	8.0	···	E-1	···	Loree *et al.* (1966a)
Fe–41 at. % Ni	AR	5.5	3.4	E-1	···	Loree *et al.* (1966a)
Fe–28.4 at. % Ni	Ann, quench liquid N 168 h	7.0–<1.0	4.1–1.2	G-8, 12	$\rho_0 = 8.032$ Mg/m^3, 7 mm, 9 various T_0 values between 298 and 663 K, γ phase recovered	Rohde (1970)
Fe–28.4 at. % Ni	Ann, quench liquid N 168 h	···	···	G-8, 16	Partial transformation at 2.0 GPa	Rohde *et al.* (1968)
Iron–chromium alloys						
Fe–4 wt % Cr	AR	12.8	···	E-1	$\rho_0 = 7.825$ Mg/m^3	Fowler *et al.* (1961)
Fe–7.7 wt % Cr	AR	12.6	···	E-1	$\rho_0 = 7.793$ Mg/m^3	Fowler *et al.* (1961)
Fe–10 wt % Cr	AR	12.5	···	E-1	···	Fowler *et al.* (1961)
Fe–13.9 wt % Cr	AR	13.3	···	E-1	$\rho_0 = 7.747$ Mg/m^3	Fowler *et al.* (1961)
Fe–17 wt % Cr	AR	14.9	···	E-1	···	Fowler *et al.* (1961)
Fe–22 wt % Cr	AR	18.2	···	E-1	···	Fowler *et al.* (1961)
Fe–9.7 wt % Cr	1273 K, 1 h, water quench	13.4–13.1	6.40–6.10	E-4	$\rho_0 = 7.757$ Mg/m^3, 6.4 mm	Gust *et al.* (1970)
Fe–17.3 wt % Cr	1273 K, 1 h, water quench	15.7–15.4	7.60–7.44	E-4	$\rho_0 = 7.724$ Mg/m^3, 6.4 mm	Gust *et al.* (1970)
Fe–25.7 wt % Cr	1273 K, 1 h, water quench	20.7	9.19	E-4	$\rho_0 = 7.644$ Mg/m^3, 6.4 mm	Gust *et al.* (1970)
Fe–30.1 wt % Cr	1273 K, 1 h, water quench	23.8–22.3	10.5–9.83	E-4	$\rho_0 = 7.618$ Mg/m^3, 6.4 mm	Gust *et al.* (1970)
Iron–Manganese alloys						
Fe–~1 at. % Mn	AR	12.4	6.1	E-1	···	Loree *et al.* (1966b)
Fe–~4 at. % Mn	AR	11.0	5.3	E-1	···	Loree *et al.* (1966b)
Fe–~7.5 at. % Mn	AR	8.5	3.8	E-1	···	Loree *et al.* (1966b)
Fe–~11 at. % Mn	AR	5.8–5.3	2.5	E-1	···	Loree *et al.* (1966b)

TABLE AI. (*Continued*)

Material	Condition	Transition conditions		Technique	Remarks	References
		Stress (GPa)	Compression (%)			
Iron–silicon alloys						
Fe–0.45 wt % Si	AR	12.8	···	E-1	25 mm	Zukas *et al.* (1963)
Fe–0.95 wt % Si	AR	13.2	···	E-1	25 mm	Zukas *et al.* (1963)
Fe–1.92 wt % Si	AR	14.0	···	E-1	25 mm, ψ	Zukas *et al.* (1963)
Fe–2.90 wt % Si	AR	14.7	···	E-1	ASTM grain size minus 2, 25 mm	Zukas *et al.* (1963)
Fe–3.82 wt % Si	AR	15.4	···	E-1	25 mm	Zukas *et al.* (1963)
Fe–4.60 wt % Si	AR	15.8	···	E-1	25 mm	Zukas *et al.* (1963)
Fe–6.85 wt % Si	AR	22.5	···	E-1	25 mm	Zukas *et al.* (1963)
Fe–2.9 wt % Si	[111] crystal, AR	14.5	···	E-1	25 mm	Zukas *et al.* (1963)
Fe–2.9 wt % Si	[112] crystal, AR	14.9	···	E-1	16 mm	Zukas *et al.* (1963)
Fe–3.25 wt % Si	Ann	15.0	···	G-15	Shock demagnetization	Graham (1968)
Iron–vanadium alloys						
Fe–2 wt % V	Ann	14.2	7.0	E-1	25 mm	Loree *et al.* (1966a)
Fe–4 wt % V	Ann	16.0	7.5	E-1	25 mm	Loree *et al.* (1966a)
Fe–6 wt % V	Ann	18.0	8.5	E-1	25 mm	Loree *et al.* (1966a)
Fe–8 wt % V	Ann	20.7	9.3	E-1	25 mm	Loree *et al.* (1966a)
Fe–10 wt % V	Ann	24.5	10.5	E-1	25 mm	Loree *et al.* (1966a)
Fe–11 wt % V	Ann	28.0	12.0	E-1	25 mm	Loree *et al.* (1966a)
Fe–20 wt % V	Ann	~50	···	E-16	25 mm	Loree *et al.* (1966a)
Fe–22 wt % V	Ann	~53	···	E-16	25 mm	Loree *et al.* (1966a)
Fe–24 wt % V	Ann	~55	···	E-16	25 mm	Loree *et al.* (1966a)
Fe–26 wt % V	Ann	~57	···	E-16	25 mm	Loree *et al.* (1966a)
Fe–8 wt % V	Ann	···	···	E-16	6 mm to 25 mm, no overdrive observed	Loree *et al.* (1966a)
Iron–molybdenum alloys						
Fe–1 wt % Mo	Ann	13.1	6.5	E-1	25 mm	Loree *et al.* (1966a)
Fe–2 wt % Mo	Ann	13.5	6.5	E-1	25 mm	Loree *et al.* (1966a)
Fe–3 wt % Mo	Ann	13.9	6.5	E-1	25 mm	Loree *et al.* (1966a)
Fe–8 wt % Mo	Ann	15.5	7.1	E-1	25 mm	Loree *et al.* (1966a)
Fe–12 wt % Mo	Ann	16.2	7.4	E-1	25 mm	Loree *et al.* (1966a)
Fe–15 wt % Mo	Ann	15.4	6.7	E-1	25 mm	Loree *et al.* (1966a)
Fe–20 wt % Mo	Ann	15.5	6.5	E-1	Mixed phase composition, 25 mm	Loree *et al.* (1966a)
Fe–30 wt % Mo	Ann	14.6	6.0	E-1	Mixed phase composition, 25 mm	Loree *et al.* (1966a)
Fe–40 wt % Mo	Ann	12.9	5.8	E-1	Mixed phase composition, 25 mm	Loree *et al.* (1966a)
Fe–45 wt % Mo	Ann	13.0	4.4	E-1	Mixed phase composition, 25 mm	Loree *et al.* (1966a)
Fe–1 wt % Mo, 1–1.5 wt % W	Ann	13.8	···	E-1	25 mm, W contamination	Loree *et al.* (1966a)
Fe–2 wt % Mo, 1–1.5 wt % W	Ann	14.3	···	E-1	25 mm, W contamination	Loree *et al.* (1966a)
Fe–3 wt % Mo 1–1.5 wt % W	Ann	14.5	···	E-1	25 mm, W contamination	Loree *et al.* (1966a)
Fe–10 wt % Mo 1–1.5 wt % W	Ann	16.4	···	E-1	25 mm, W contamination	Loree *et al.* (1966a)
Iron–cobalt alloys						
Fe–2 wt % Co	Ann	13.2	6.5	E-1	25 mm	Loree *et al.* (1966a)
Fe–4 wt % Co	Ann	13.5	7.1	E-1	25 mm	Loree *et al.* (1966a)
Fe–8 wt % Co	Ann	14.5	7.1	E-1	25 mm	Loree *et al.* (1966a)
Fe–12 wt % Co	Ann	16.5	7.8	E-1	25 mm	Loree *et al.* (1966a)
Fe–16 wt % Co	Ann	18.0	8.5	E-1	25 mm	Loree *et al.* (1966a)
Fe–20 wt % Co	Ann	18.7	8.5	E-1	25 mm	Loree *et al.* (1966a)
Fe–25 wt % Co	Ann	21.7	9.6	E-1	25 mm	Loree *et al.* (1966a)
Fe–30 wt % Co	Ann	23.0	9.9	E-1	25 mm	Loree *et al.* (1966a)
Fe–35 wt % Co	Ann	24.5	10.4	E-1	25 mm	Loree *et al.* (1966a)
Fe–40 wt % Co	Ann	28.0	11.0	E-1	25 mm	Loree *et al.* (1966a)
Fe–45 wt % Co	Ann	32.0	12.5	E-1	25 mm	Loree *et al.* (1966a)
Fe–50 wt % Co	Ann	36.7	12.4	E-1	25 mm	Loree *et al.* (1966a)

TABLE AI. (*Continued*)

Material	Condition	Transition conditions: Stress (GPa)	Transition conditions: Compression (%)	Technique	Remarks	References
Iron–carbon alloys						
Fe–0.5 wt % C	593 K, 2 h	13.9	6.4	E-1	25 mm	Loree *et al.* (1966a)
Fe–0.5 wt % C	948 K, 2 h	13.1	6.4	E-1	25 mm	Loree *et al.* (1966a)
Fe–0.5 wt % C	Ann	13.0	6.4	E-1	25 mm	Loree *et al.* (1966a)
Fe–1 wt % C	593 K, 2 h	15.0	6.7	E-1	25 mm	Loree *et al.* (1966a)
Fe–1 wt % C	948 K, 2 h	13.2	6.4	E-1	25 mm	Loree *et al.* (1966a)
Fe–1 wt % C	Ann	13.1	6.4	E-1	25 mm	Loree *et al.* (1966a)
Fe–15 wt % C	593 K, 2 h	14.8	6.6	E-1	25 mm	Loree *et al.* (1966a)
Fe–15 wt % C	948 K, 2 h	13.3	6.4	E-1	25 mm	Loree *et al.* (1966a)
Fe–15 wt % C	Ann	13.4	6.4	E-1	25 mm	Loree *et al.* (1966a)
Fe–2 wt % C	593 K, 2 h	15.6	6.6	E-1	25 mm	Loree *et al.* (1966a)
Fe–2 wt % C	948 K, 2 h	13.6	6.6	E-1	25 mm	Loree *et al.* (1966a)
Fe–2 wt % C	Ann	14.7	5.75	E-1	25 mm	Loree *et al.* (1966a)
Iron-nickel-chromium alloys						
Fe–8.1 wt % Cr, 8.1 wt % Ni	AR	10.0	···	E-1	$\rho_0 = 7.817$ Mg/m^3	Fowler *et al.* (1961)
Fe–17.4 wt % Cr, 8.2 wt % Ni	AR	3.0	···	E-1	$\rho_0 = 7.764$ Mg/m^3	Fowler *et al.* (1961); see also Gust *et al.* (1970)
Fe–8 wt % Cr, 8 wt % Ni	AR	10.0–9.5	···	E-1	···	Fowler *et al.* (1961) as reported by Gust *et al.* (1970)
Fe–12 wt % Cr, 8 wt % Ni	AR	8.0	···	E-1	···	Fowler *et al.* (1961) as reported by Gust *et al.* (1970)
Fe–6 wt % Cr, 12 wt % Ni	AR	8.5	···	E-1	···	Fowler *et al.* (1961) as reported by Gust *et al.* (1970)
Fe–7 wt % Cr, 12 wt % Ni	AR	8.5	···	E-1	···	Fowler *et al.* (1961) as reported by Gust *et al.* (1970)
Fe–5.93 wt % Cr, 8.79 wt % Ni	1303 K, 1 h, water quench	11.0–10.7	5.24–5.13	E-4	$\rho_0 = 7.822$ Mg/m^3	Gust *et al.* (1970)
Fe–12.1 wt % Cr, 7.73 wt % Ni	1303 K, 1 h, water quench	8.7	4.36	E-4	$\rho_0 = 7.778$ Mg/m^3	Gust *et al.* (1970)
Fe–15.9 wt % Cr, 7.8 wt % Ni	1303 K, 1 h, water quench	8.1–7.9	4.19–4.12	E-4	$\rho_0 = 7.760$ Mg/m^3	Gust *et al.* (1970)
Fe–18.1 wt % Cr, 8.22 wt % Ni	1303 K, 1 h, water quench	8.1–7.0	4.65–3.00	E-4	$\rho_0 = 7.827$–7.833 Mg/m^3, τ	Gust *et al.* (1970)
Fe–6.32 wt % Cr, 12.2 wt % Ni	1303 K, 1 h, water quench	9.8	5.49	E-4	$\rho_0 = 7.852$ Mg/m^3	Gust *et al.* (1970)
Fe–11.7 wt % Cr, 12.1 wt % Ni	1303 K, 1 h, water quench	8.2	4.22	E-4	$\rho_0 = 7.888$ Mg/m^3	Gust *et al.* (1970)
Fe–5.91 wt % Cr, 16.0 wt % Ni	1303 K, 1 h, water quench	7.8	4.14	E-4	$\rho_0 = 7.852$ Mg/m^3	Gust *et al.* (1970)
Fe–20 wt % Cr, 8.5 wt % Ni	168 h, liquid N	7.0	···	G-12	$\rho_0 = 7.79$ Mg/m^3	Graham *et al.* (1968)
B. Elements						
Antimony						
Antimony	AR	11.4–8.6	···	E-1	10 to 25 mm, +	Minshall as reported by McQueen (1964)
Antimony	AR	~9.5	···	E-1	Wedge sample, optical lever	Katz *et al.* (1959)
Antimony	Cast	10.8–9.1	16.4–13.9	E-1	5 to 49 mm, +, τ	Warnes (1967)
Antimony	Cast	···	···	E-20	Direct observation of transformation times	Breed *et al.* (1968)

TABLE AI. (*Continued*)

Material	Condition	Transition conditions: Stress (GPa)	Transition conditions: Compression (%)	Technique	Remarks	References
Bismuth						
Bismuth	Cast and hot pressed	2.72	6.54	E-1	6.6 to 25.2 mm, 3 mm grain size $\rho_0 = 9.80$ Mg/m^3	Duff *et al.* (1957)
Bismuth	Cast and hot pressed	3.13	7.54	E-1	22 mm, $T_0 = 300$ K, 3 mm grain size $\rho_0 = 9.80$ Mg/m^3	Duff *et al.* (1957)
Bismuth	Cast and hot pressed	2.53	6.12	E-1	20 mm, $T_0 = 360$ K, 3 mm grain size $\rho_0 = 9.80$ Mg/m^3	Duff *et al.* (1957)
Bismuth	Cast and hot pressed	1.76	3.83	E-1	20.4 mm, $T_0 = 509$ K, 3 mm grain size $\rho_0 = 9.80$ Mg/m^3	Duff *et al.* (1957)
Bismuth	Cast	2.98–2.27	7.2–5.6	G-7	3 to 6 mm	Hughes *et al.* (1961)
Bismuth	Cast	2.65–2.46	6.1–5.9	E-8	1.6 to 12.7 mm, τ, 21 samples $\rho_0 = 9.80$ Mg/m^3	Larson (1967)
Bismuth	Pressed	2.65–2.45	6.3–5.8	E-8	1.4 to 4.5 mm, τ, 7 samples	Larson (1967)
Bismuth	Crystal, *a* axis	2.46	5.8	E-8	3.1 to 4.4 mm, τ, 3 samples	Larson (1967)
Bismuth	Crystal, *c* axis	2.56	6.1	E-8	1.2 to 4.4 mm, τ, 7 samples	Larson (1967)
Bismuth	Pressed	2.50–2.53	5.8	G-9	$\rho_0 = 9.756$ Mg/m^3, grain size 30 μm	Asay (1974)
Bismuth	···	7.0	···	E	$\rho_0 = 9.80$ Mg/m^3, thermoelectric effect	Romain (1974)
Carbon						
Carbon	Spectroscopically pure artificial graphite	···	···	E-17, 19	Diamonds recovered	DeCarli *et al.* (1961)
Carbon	Natural Ceylon graphite, high purity	40 and 60	···	···	75% to 95% theoretical density, +, ?	Alder *et al.* (1961), see Trunin *et al.* (1969) and Pavlovskii *et al.* (1966)
Carbon	Pyrolytic graphite	···	···	E, P-3	$\rho_0 = 2.2$ Mg/m^3, no transition	Coleburn (1964)
Carbon	Pyrolytic graphite	···	···	E-4	$\rho_0 = 2.18$–2.20 Mg/m^3, optical lever	Doran (1963a)
Carbon	Pyrolytic graphite	···	···	P-2	$\rho_0 = 2.20$ Mg/m^3, possible transition at 40 GPa	McQueen (1964)
Carbon	Pressed graphite	···	···	P-2	$\rho_0 = 2.15$ Mg/m^3, possible transition at 27 GPa	McQueen (1964)
Carbon	Synthetic graphite	···	···	P-1	$\rho_0 = 1.77$ Mg/m^3, +	Pavlovskii *et al.* (1966)
Carbon	Synthetic graphite	···	···	P-1	$\rho_0 = 1.85$ Mg/m^3, +	Pavlovskii *et al.* (1966)
Carbon	Ceylon graphite, ground pressed	···	···	P-1	$\rho_0 = 2.23$ Mg/m^3, +	Pavlovskii *et al.* (1966)
Carbon	Pyrolytic graphite	40	28	P-2	$\rho_0 = 2.20$ Mg/m^3	McQueen *et al.* (1968)
Carbon	Pressed graphite	23	···	P-2	$\rho_0 = 2.13$ Mg/m^3	McQueen *et al.* (1968)
Carbon	Pressed graphite	23	···	P-2	$\rho_0 = 2.03$ Mg/m^3	McQueen *et al.* (1968)
Carbon	ZTA graphite	23	···	P-2	$\rho_0 = 1.95$ Mg/m^3	McQueen *et al.* (1968)
Carbon	Pressed graphite	23	···	P-2	$\rho_0 = 1.88$ Mg/m^3	McQueen *et al.* (1968)
Carbon	ATJ graphite	23	···	P-2	$\rho_0 = 1.79$ Mg/m^3	McQueen *et al.* (1968)
Carbon	PT0178 graphite	23	···	P-2	$\rho_0 = 1.54$ Mg/m^3	McQueen *et al.* (1968)
Carbon	Graphite, chemically pure	···	···	P-1	$\rho_0 = 1.878$ Mg/m^3; found evidence that high pressure metallic phase reported by Alder was in error	Trunin *et al.* (1969)
Carbon	Decalcified natural graphite	25	~31	P-1	$\rho_0 = 2.08$ Mg/m^3, +	Dremin *et al.* (1968)
Carbon	Iron-graphite mixture	···	···	P-19	Electron microscopy, diamonds recovered	Trueb (1968)
Carbon	Copper-graphite mixtures	···	···	E-19	Electron microscopy, diamonds recovered	Trueb (1971)
Carbon	Madagascar graphite	···	···	P-19	$\rho_0 = 2.05$ Mg/m^3, pulse duration 300 ns	Pujols *et al.* (1970)
Carbon	Graphite	···	···	P	Diamonds recovered	Fournier *et al.* (1971)
Carbon	Diamond pressed powder	···	···	P-2	$\rho_0 = 3.20$ Mg/m^3, no transition observed between 43 and 128 GPa	McQueen *et al.* (1968)

TABLE AI. (*Continued*)

Material	Condition	Transition conditions: Stress (GPa)	Transition conditions: Compression (%)	Technique	Remarks	References
Carbon (*Continued*)						
Carbon	Diamond crystal	···	···	P-1	No transition observed between 100 and 580 GPa	Pavlovskii (1971)
Carbon	Diamond pressed powder	···	···	P-1	$\rho_0 = 1.90$ Mg/m^3, no transition observed between 40 and 160 GPa	Pavlovskii (1971)
Germanium						
Germanium	[111], [100], and [114] orientations	12.5	···	E-2, 5	···	McQueen (1964)
Germanium	[111] orientation	13.9±0.3	12–13	G-14	Electrical resistance, τ	Graham *et al.* (1966)
Germanium	[111] orientation	14.3	16.0	E-1, 10	τ	Pavlovskii (1968)
Germanium	[111] orientation	···	···	E	Thermoelectric effect, wave velocities	Jacquesson *et al.* (1970)
Silicon						
Silicon	Crystal	···	···	E-4, 5	Wave profiles, ϕ, ψ	McQueen (1964)
Silicon	[111] orientation	11.2	9.9	E-1, 10	τ	Pavlovskii (1968)
Silicon	[100] orientation	14.0±0.4	10.3	E-6	6.4 mm, τ	Gust *et al.* (1971)
Silicon	[110] orientation	10.3±0.7 12.8±0.7	7.2 10.3	E-6	6.4 mm, two successive transitions observed τ	Gust *et al.* (1971)
Silicon	[111] orientation	10.1±0.3 13.7±0.5	6.8 10.7	E-6	6.4 mm, two successive transitions observed, τ	Gust *et al.* (1971)
Iodine						
Iodine	Pressed pellet, commercial grade	<25	···	E-14	Electrical resistance	Alder *et al.* (1956a)
Iodine	Pressed pellet, commercial grade	>8, <13	···	E-14	Electrical resistance	Alder *et al.* (1956b)
Iodine	Crystalline	~70	47	?	?	Alder *et al.* (1960), see also McMahan *et al.* (1975)
Iodine	···	···	···	···	Calculations show no 70 GPa transition	McMahan *et al.* (1975)
Phosphorus						
Phosphorus	Red, pressed pellet	<25	···	E-14	Electrical resistance	Alder *et al.* (1956a)
Phosphorus	Red, pressed pellet	<10	···	E-14	···	Alder *et al.* (1956b)
Phosphorus	Red	~2.5	···	···	···	Grover *et al.* (1958)
Phosphorus	Yellow	~8.0	···	···	···	Grover *et al.* (1958)
Other elements						
Cerium	···	~2.5	~2.5	P-2	···	Carter (1973a)
Gadolinium	···	~38	···	P-2	$T_H \approx 1500$ K	Carter (1973a)
Hafnium	···	~47	~23	P-2	···	Carter (1973a)
Selenium	···	···	···	G-14	Resistance change	Cole *et al.* (1971)
Sulfur	···	···	···	D-14	Resistance change, see also Table VII	David *et al.* (1958)
Tin	···	9.4	···	E-6	···	Duff *et al.* (1968)
Titanium	···	~18	~12	P-2	···	Carter (1973b)
Titanium	···	···	···	D-17	bcc phase recovered for $p_x > 12$ GPa	German *et al.* (1970a)
Zirconium	···	~23	~16	P-2	···	Carter (1973b)
Zirconium	···	···	···	D-17	bcc phase recovered for $p_x = 3.0$ GPa	German *et al.* (1970a)
Uranium	···	~50	20	E-2	$\rho_0 = 19.05$ Mg/m^3	Viard (1962)
Ytterbium	Foil	~3.3	···	G-14	Electrical resistance	Ginsberg *et al.* (1973)
Plutonium	δ phase	~0.6	···	G-8, 11	Reversion on unloading at 0.8 GPa	Kamegai (1975)
C. Compounds						
Alkali halides						
KCl	Crystal	~2.1	···	P-1	3.5 mm, $\rho_0 = 1.99$ Mg/m^3	Al'tshuler *et al.* (1963)
KCl	Crystal	2.0±0.08	···	E-8	···	Larson (1965)
KCl	Pressed	1.89	9.75	E-10	1.6 to 16.5 mm, $\rho_0 = 1.90$ Mg/m^3	Dremin *et al.* (1965)
KCl	[001] crystal	1.9	7.8	E-10	Unloading showed hysteresis of 1.0 GPa	Al'tshuler *et al.* (1967)
KCl	[111], [100] crystal	2.08±0.05	8.6	G-8	Impact surface measurement, rates	Hayes (1974)

TABLE AI. (*Continued*)

Material	Condition	Transition conditions: Stress (GPa)	Transition conditions: Compression (%)	Technique	Remarks	References
Alkali halides (*Continued*)						
KBr	Crystal	~2.2	···	P-1	3.5 mm, $\rho_0 = 1.999$ Mg/m^3	Al'tshuler *et al.* (1963)
KBr	Crystal	1.85 ± 0.08	···	E-8	···	Larson (1965)
KBr	Pressed	2.38	11.3	E-10	4.9 to 30.2 mm, $\rho_0 = 2.70$ Mg/m^3	Dremin *et al.* (1965)
KBr	[001] crystal	···	···	E-10	Unloading hysteresis of 1 GPa	Al'tshuler *et al.* (1967)
KBr	Pressed powder	2.05	10.9	E-10	$\rho_0 = 2.70$ Mg/m^3	Adadurov *et al.* (1970)
KBr	Pressed powder	···	···	E-10	$\rho_0 = 2.57$, 2.45, and 2.00 Mg/m^3	Adadurov *et al.* (1970)
KBr	···	2.1	11.5	–10	$\rho_0 = 2.70$ Mg/m^3	Khristoforov *et al.* (1971)
NaCl	Crystal	2.9	···	E-8	?	Larson (1965) See Royce (1969)
NaCl	Pressed powder	2.3	···	E-8	?	Larson (1965) See Royce (1969)
NaCl	···	~3.0	···	E-5	?	Larson *et al.* (1966) See Royce (1969)
NaCl	Pressed powder	···	···	E-6	No transition observed, problem with explosive driver used by Larson (1965)	Royce (1969)
NaCl	[100], [111] crystal	23.1	30.6	P-2	$\rho_0 = 2.165$ Mg/cm^3	Fritz *et al.* (1971)
NaCl	Crystal	···	···	P-17	Recovery of samples loaded between 4.0 and 3.5 GPa. $T_0 = 113$, 253, 293, 328 and 348 K. Evidence for recrystallization from dense phase.	Brazhnik *et al.* (1969)
CsI	Crystal	<25	···	E-14	Electrical resistance	Alder *et al.* (1956a)
CsI	Crystal	<28	···	E-14	Electrical resistance	Alder *et al.* (1956b)
CsI	Pressed pellet	<28	···	E-14	Electrical resistance	Alder *et al.* (1956b)
CsI	···	···	···	···	Calculated temperature rise to explain Alder's results	Pospelov *et al.* (1966)
RbI	Pressed pellet	<28	···	E-14	Electrical resistance	Alder *et al.* (1956b)
RbCl and CsCl	···	···	···	–17	Solid solutions of RbCl–CsCl synthesized from RbCl and CsCl starting materials	Batsanov *et al.* (1969)
III–V, II–VI Compounds						
CdS	Crystal *c* axis	3.15	3.3	E-8	*, τ	Kennedy *et al.* (1966)
CdS	Crystal *a* axis	2.8	3.3	E-8	ϕ, τ	Kennedy *et al.* (1966)
CdS	CdS–water mixture	···	···	D-17	Zinc blende structure recovered	Leiserowitz *et al.* (1966)
InSb	Crystal [100]	2.0	3.0	E-8	···	Kennedy *et al.* (1965)
InSb	Crystal [111]	1.7	2.1	E-8	ϕ, τ	Kennedy *et al.* (1965)
BN	Graphitelike	12.0	28.8	E-1	$\rho_0 = 1.95$ Mg/m^3 rarefaction shock not observed	Al'tshuler *et al.* (1967)
BN	Hexagonal powder pressed to 98.5% of theoretical density	12.2	20	P-3	3.2 to 3.8 mm, T_0 values 298 K, 393 K, 473 K, 573 K, 658 K, 713 K, $\Delta V = \sim 19\%$, cubic zinc blende phase and wurtzite recovery	Coleburn *et al.* (1968)
BN	Graphitelike	12.8	29.6	···	$\rho_0 = 2.00$ Mg/m^3, wurtzite phase recovered	Adadurov *et al.* (1967)
BN	Hexagonal	···	···	P-17	$\rho_0 = 0.8$ Mg/m^3, 1.98 Mg/m^3, $T_0 = 300$ K and 800 K cubic and wurtzite phases recovered after shocking to 12.0 GPa	Dulin *et al.* (1969)
BN	Powder	···	···	D	Dense phase recovered	Batsanov *et al.* (1965)
BN	Pressed powder	13.5	···	P-14	$\rho_0 = 1.97$ Mg/m^3, electrical resistance	Kuleshova (1969)
BN	Graphitelike	···	···	G, P-17	Recovered samples showed no zinc blende structure, wurtzite structure recovered, crystallites ~200 Å	Soma *et al.* (1975)

TABLE AI. (*Continued*)

Material	Condition	Transition conditions: Stress (GPa)	Transition conditions: Compression (%)	Technique	Remarks	References
III–V, II–VI Compounds (*Continued*)						
GaAs	High purity polycrystal	20±1.1	19	E-4	$\rho_0 = 5.326$ Mg/m^3	Goto *et al.* (1976)
GaP	High purity polycrystal	26	22	E-4	$\rho_0 = 4.127$ Mg/m^3	Syono *et al.* (1977)
Oxides						
TiO_2	Rutile phase crystal	33	12	P-2, 17	$\Delta V \sim 21\%$, orthorhombic lead dioxide structure recovered	McQueen *et al.* (1967)
TiO_2	Hot pressed powder	<20	···	E, P-11, 17	6 mm, $\rho_0 = 4.18$, 4.15, 4.07, 2.83 Mg/m^3, orthorhombic lead dioxide structure recovered, τ	Linde *et al.* (1969)
SiO_2	α-Crystal x-cut	14.5	16.5	E, P-5	3.2 to 12.7 mm, τ	Wackerle (1962)
SiO_2	α-Crystal y-cut	14.5	16.5	E, P-5	3.2 to 9.5 mm, τ	Wackerle (1962)
SiO_2	α-Crystal z-cut	14.5	16.5	E, P-5	3.2 to 9.5 mm, τ	Wackerle (1962)
SiO_2	α-Crystal x,y,z-cut	···	···	P-	Examination of samples shocked at 50 GPa shows amorphous quartz; those shocked at 25 GPa show α-quartz	Wackerle (1962)
SiO_2	Fused	···	···	P-	Recovered samples show permanent densification at 25 GPa	Wackerle (1962)
SiO_2	α-Crystal	···	···	P-	Recovered samples show amorphous quartz when shocked to 36 and 60 GPa	DeCarli *et al.* (1959)
SiO_2	α-Crystal, quartz rocks	···	···	D-17	Traces stishovite recovered	DeCarli *et al.* (1965)
SiO_2	α-Crystal	···	···	?	Very high pressure	Al'tshuler *et al.* (1965)
SiO_2	Powder	···	···	D-17	Coesite recovered	Deribas *et al.* (1968)
SiO_2	α-Crystal	···	···	E, P-4	Loading and unloading	Ahrens *et al.* (1968)
SiO_2	α-Crystal	···	···	P-1	Very high pressure	Trunin *et al.* (1971a)
SiO_2	Powder	···	···	P-	$\rho_0 = 1.15$, 1.35, 1.55, and 1.75 Mg/m^3	Trunin *et al.* (1971b)
SiO_2	x- and z-cut crystals	···	···	E, P	Recovered amorphous quartz above HEL	Anan'in *et al.* (1974)
SiO_2	α-Quartz	···	···	···	Pulsed electron beam, $\alpha \rightarrow \beta$ transition	Gauster *et al.* (1973)
SiO_2	Quartzite, α-quartz	···	···	···	Orthorhombic quartz in recovered samples	German *et al.* (1973)
PbO_2	···	···	···	D-17	Dense phase recovered	Leiserowitz *et al.* (1966)
PbO_2	PbO_2–water mixture	···	···	D-17	Dense phase recovered	Leiserowitz *et al.* (1966)
D. Ferroelectric ceramics						
$Pb(Zr_{0.52}Ti_{0.48})O_3$	Polycrystalline ceramic	···	···	E-5	Multiple wave structure observed	Reynolds *et al.* (1961)
$Pb(Zr_{0.52}Ti_{0.48})O_3$ 1 wt % Nb_2O_5	Polycrystalline ceramic	···	···	E-5	12.7 mm, multiple waves not associated with ferroelectric to paraelectric transition	Reynolds *et al.* (1962)
$BaTiO_3$	Polycrystalline ceramic	···	···	E-5	Multiple wave structure observed	Reynolds *et al.* (1961)
$BaTiO_3$	Polycrystalline ceramic	···	···	E-5	12.7 mm, multiple waves not associated with ferroelectric to paraelectric transition	Reynolds *et al.* (1962)

TABLE AI. (*Continued*)

Material	Condition	Transition conditions: Stress (GPa)	Transition conditions: Compression (%)	Technique	Remarks	References
Ferroelectric ceramics (*Continued*)						
95% $BaTiO_3$ 5% $CaTiO_3$	Polycrystalline	···	···	E-5	Multiple wave structure observed	Reynolds *et al.* (1961)
95% $BaTiO_3$ 5% $CaTiO_3$	Polycrystalline	~0.7 GPa	···	E-4	$\rho_0 = 5.52$ to 5.56 Mg/m^3	Doran (1968)
$Pb(Zr_{0.95}Ti_{0.05})O_3$ 1 wt % Nb_2O_5	Polycrystalline ceramic	~0.2 GPa	···	E-4	$\rho_0 = 7.61$ to 7.89 Mg/m^3	Doran (1968)
$Pb(Zr_{0.95}Ti_{0.05})O_3$	Polycrystalline ceramic	···	···	G	Electrical response, multiaxial strain	Lysne (1977)
$Pb_{0.99}Nb_{0.02}(Zr_{0.65}Ti_{0.35})_{0.98}O_3$	Polycrystalline ceramic	~6	···	G	Electrical response	Lysne *et al.* (1975)
$Pb_{0.99}Nb_{0.02}[(Zr_{0.70}-Sn_{0.30})_{0.94}Ti_{0.06}]_{0.98}O_3$	Polycrystalline ceramic	~0.3	···	G	Electrical response	Lysne (1975)
E. Others						
BaF_2	[111], [100] crystals	···	···	G-8	Transition uncertain	Dandekar *et al.* (1973)
$LiAlH_4$	Pressed powder	<25	···	E-14	Electrical resistance	Alder and Christian (1956a)
$LiAlH_4$	Pressed powder	<5	···	E-14	Electrical resistance	Alder and Christian (1956a)
Teflon	···	0.5±0.01	8.3	G-8	···	Champion (1971)
Fe_3O_4	Crystal	22±2	~8	E, P-4, 2	$\rho_0 = 5.20$ Mg/m^3	Syono *et al.* (1975)
αFe_2O_3	Crystal	~80	···	E, P-4,3	$\rho_0 = 5.26$ Mg/m^3	Syono *et al.* (1975)
Nb_3Sn	···	···	···	···	Synthesis by shock loading	Otto *et al.* (1971)
Nb_3Sn	···	···	···	···	Synthesis by shock loading	Barskii *et al.* (1972)
Nb–Ge	···	···	···	···	Phases of unknown character synthesized	Barskii *et al.* (1972)
Nb–Pb	···	···	···	···	Phase of unknown character synthesized	Barskii *et al.* (1972)
Epoxy	···	···	···	P-2	High pressure transition	Carter (1973b)
Polyimide	···	···	···	P-2	High pressure transition	Carter (1973b)
Polycarbonate	···	···	···	P-2	High pressure transition	Carter (1973b)
Polysulfate	···	···	···	P-2	High pressure transition	Carter (1973b)
AlN	Wurtzite powder	···	···	D-17	ρ_0 from 0.41 to 1.14 Mg/m^3	Vereshchagin *et al.* (1969b)
Methacrylamide/trioxane	Pressed powder	···	···	D-19	Polymerization at pressures between 1.5 and 3 GPa	Adadurov *et al.* (1965)
Diphenylbutadiene	Purified, recrystallized pressed powder	···	···	D-19	Polymerization at pressures between 2.8 and 13 GPa	Al'tshuler *et al.* (1968b)

[a]Starting material: wt % indicates weight percent, at. % indicates atomic percent. Condition: AR indicates "as received" or no treatment specified; Ann indicates annealed; CR indicates cold rolled; other treatments as specified. Transition conditions: Stress (GPa)—Values quoted are longitudinal component of stress associated with the transition. In those cases where it is difficult to assign a value to the transition but evidence for a transition is given, an entry is made without specific value. Compression (%)—Compression to initiate the transition. Technique: Loading methods: E—plane-wave explosive loading, D—divergent wave explosive loading, P—explosively driven flying plate, G—projectile impact from gun. Numbers indicate instrumentation scheme as numbered in Table I. Remarks: Sample thicknesses in mm, initial sample temperature T_0 if different from room temperature, + indicates the original author quotes an explicit dependence on sample thickness, ϕ indicates a finite rise time, * indicates stress relaxation, τ indicates that shear strength correction is possible from data in the paper, ψ indicates an explicit dependence on driving pressure, ? indicates other authors question data. Reference: Reference as cited at end of paper.

REFERENCES

Adadurov, G. A., A. N. Dremin, S. V. Pershin, V. N. Rodionov, and Y. N. Ryabinin, 1962, Zh. Prikl. Mekh. Tekh. Fiz. **4**, 81.

Adadurov, G. A., I. M. Barkalov, V. I. Gol'danskii, A. N. Dremin, T. N. Ignatovich, A. N. Mikhailov, V. L. Tal'roze, and P. A. Yampol'skii, 1965, Polym. Sci. USSR **7**, 196.

Adadurov, G. A., Z. G. Aliev, L. O. Atovmyan, T. V. Bavina, Yu. G. Borod'ko, O. N. Breusov, A. N. Dremin, A. Kh. Muranevich, and S. V. Pershin, 1967, Sov. Phys.—Dokl. **12**, 173.

Adadurov, G. A., A. N. Dremin, and G. I. Kanel', 1970, Combust. Explos. Shock Waves **6**, 456.

Ahrens, T. J., 1972, Tectonophysics **13**, 189.

Ahrens, T. J., and J. T. Rosenberg, 1968, in *Shock Metamorphism of Natural Materials*, edited by B. M. French and N. M. Short (Mono Book Corp., Baltimore), p. 59.

Ahrens, T. J., D. L. Anderson, and A. E. Ringwood, 1969, Rev. Geophys. **7**, 667.

Ahrens, T. J., T. Takahashi, and G. F. Davies, 1970, J. Geophys. Res. **75**, 310.

Alder, B. J., and R. H. Christian, 1956a, Phys. Rev. **104**, 550.

Alder, B. J., and R. H. Christian, 1956b, Discuss. Faraday Soc. **22**, 44.

Alder, B. J., and R. H. Christian, 1960, Phys. Rev. Lett. **4**, 450.

Alder, B. J., and R. H. Christian, 1961, Phys. Rev. Lett. **7**, 367.

Al'tshuler, L. V., 1965, Sov. Phys.—Usp. **8**, 52.

Al'tshuler, L. V., A. A. Bakanova, and R. F. Trunin, 1958, Sov. Phys.—Dokl. **3**, 761.

Al'tshuler, L. V., S. B. Kormer, M. I. Brazhnik, L. A. Vladimirov, M. P. Speranskaya, and A. I. Funtikov, 1960, Sov. Phys.—JETP **11**, 766.

Al'tshuler, L. V., A. A. Bakanova, and R. F. Trunin, 1962, Sov. Phys.—JETP **15**, 65.

Al'tshuler, L. V., M. N. Pavlovskii, L. V. Kuleshova, and G. V. Simakov, 1963, Sov. Phys.—Solid State **5**, 203.

Al'tshuler, L. V., R. F. Trunin, and G. V. Simakov, 1965, Bull. Acad. Sci. USSR, Physics Solid Earth No. 10, p. 657.

Al'tshuler, L. V., M. N. Pavlovskii, and V. P. Drakin, 1967, Sov. Phys.—JETP **25**, 260.

Al'tshuler, L. V., B. N. Moiseev, L. V. Popov, G. V. Simakov, and R. F. Trunin, 1968a, Sov. Phys.—JETP **27**, 420.

Al'tshuler, L. V., I. M. Barkalov, I. N. Dulin, V. N. Zubarev, T. N. Ignatovich, and P. A. Yampol'skii, 1968b, High Energy Chem. **2**, 73.

Anan'in, A. V., A. N. Dremin, and G. I. Kanel', 1973, Combust. Explos. Shock Waves **9**, 381.

Anan'in, A. V., O. N. Breusov, A. N. Dremin, S. V. Pershin, and V. F. Tatsil, 1974, Combust. Explos. Shock Waves **10**, 372.

Anderson, D. L., and H. Kanamori, 1968, J. Geophys. Res. **73**, 6477.

Andrews, D. J., 1970, Ph.D. thesis, Washington State University.

Andrews, D. J., 1971, J. Comput. Phys. **7**, 310.

Andrews, D. J., 1973, J. Phys. Chem. Solids **34**, 825.

Asay, J. R., 1974, J. Appl. Phys. **45**, 4441.

Asay, J. R., 1977, J. Appl. Phys., accepted for publication.

Asay, J. R., and D. B. Hayes, 1975, J. Appl. Phys. **46**, 4789.

Balchan, A. S., 1963, J. Appl. Phys. **34**, 241.

Balchan, A. S., and H. G. Drickamer, 1961, Rev. Sci. Instrum. **32**, 308.

Bancroft, D., E. L. Peterson, and S. Minshall, 1956, J. Appl. Phys. **27**, 291.

Band, W., and G. E. Duvall, 1961, Am. J. Phys. **29**, 780.

Banks, E. E., 1968, J. Iron Steel Inst. **206**, 1022.

Banus, M. D., 1969, High Temp.-High Pressures **1**, 483.

Barker, L., 1975, J. Appl. Phys. **46**, 2544.

Barker, L. M., and R. E. Hollenbach, 1964, Rev. Sci. Instrum. **35**, 742.

Barker, L. M., and R. E. Hollenbach, 1970, J. Appl. Phys. **41**, 4208.

Barker, L., and R. E. Hollenbach, 1972, J. Appl. Phys. **43**, 4669.

Barker, L., and R. E. Hollenbach, 1974, J. Appl. Phys. **45**, 4872.

Barskii, I. M., V. Y. Dikovskii, and A. I. Matysin, 1972, Combust. Explos. Shock Waves **8**, 474.

Bassett, W. A., T. Takahashi, H. Mao, and J. S. Weaver, 1968, J. Appl. Phys. **39**, 319.

Bassett, W. A., and J. D. Barnett, 1970, Phys. Earth Planet. Inter. **3**, 54.

Batsanov, S. S., G. E. Blokhina, and A. A. Deribas, 1965, J. Struct. Chem. **6**, 209.

Batsanov, S. S., 1968, in *Behavior of Dense Media Under High Dynamic Pressures* (Gordon and Breach, New York), p. 371.

Batsanov, S. S., G. S. Doronin, E. M. Moroz, I. A. Ovsyannikova, and O. I. Ryabinina, 1969, Combust. Explos. Shock Waves **5**, 193.

Belyakov, L. V., V. P. Valitskii, N. A. Zlatin, 1965, Sov. Phys.—Dokl. **10**, 69.

Belyakov, L. V., V. P. Valitskii, N. A. Zlatin, and S. M. Mochalov, 1967, Sov. Phys.—Dokl. **11**, 808.

Benedick, W. B., 1965, Rev. Sci. Instrum. **36**, 1309.

Berger, M. J., S. Joigneau, and M. G. Bottet, 1960, C. R. Acad. Sci. (Paris) **250**, 4331.

Berger, J., S. Joigneau, and C. Fauquignon, 1962, in *Les Ondes de Detonation* (Centre de la Recherche Scientifique 15, Quai Anatole-France, Paris), p. 353.

Bertholf, L. D., L. D. Buxton, B. J. Thorne, R. K. Byers, A. L. Stevens, and S. L. Thompson, 1975, J. Appl. Phys. **46**, 3776.

Bethe, H. A., 1942, Office of Scientific Research and Development Report No. 545, Serial No. 237.

Blackburn, L. D., L. Kaufman, and M. Cohen, 1965, Acta Metall. **13**, 533.

Boreskov, G., I. Sazonova, N. Keyer, V. Kudinov, G. Gridasova, V. Maly, and L. Kefely, 1968, in *Behavior of Dense Media Under High Dynamic Pressures* (Gordon and Breach, New York), p. 389.

Brazhnik, M. I., L. V. Al'tshuler, and L. A. Tarasova, 1969, Combust. Explos. Shock Waves **5**, 352.

Breed, B. R., and D. Venable, 1968, J. Appl. Phys. **39**, 3222.

Bridgman, P. W., 1935, Phys. Rev. **48**, 893.

Bridgman, P. W., 1942, Proc. Am. Acad. Arts. Sci. **74**, 425.

Bridgman, P. W., 1948, Proc. Am. Acad. Arts. Sci. **76**, 71.

Bridgman, P. W., 1956, J. Appl. Phys. **27**, 659.

Bundy, F. P., 1958, Phys. Rev. **110**, 314.

Bundy, F. P., 1965, J. Appl. Phys. **36**, 616.

Bundy, F. P., 1967, J. Appl. Phys. **38**, 2446.

Bundy, F. P., 1975, Rev. Sci. Instrum. **46**, 1318.

Bundy, F. P., and R. H. Wentorf, Jr., 1963, J. Chem. Phys. **38**, 1144.

Carter, W. J., 1973a, in *Metallurgical Effects at High Strain Rates*, edited by R. W. Rohde, B. M. Butcher, J. R. Holland, and C. H. Karnes (Plenum, New York), p. 171.

Carter, W. J., 1973b, in *Phase Transitions—1973 Proceedings of the Conference on Phase Transitions and Their Applications in Materials Science*, edited by L. E. Cross (Pergamon, New York), p. 223.

Champion, A. R., 1971, J. Appl. Phys. **42**, 5546.

Chao, E. C. T., 1967, Science **156**, 192.

Chao, E. C. T., E. M. Shoemaker, and B. M. Madsen, 1960, Science **132**, 220.

Chao, E. C. T., J. J. Fahey, J. Littler, D. J. Milton, 1962, Am. Mineral. **47**, 807.

Christian, J. W., 1965, *The Theory of Transformation in Metals and Alloys* (Pergamon, New York).

Christian, Russell H., 1957, "The Equation of State of the Alkali Halides at High Pressure," Lawrence Livermore Laboratory Report No. UCRL-4900. Also available as a doctoral thesis from University of California, Berkeley.
Christou, A., 1972, Phil. Mag. **26**, 97.
Christou, A., 1973, Phil. Mag. **27**, 833.
Christou, A., and N. Brown, 1971, J. Appl. Phys. **42**, 4160.
Claussen, W. F., 1961, in *Progress in Very High Pressure Research* (Wiley, New York), p. 193.
Claussen, W. F., 1963, in *High Pressure Measurement*, edited by A. A. Giardini and E. C. Lloyd (Butterworths, Washington, D. C.), p. 125.
Clendenen, R. L., and H. G. Drickamer, 1964, J. Phys. Chem. Solids **25**, 865.
Clougherty, E. V., and L. Kaufman, 1963, in *High Pressure Measurement*, edited by A. A. Giardini and E. C. Lloyd (Butterworths, Washington, D. C.), p. 152.
Coes, L., Jr., 1953, Science **118**, 131.
Cohen, L. H., and W. Klement, Jr., 1967, J. Geophys. Res. **72**, 4245.
Cole, T. T., and J. W. Lyle, 1971, Rev. Sci. Instrum. **42**, 1258.
Coleburn, N. L., 1964, J. Chem. Phys. **40**, 71.
Coleburn, N. L., and J. W. Forbes, 1968, J. Chem. Phys. **48**, 555.
Coleburn, N. L., J. W. Forbes, and H. D. Jones, 1972, J. Appl. Phys. **43**, 5007.
Cook, M. A., and L. A. Rodgers, 1963, J. Appl. Phys. **34**, 2330.
Corll, J. A., and G. A. Samara, 1966, Solid State Commun. **4**, 283.
Courant, R., and K. O. Friedrichs, 1948, *Supersonic Flow and Shock Waves* (Interscience, New York).
Cowperthwaite, M., 1966, Am. J. Phys. **34**, 1025.
Curran, D. R., 1961, J. Appl. Phys. **32**, 1811.
Curran, D. R., 1971, in *Shock Waves and the Mechanical Properties of Solids*, edited by J. J. Burke and V. Weiss (Syracuse University, New York), p. 121.
Curran, D. R., S. Katz, J. J. Kelly, and M. E. Nicholson, 1959, Trans. Metall. Soc. AIME (Am. Inst. Min. Metall. Pet. Eng.) **215**, 151.
Dandekar, D. P., and G. E. Duvall, 1973, in *Metallurgical Effects at High Strain Rates*, edited by R. W. Rohde, B. M. Butcher, J. R. Holland, and C. H. Karnes (Plenum, New York), p. 185.
Darnel, A. J., and W. A. McCollum, 1970, High Temp. Sci. **2**, 331.
Darnel, A. J., and W. A. McCollum, 1971, High Temp. Sci. **3**, 73.
David, H. G., and S. D. Hamann, 1958, J. Chem. Phys. **28**, 1006.
Davies, G. F., 1972, J. Geophys. Res. **77**, 4920.
Davis, W. C., and B. G. Craig, 1961, Rev. Sci. Instrum. **32**, 579.
Deal, W. E., Jr., 1962, in *Modern Very High Pressure Techniques*, edited by R. H. Wentorf, Jr. (Butterworths, Washington, D. C.), p. 200.
DeCarli, P. S., 1966, Method of Making Diamond, U. S. Patent 3,238,019.
DeCarli, P. S., 1967, in *Science and Technology of Industrial Diamonds, Vol. I*, edited by J. Burls (Industrial Diamond Information Bureau, London).
DeCarli, P. S., 1976, Stanford Research Institute, private communication.
DeCarli, P. S., and J. C. Jamieson, 1959, J. Chem. Phys. **31**, 1675.
DeCarli, P. S., and J. C. Jamieson, 1961, Science **133**, 1821.
DeCarli, P. S., and D. J. Milton, 1965, Science **147**, 144.
Decker, D. L., 1971, J. Appl. Phys. **42**, 3239.
Deribas, A., N. Dobretsov, V. Kudinov, V. Maly, A. Serebrjakov, and A. Stauer, 1968, in *Behavior of Dense Media Under High Dynamic Pressures* (Gordon and Breach, New York), p. 385.
Dick, J. J., and D. L. Styris, 1975, J. Appl. Phys. **46**, 1602.
Dick, R. D., 1964, Bull. Am. Phys. Soc. **9**, 547.
Dick, R. D., 1970, J. Chem. Phys. **52**, 6021.
Doran, D. G., 1963a, in *High Pressure Measurement*, edited by A. A. Giardini and E. C. Lloyd (Butterworths, Washington, D. C.), p. 59.
Doran, D. G., 1963b, J. Appl. Phys. **34**, 844.
Doran, D. G., 1968, J. Appl. Phys. **39**, 40.
Doran, D. G., and T. J. Ahrens, 1963, Stanford Research Institute Final Report, PGU-4100, Contract DA-04-200-ORD-1279, Ballistics Research Laboratory, 31 August.
Dremin, A. N., S. V. Pershin, and V. F. Pogorelov, 1965, Combust. Explos. Shock Waves **1**, 1.
Dremin, A. N., and S. V. Pershin, 1968, Combust. Explos. Shock Waves **4**, 66.
Drickamer, H. G., 1970, Rev. Sci. Instrum. **41**, 1667.
Drummond, W. E., 1957, J. Appl. Phys. **28**, 998.
Duff, R. E., and F. S. Minshall, 1957, Phys. Rev. **108**, 1207.
Duff, R. E., W. H. Gust, E. B. Royce, M. Ross, A. C. Mitchell, R. N. Keeler, and W. G. Hoover, 1968, in *Behavior of Dense Media Under High Dynamic Pressures* (Gordon and Breach, New York), p. 397.
Dublin, I. N., L. V. Al'tshuler, V. Ya Vashchenko, and V. N. Zubarev, 1969, Sov. Phys.—Solid State **11**, 1016.
Duvall, G. E., 1962, in *Les Ondes de Detonation* (Centre National de la Recherche Scientifique, 15 Quai Anatole-France, Paris), p. 337.
Duvall, G. E., 1964, in *Dynamic Response of Materials to Intense Impulsive Loading*, edited by P. C. Chou and A. K. Hopkins (Air Force Materials Laboratory, Ohio), Chap. 4, p. 89.
Duvall, G. E., 1968, in *Shock Metamorphism of Natural Materials*, edited by B. M. French and N. M. Short (Mono Book Corp, Baltimore), p. 19.
Duvall, G. E., 1973, Semiannual Report, 1 February 1973 to 31 July 1973, Contract No. DAAG-46-73-C-0104, AMMRC, Watertown, Ma.
Duvall, G. E., 1976, in *Propagation of Shock Waves in Solids AMD, Vol. 17*, edited by E. Varley (The American Society of Mechanical Engineers, New York), p. 97.
Duvall, G. E., and G. R. Fowles, 1963, in *High Pressure Physics and Chemistry Vol. 2*, edited by R. S. Bradley (Academic, New York), p. 209.
Duvall, G. E., and Y. Horie, 1965, in *Fourth Symposium on Detonation*, edited by S. J. Jacobs, Office of Naval Research Report ACR-126, p. 248.
Duvall, G. E., and B. J. Zwolinskii, 1955, J. Acoust. Soc. Am. **27**, 1054.
Ebert, H., and A. Kussman, 1937, Phys. Z. **38**, 437.
Eden, G., and P. W. Wright, 1965, in *Fourth Symposium on Detonation*, edited by S. J. Jacobs, Office of Naval Research Report ACR-126, p. 573.
Edwards, L. R., 1976, private communication.
Edwards, L. R., and L. C. Bartel, 1974, Phys. Rev. B **10**, 2044.
Evdokimova, V. V., and L. F. Vereshchagin, 1963a, Sov. Phys.—JETP **16**, 855.
Evdokimova, V. V., and L. F. Vereshchagin, 1963b, Sov. Phys.—Solid State **4**, 1438.
Erkman, J. O., 1961, J. Appl. Phys. **32**, 939.
Flinn, J. E., G. E. Duvall, G. R. Fowles, and R. F. Tinder, 1975, J. Appl. Phys. **46**, 3752.
Forbes, J. W., 1976, Ph.D. thesis, Washington State University.
Forbes, J. W., and G. E. Duvall, 1975, in *Proceedings of the Fourth International Conference on High Pressure, Kyoto, 1974*, edited by J. Osugi (The Physico-Chemical Society of Japan, Kyoto), p. 480.
Fournier, C., and A. Oberlin, 1971, C. R. Acad. Sci. (Paris) **272**, 977.

Fowler, C. M., F. S. Minshall, and E. G. Zukas, 1961, in *Response of Metals to High Velocity Deformation*, edited by P. G. Shewmon and Z. F. Zackay (Interscience, New York), p. 275.
Fowles, G. R., 1962, Ph.D. thesis, Stanford University.
Fowles, G. R., 1967, J. Geophys. Res. **72**, 5729.
Fowles, G. R., 1973, in *Dynamic Response of Materials to Intense Impulsive Loading*, edited by P. C. Chou and A. K. Hopkins (Air Force Materials Laboratory, Ohio), p. 405.
Fowles, G. R., 1976, Phys. Fluids, **19**, 227.
Fowles, G. R., G. E. Duvall, J. Asay, P. Bellamy, F. Feistmann, D. Grady, T. Michaels, and R. Mitchell, 1970, Rev. Sci. Instrum. **41**, 984.
Fritz, J. N., S. P. Marsh, W. J. Carter, and R. G. McQueen, 1971, in *Accurate Characterization of the High-Pressure Environment*, edited by E. C. Lloyd, National Bureau of Standards Special Publication 326 (U. S. Government Printing Office), p. 201.
Fuller, P. J. A., and J. H. Price, 1962, Nature (Lond.) **193**, 262.
Gauster, W. B., F. C. Perry, and W. H. Buckalew, 1973, J. Appl. Phys. **44**, 4970.
German, V. N., A. A. Bakanova, L. A. Tarasova, and Yu. N. Sumulov, 1970a, Sov. Phys.—Solid State **12**, 490.
German, V. N., M. P. Speranskaya, L. V. Al'tshuler, and L. A. Tarasova, 1970b, Phys. Met. Metallogr. **30**, No. 5, 124.
German, V. N., M. A. Podurets, and R. F. Trunin, 1973, Sov. Phys.—JETP **37**, 107.
Giardini, A. A., and G. A. Samara, 1965, J. Phys. Chem. Solids **26**, 1523.
Gibbs, J. W., 1925, *The Collected Papers of J. Willard Gibbs*, Introductory Note by W. R. Longley and R. G. Van Name (Yale University, New Haven), p. 1.
Giles, P. M., M. H. Longenbach, and A. R. Marder, 1971, J. Appl. Phys. **42**, 4290.
Giles, P. M., and A. R. Marder, 1971, Trans. Metall. Soc. AIME (Am. Inst. Min. Metall. Pet. Eng.) **2**, 1371.
Ginsberg, M. J., D. E. Grady, P. S. DeCarli, and J. T. Rosenberg, 1973, Stanford Research Institute Report DNA 3577F, August.
Glass, I. I., 1974, *Shock Waves and Man* (University of Toronto Institute for Aerospace Studies, Toronto).
Goranson, R. W., D. Bancroft, B. L. Burton, T. Blechar, E. E. Houston, E. F. Gittings, and S. A. Landeen, 1955, J. Appl. Phys. **26**, 1472.
Goto, T., Y. Syono, J. Nakai, and Y. Nakagawa, 1976, Solid State Commun. **18**, 1607.
Grady, D. E., 1976, in *Proceedings of the United States–Japan Seminar on High Pressure Research Applications and Geophysics, July 6–9, 1976*, in press.
Grady, D. E., 1977, in *High Pressure Research Applications in Geophysics*, edited by M. H. Manghnani and S. Akimoto (Academic, New York), p. 389.
Graham, R. A., 1967, J. Basic Eng. **89**, 911.
Graham, R. A., 1968, J. Appl. Phys. **39**, 437.
Graham, R. A., 1971, J. Acoust. Soc. Am. **51**, 1576.
Graham, R. A., 1974, J. Phys. Chem. Solids **35**, 355.
Graham, R. A., 1975, J. Appl. Phys. **46**, 1901.
Graham, R. A., F. W. Neilson, and W. B. Benedick, 1965, J. Appl. Phys. **36**, 1775.
Graham, R. A., O. E. Jones, and J. R. Holland, 1966, J. Phys. Chem. Solids **27**, 1519.
Graham, R. A., D. H. Anderson, and J. R. Holland, 1967, J. Appl. Phys. **38**, 223.
Graham, R. A., and G. E. Ingram, 1968, in *Behavior of Dense Media Under High Dynamic Pressures* (Gordon and Breach, New York), p. 469.
Graham, R. A., and W. P. Brooks, 1971, J. Phys. Chem. Solids **32**, 2311.
Graham, R. A., and R. D. Jacobson, 1973, Appl. Phys. Lett. **23**, 584.
Graham, R. A., and J. R. Asay, 1977, "Measurement of wave profiles in shock loaded solids," submitted to High Temp–High Pressures.
Grigor'ev, F. V., S. B. Kormer, O. L. Mikhailov, A. P. Tolochko, and V. D. Urlin, 1972, JETP Lett. **16**, 201.
Grover, R., R. H. Christian, and B. J. Alder, 1958, Bull. Am. Phys. Soc. **3**, 230.
Grover, R., and P. A. Urtiew, 1974, J. Appl. Phys. **45**, 146.
Gupta, Y. M., and G. E. Duvall, 1975, Bull. Am. Phys. Soc. **20**, 1513.
Gugan, D., 1958, Proc. Phys. Soc. Lond. **72**, 1013.
Gust, W. H., and E. B. Royce, 1970, J. Appl. Phys. **41**, 2443.
Gust, W. H., and E. B. Royce, 1971, J. Appl. Phys. **42**, 1897.
Gust, W. H., and E. B. Royce, 1972, J. Appl. Phys. **43**, 4437.
Gust, W. H., and D. A. Young, 1977, Phys. Rev. B, in press.
Halpin, W. J., O. E. Jones, and R. A. Graham, 1963, in *Symposium on Dynamic Behavior of Materials*, ASTM Special Technical Publication No. 336 (American Society for Testing and Materials, Philadelphia), p. 208.
Hanneman, R. E., M. D. Banus, and H. L. Gatos, 1964, J. Phys. Chem. Solids **25**, 293.
Haussühl, S., 1960, Z. Phys. **159**, 223.
Hauver, G. E., 1966a, Ballistics Research Laboratory, private communication.
Hauver, G. E., 1966b, Ballistics Research Laboratory Technical Note No. 1628.
Hauver, G. E., and A. Melani, 1964, Ballistics Research Laboratory Report No. 1259.
Hauver, G. E., and A. Melani, 1970, Ballistics Research Laboratory Memorandum Report No. 2061.
Hawke, R. S., 1977, Lawrence Livermore Laboratory, private communication.
Hawke, R. S., D. E. Duerre, J. G. Huebel, and H. Klapper, 1972, Phys. Earth Planet. Interiors **6**, 44.
Hayes, D. B., 1972, Ph.D. thesis, Washington State University.
Hayes, D. B., 1974, J. Appl. Phys. **45**, 1208.
Hayes, D. B., 1975, J. Appl. Phys. **46**, 3438.
Hayes, D. B., 1977, "The Kinetics of Shock-Induced Polymorphic Phase Transitions," Sandia Laboratories Report SAND 77-0267.
Heydemann, P. L. M., 1967a, J. Appl. Phys. **38**, 2640.
Heydemann, P. L. M., 1967b, J. Appl. Phys. **38**, 3424.
Hord, L., 1975, Lawrence Livermore Laboratory H-Division Quarterly Report 24, UCRL 50028-75-3, July–September, p. 24.
Horie, Y., 1967, J. Phys. Chem. Solids **28**, 1569.
Horie, Y., and G. E. Duvall, 1968a, in *Behavior of Dense Media Under High Dynamic Pressures* (Gordon and Breach, New York), p. 355.
Horie, Y., and G. E. Duvall, 1968b, *Proceedings of the Army Symposium on Solid Mechanics*, The Johns Hopkins University, Baltimore, Md., 10–11 September (AMMRC Report MS-68-09, September 1968), available from Army Materials and Mechanics Research Center, Watertown, Ma. 02172.
Hornung, K., and K. W. Michel, 1972, J. Chem. Phys. **56**, 2072.
Hughes, D. S., L. E. Gourley, and M. F. Gourley, 1961, J. Appl. Phys. **32**, 624.
Ingram, G. E., and R. A. Graham, 1970, in *Fifth Symposium on Detonation*, Office of Naval Research Report ACR-184 (U. S. Government Printing Office), p. 369.
Isbell, W. M., F. H. Shipman, and A. H. Jones, 1968, in *Behavior of Dense Media Under High Dynamic Pressures* (Gordon and Breach, New York), p. 179.
Ivanov, A. G., S. A. Novikov, and Yu. I. Tarasov, 1962, Sov. Phys–Solid State **4**, 177.
Ivanov, A. G., and S. A. Novikov, 1963, Instrum. Exp. Tech., No. 1, 128.
Jacquesson, J., J. P. Romain, M. Hallouin, and J. C. Desoyer,

1970, in *Fifth Symposium on Detonation*, Office of Naval Research Report ACR-184 (U. S. Government Printing Office), p. 403.
Jamieson, J. C., 1963a, Science **139**, 762.
Jamieson, J. C., 1963b, in *High Pressure Measurement*, edited by A. A. Giardini and E. C. Lloyd (Butterworths, Washington, D. C.), p. 165.
Jamieson, J. C., and A. W. Lawson, 1962, J. Appl. Phys. **33**, 776.
Jamieson, J. C., and B. Olinger, 1971, in *Accurate Characterization of the High Pressure Environment*, edited by E. C. Lloyd, National Bureau of Standards Special Publication 326, p. 321.
Johnson, J. N., 1972, Sandia Laboratories Report SC-RR-72 0626, September.
Johnson, J. N., D. B. Hayes, and J. R. Asay, 1974, J. Phys. Chem. Solids **35**, 501.
Johnson, P. C., B. A. Stein, and R. S. Davis, 1962, J. Appl. Phys. **33**, 557.
Johnson, Q., 1966, Science **153**, 419.
Johnson, Q., A. Mitchell, R. N. Keller, and L. Evans, 1970, Phys. Rev. Lett. **25**, 1099.
Johnson, Q., A. Mitchell, and L. Evans, 1971, Nature (Lond.) **231**, 310.
Johnson, Q., A. Mitchell, and L. Evans, 1972, Appl. Phys. Lett. **21**, 29.
Johnson, Q., and A. Mitchell, 1972, Phys. Rev. Lett. **29**, 1369.
Jones, A. H., 1975, Terra Tek, Inc., Salt Lake City, private communication.
Jones, A. H., W. M. Isbell, and C. J. Maiden, 1966, J. Appl. Phys. **37**, 3493.
Jones, O. E., and R. A. Graham, 1971, in *Accurate Characterization of the High Pressure Environment*, edited by E. C. Lloyd, National Bureau of Standards Special Publication 326, p. 229.
Kabalkina, S. S., and Z. V. Troitskaya, 1964, Sov. Phys.—Dokl. **8**, 800.
Kabalkina, S. S., T. N. Kolobyanina, and L. F. Vereshchagin, 1970, Sov. Phys.—JETP **31**, 259.
Kamegai, M., 1975, J. Appl. Phys. **46**, 1618.
Kasper, J. S., and H. Brandhorst, 1964, J. Chem. Phys. **41**, 3768.
Kasper, J. S., and S. M. Richards, 1964, Acta Crystallogr. **17**, 752.
Katz, S., 1955, Phys. Rev. **100**, 1800.
Katz, S., D. G. Doran, and D. R. Curran, 1959, J. Appl. Phys. **30**, 568.
Kaufman, L., 1961, in *Response of Metals to High Velocity Deformation*, edited by P. G. Shewman and V. F. Zackay (Interscience, New York), p. 300.
Kaufman, L., 1969, in *Progress in Materials Science Vol. 14*, edited by O. Kubaschewski and W. Slough (Pergamon, Oxford), p. 55.
Kaufman, L., and H. Bernstein, 1970, *Computer Calculations of Phase Diagrams* (Academic, New York).
Keeler, R. N., and A. C. Mitchell, 1969, Solid State Commun. **7**, 271.
Kennedy, G. C., and R. C. Newton, 1961, J. Geophys. Res. **66**, 1491.
Kennedy, G. C., and R. C. Newton, 1963, in *Solids Under Pressure*, edited by W. Paul and D. M. Warschauer (McGraw-Hill, New York), p. 163.
Kennedy, J. D., and W. B. Benedick, 1965, Bull. Am. Phys. Soc. **10**, 1112.
Kennedy, J. D., and W. B. Benedick, 1966, J. Phys. Chem. Solids **27**, 125.
Keough, D. D., and J. Y. Wong, 1970, J. Appl. Phys. **41**, 3508.
Khristoforov, B. D., E. E. Goller, Y. Sidorin, and L. D. Livshits, 1971, Combust. Explos. Shock Waves **4**, 525.
Kirkinsky, V. A., 1968, in *Behavior of Dense Media Under High Dynamic Pressures* (Gordon and Breach, New York), p. 367.
Klement, W., Jr., A. Jayaraman, and G. C. Kennedy, 1963, Phys. Rev. **131**, 632.
Klement, W., Jr., and A. Jayaraman, 1967, in *Progress in Solid State Chemistry, Vol. 3*, edited by H. Reiss (Pergamon, New York), p. 289.
Kondo, K., A. Sawaoka, and S. Saito, 1975, in *Proceedings of the Fourth International Conference on High Pressure, Kyoto*, 1974, edited by J. Osugi (The Physico-Chemical Society of Japan, Kyoto), p. 845.
Kondorsky, E. I., and V. L. Sedov, 1960, J. Appl. Phys. Suppl. **31**, 331S.
Kormer, S. B., 1968, Sov. Phys. Uspeki **11**, 229.
Kormer, S. B., M. V. Sinitsyn, A. I. Funtikov, V. D. Urlin, and A. V. Blinov, 1965a, Sov. Phys.—JETP **20**, 811.
Kormer, S. B., M. V. Sinitsyn, G. A. Kirillov, and V. D. Urlin, 1965b, Sov. Phys.—JETP **21**, 689.
Kormer, S. B., K. B. Yushko, and G. V. Kirshkevich, 1966, JETP Lett. **3**, 39.
Kormer, S. B., K. B. Yushko, and G. V. Kirshkevich, 1968, Sov. Phys.—JETP **27**, 879.
Kouvel, J. S., 1963, in *Solids Under Pressure*, edited by W. Paul and D. M. Warschauer (McGraw-Hill, New York), p. 277.
Kouvel, J. S., and R. H. Wilson, 1961, J. Appl. Phys. **32**, 435.
Krupnikov, K. K., A. A. Bakanova, M. I. Brazhnik, and R. F. Trunin, 1963, Sov. Phys.—Dokl. **8**, 205.
Kuleshova, L. V., 1969, Sov. Phys.—Solid State **11**, 886.
Larson, D. B., 1965, in *Physics of Solids at High Pressures*, edited by C. T. Tomizuka and R. M. Emrick (Academic, New York), p. 459.
Larson, D. B., 1967, J. Appl. Phys. **38**, 1541.
Larson, D. B., R. N. Keeler, A. Kusubov, and B. L. Hord, 1966, J. Phys. Chem. Solids **27**, 476.
Leger, J. M., C. Susse, and B. Vodar, 1971, in *Accurate Characterization of the High-Pressure Environment*, edited by E. C. Lloyd, National Bureau of Standards Special Publication 326, p. 251.
Lethaby, J. W., and I. C. Skidmore, 1959, S. W. A. Branch Note No. 3, AWRE (England).
Leiserowitz, L., G. M. J. Schmidt, and A. Shamgar, 1966, J. Phys. Chem. Solids **27**, 1453.
Linde, R. K., and D. N. Schmidt, 1966, Rev. Sci. Instrum. **37**, 1.
Linde, R. K., and P. S. DeCarli, 1969, J. Chem. Phys. **50**, 319.
Lipschutz, M. E., 1964, Science **143**, 1431.
Lipschutz, M. E., 1968, in *Shock Metamorphism of Natural Materials*, edited by B. M. French and N. M. Short (Mono Book Corp., Baltimore), p. 571.
Liu, C. Y., K. Ishizaki, J. Paauwe, and I. L. Spain, 1973, High Temp.-High Pressures **5**, 359.
Loree, T. R., C. M. Fowler, E. G. Zukas, and F. S. Minshall, 1966a, J. Appl. Phys. **37**, 1918.
Loree, T. R., R. H. Warnes, E. G. Zukas, and C. M. Fowler, 1966b, Science **153**, 1277.
Los Alamos, Group GMX-6, 1969, Los Alamos Scientific Laboratory Report LA-4167-MS, "Selected Hugoniots."
Lubkin, G. B., 1976, "Search and Discovery News" note, Phys. Today **26**, No. 3, 17.
Lysne, P. C., 1971, J. Chem. Phys. **55**, 5242.
Lysne, P. C., 1975, J. Appl. Phys. **46**, 4078.
Lysne, P. C., 1977, J. Appl. Phys. **48**, 1020.
Lysne, P. C., and L. C. Bartel, 1975, J. Appl. Phys. **46**, 222.
Mao, H. K., W. A. Bassett, and T. Takahashi, 1967, J. Appl. Phys. **38**, 272.
McDonald, T. T., E. Gregory, G. S. Barberich, D. B. McWhan, T. H. Geballe, and G. W. Hull, Jr., 1965, Phys. Lett. **14**, 16.
McQueen, R. G., 1964, in *Metallurgy at High Pressures and High Temperatures*, edited by K. Gschneider, Jr., M. T.

Hepworth and N. A. D. Parlee (Gordon and Breach, New York), p. 44.
McQueen, R. G., W. J. Carter, J. N. Fritz, and S. P. Marsh, 1971, in *Accurate Characterization of the High Pressure Environment*, edited by E. C. Lloyd, National Bureau of Standards Special Publication 326, U. S. Government Printing Office, p. 219.
McQueen, R. G., and S. P. Marsh, 1960, J. Appl. Phys. **31**, 1253.
McQueen, R. G., J. N. Fritz, and S. P. Marsh, 1963, J. Geophys. Res. **68**, 2319.
McQueen, R. G., J. C. Jamieson, and S. P. Marsh, 1967, Science **155**, 1401.
McQueen, R. G., and S. P. Marsh, 1968, in *Behavior of Dense Media Under High Dynamic Pressures* (Gordon and Breach, New York), p. 207.
McQueen, R. G., S. P. Marsh, J. W. Taylor, J. N. Fritz, and W. J. Carter, 1970, in *High Velocity Impact Phenomena*, edited by R. Kinslow (Academic, New York), p. 293.
McMahan, A. K., M. Ross, and R. Grover, 1975, Bull. Am. Phys. Soc. **20**, 1514.
McWhan, D. B., 1967, J. Appl. Phys. **38**, 347.
Millet, L. E., and D. L. Decker, 1969, Phys. Lett. A **29**, 7.
Mineev, V. N., and E. V. Savinov, 1967, Sov. Phys.—JETP **25**, 411.
Mineev, V. N., A. G. Ivanov, V. V. Lisitsyn, E. Z. Novitskii, and Y. N. Tyunyaev, 1971, Sov. Phys.—JETP **32**, 592.
Minomura, S., and H. G. Drickamer, 1962, J. Phys. Chem. Solids **23**, 451.
Minshall, S., 1955a, Phys. Rev. **98**, 271.
Minshall, S., 1955b, J. Appl. Phys. **26**, 463.
Minshall, S., 1961, in *Response of Metals to High Velocity Deformation*, edited by P. G. Shewmon and V. F. Zackay (Interscience, New York), p. 249.
Mitchell, A. C., Q. Johnson, and L. Evans, 1973a, Rev. Sci. Instrum. **44**, 597.
Mitchell, A. C., Q. Johnson, and L. Evans, 1973b, in *Advances in X-Ray Analysis Vol. 16*, edited by L. S. Birks, C. S. Barrett, J. B. Newkirk, and C. O. Ruud (Plenum, New York), p. 242.
Neilson, F. W., W. B. Benedick, W. P. Brooks, R. A. Graham, and G. W. Anderson, 1962, in *Les Ondes de Detonation* (Centre National de la Recherche Scientifique, 15, Quai Anatole-France, Paris), p. 391.
Novikov, I., I. Divnov, and A. G. Ivanov, 1965, Sov. Phys.—JETP **20**, 545.
Novikov, V. V., and V. N. Mineev, 1974, Sov. Phys.—JETP **4**, 717.
O'Brien, J. L., and R. S. Davis, 1961, in *Response of Metals to High Velocity Deformation*, edited by P. G. Shewman and V. F. Zackay (Interscience, New York), p. 371.
Otto, G., O. Y. Reece, and U. Roy, 1971, Appl. Phys. Lett. **18**, 418.
Panova, G. K., S. S. Sekoyan, and L. F. Vereshchagin, 1961, Phys. Met. Metallogr. **11**, No. 2, 61.
Parsons, C. A., 1920, Philos. Trans. R. Soc. Lond. **A220**, 67.
Paterson, M. S., 1973, Rev. Geophys. and Space Phys. **11**, 355.
Pavlovskii, M. N., 1968, Sov. Phys.—Solid State **9**, 2514.
Pavlovskii, M. N., 1971, Sov. Phys.—Solid State **13**, 741.
Pavlovskii, M. N., and V. P. Drakin, 1966, Sov. Phys.—JETP **4**, 116.
Peyre, C., J. Pujol, and J. Thouvenin, 1965, in *Fourth Symposium on Detonation*, edited by S. Jacobs, Office of Naval Research ACR-126, 566.
Pipkorn, D. N., C. K. Edge, P. Debrunner, G. De Pasquali, H. G. Drickamer, and H. Frauenfelder, 1964, Phys. Rev. **135**, A1604.
Pistorius, C. W. F. T., 1964, J. Phys. Chem. Solids **25**, 1477.
Podurets, A. M., and R. F. Trunin, 1971, Sov. Phys.—Dokl. **15**, 1117.
Podurets, A. M., and R. F. Trunin, 1974, Bull. Acad. Sci. USSR, Physics of the Solid Earth No. 7, p. 427.
Pope, L. E., and L. R. Edwards, 1973, Acta Metall. **21**, 281.
Pope, L. E., and W. E. Warren, 1974, Acta Metall. **22**, 751.
Pope, L. E., and J. N. Johnson, 1975, J. Appl. Phys. **46**, 720.
Pospelov, Yu. A., and N. N. Kuzin, 1966, Sov. Phys.—Solid State **8**, 134.
Primak, W., 1975, *The Compacted States of Vitreous Silica* (Gordon and Breach, New York), p. 81.
Pujols, H., and F. Boisard, 1970, Carbon **8**, 781.
Reynolds, C. E., and G. E. Seay, 1961, J. Appl. Phys. **32**, 1401.
Reynolds, C. E., and G. E. Seay, 1962, J. Appl. Phys. **33**, 2234.
Riabinin, I. N., 1956, Sov. Phys.—Tech. Phys. **1**, 2575.
Rice, M. H., 1961, Rev. Sci. Instrum. **32**, 449.
Rice, M. H., and J. M. Walsh, 1957, J. Chem. Phys. **26**, 824.
Rice, M. H., R. G. McQueen, and J. M. Walsh, 1958, in *Solid State Physics Vol. VI*, edited by F. Seitz and D. Turnbull (Academic, New York), p. 1.
Rinehart, J. S., and J. Pearson, 1954, *Behavior of Metals Under Impulsive Loads* (American Society of Metals, Cleveland).
Ritter, J. R., Jr., 1973, J. Chem. Phys. **59**, 1538.
Robin, P. Y. F., 1974, Am. Mineral. **59**, 1286.
Rohde, R. W., 1970, Acta Metall. **18**, 903.
Rohde, R. W., J. R. Holland, and R. A. Graham, 1968, Trans. Metall. Soc. AIME (Am. Inst. Min. Metall. Pet. Eng.) **242**, 2017.
Rohde, R. W., and R. A. Graham, 1969, Trans. Metall. Soc. AIME (Am. Inst. Min. Metall. Pet. Eng.) **245**, 2441.
Rohde, R. W., and C. E. Albright, 1971, Scr. Metall. **5**, 151.
Rohde, R. W., and R. A. Graham, 1973, Phil. Mag. **28**, 941.
Romain, J. P., 1974, J. Appl. Phys. **45**, 135.
Rooymans, C. J. M., 1969, in *Advances in High Pressure Research*, Vol. 2, edited by R. S. Bradley (Academic, New York), p. 1.
Ross, Marvin, 1974, J. Chem. Phys. **60**, 3634.
Ross, M., F. H. Ree, and R. N. Keeler, 1975, in *Proceedings of the Fourth International Conference on High Pressure, Kyoto, Japan*, edited by J. Osugi (The Physico-Chemical Society of Japan, Kyoto), p. 852.
Roy, R., 1969, in *Reactivity of Solids*, Proceedings of the Sixth International Symposium on the Reactivity of Solids, Schenectady, New York, 25–30 August 1968, edited by J. W. Mitchell, R. C. DeVries, R. W. Roberts, and P. Cannon (Wiley, New York), p. 777.
Roy, R., and H. M. Cohen, 1961, Nature (Lond.) **190**, 798.
Royce, E. B., 1968, in *Behavior of Dense Media Under High Dynamic Pressures* (Gordon and Breach, New York), p. 419.
Royce, E. B., 1969, Lawrence Radiation Laboratory Report UCID-15454, January.
Ruchkin, E. D., I. A. Ovsjannikova, and S. S. Batsanov, 1968, in *Behavior of Dense Media Under High Dynamic Pressures* (Gordon and Breach, New York), p. 361.
Samara, G. A., and H. G. Drickamer, 1962, J. Phys. Chem. Solids **23**, 457.
Samara, G. A., and W. L. Chrisman, 1971, in *Accurate Characterization of the High Pressure Environment*, edited by E. C. Lloyd, National Bureau of Standards Special Publication No. 326, U. S. Government Printing Office, p. 243.
Schardin, H., 1941, Jahrbuch Der Deutsche Akademie Der Luftfahrtforschung, p. 314.
Schumann, H., 1973, Phil. Mag. **28**, 1153.
Shockey, D. A., D. R. Curran, and P. S. DeCarli, 1975, J. Appl. Phys. **46**, 3766.
Smith, C. S., 1958, Trans. Metall. Soc. AIME (Am. Inst. Min. Metall. Pet. Eng.) **212**, 574.
Soma, T., A. Sawaoka, and S. Saito, 1975, in *Proceedings of the Fourth International Conference on High Pressure, Kyoto, 1974*, edited by J. Osugi (The Physico-Chemical Society

of Japan, Kyoto), p. 446.
Snay, H., and G. Rosenbaum, 1952, U. S. Naval Ordnance Laboratory Report No. 2383 (U. S. Naval Ordnance Laboratory, White Oak, Md.).
Stishov, S. M., and S. V. Popova, 1961, Geochemistry No. 10, 923 (translation of Geokhimiya).
Stoffler, D., 1971, J. Geophys. Res. **76**, 5474.
Stoffler, D., 1972, Fortschr. Mineral. **49**, 50.
Syono, Y., T. Goto, J. Nakai, and Y. Nakagawa, 1975, in *Proceedings of the Fourth International Conference on High Pressure, Kyoto, 1974*, edited by J. Osugi (The Physico-Chemical Society of Japan, Kyoto), p. 466.
Syono, Y., T. Goto, and Y. Nakagawa, 1977, in *High Pressure Research Applications in Geophysics*, edited by M. H. Manghnani and S. K. Akimoto (Academic, New York).
Takahashi, T., and W. A. Bassett, 1964, Science **145**, 483.
Taylor, J. W., and M. H. Rice, 1963, J. Appl. Phys. **34**, 364.
Temperley, H. N. V., 1956, *Changes of State* (Cleaver-Hume, London).
Thunborg, S., G. E. Ingram, and R. A. Graham, 1964, Rev. Sci. Instrum. **35**, 11.
Trueb, L. F., 1968, J. Appl. Phys. **39**, 4207.
Trueb, L. F., 1970, J. Appl. Phys. **41**, 5029.
Trueb, L. F., 1971, J. Appl. Phys. **42**, 503.
Trunin, R. F., G. V. Simakov, B. N. Moiseev, L. V. Popov, and M. A. Podurets, 1969, Sov. Phys.—JETP **29**, 628.
Trunin, R. F., G. V. Simakov, M. A. Podurets, B. N. Moiseev, and L. V. Popov, 1971a, Bull. Acad. Sci. USSR, Physics of the Solid Earth, No. 1, p. 8.
Trunin, R. F., G. V. Simakov, and M. Podurets, 1971b, Bull. Acad. Sci. USSR, Physics of the Solid Earth, No. 2, p. 102.
Urtiew, P. A., and R. Grover, 1971, in *Temperature—Its Measurement and Control In Science and Industry*, Vol. 4, Part 1 (Instrument Society of America, Pittsburgh), p. 677.
Urtiew, P. A., and R. Grover, 1974, J. Appl. Phys. **45**, 140.
Urtiew, P. A., and R. Grover, 1977, J. Appl. Phys. **48**, 1122.
Vanfleet, H. B., and R. J. Zeto, 1971, J. Appl. Phys. **42**, 4955.
Van Thiel, M., L. B. Hord, W. H. Gust, A. C. Mitchell, M. D'Addario, K. Boutwell, E. Wilbarger, and B. Barrett, 1974, Phys. Earth Planet. Inter. **9**, 57.
Vdovykin, G. P., A. N. Dremin, S. N. Pershin, and I. D. Shevaleevskii, 1973, Combust. Explos. Shock Waves **9**, 464.
Vereshchagin, L. F., and S. S. Kabalkina, 1965, Sov. Phys.—JETP **20**, 274.
Vereshchagin, L. F., G. A. Adadurov, O. N. Breusov, K. P. Burdina, L. N. Burenkova, A. N. Dremin, E. V. Zubova, and A. T. Rogacheva, 1969a, Sov. Phys.—Dokl. **13**, 896.
Vereshchagin, L. F., A. A. Semerchan, N. N. Kuzin, and Yu. A. Sadkov, 1969b, Sov. Phys.—Dokl. **14**, 340.
Vereshchagin, L. F., E. N. Yakovlev, and Yu. A. Timofeev, 1975, JETP Lett. **21**, p. 85.
Viard, J., 1962, in *Les Ondes de Detonation* (Centre National de la Recherche Scientifique, 15, Quai Anatole-France, Paris), p. 383.
Voskoboinikov, I. N., and V. N. Bogomolov, 1968, JETP Lett. **7**, 264.
Wackerle, J., 1962, J. Appl. Phys. **33**, 922.
Walsh, J. M., 1969, J. Geophys. Res. **74**, 4333.
Walsh, J. M., and R. H. Christian, 1955, Phys. Rev. **97**, 1544.
Walsh, J. M., and M. H. Rice, 1957, J. Chem. Phys. **26**, 815.
Warnes, R. H., 1967, J. Appl. Phys. **38**, 4629.
Warnes, R. H., 1968, Bull. Am. Phys. Soc. **13**, 579.
Wayne, R. C., 1969, J. Appl. Phys. **40**, 15.
Weidner, D. J., and E. B. Royce, 1970, Lawrence Radiation Laboratory Report UCID 15629.
Wentorf, R. H., Jr., and J. S. Casper, 1963, *Science* **139**, 338.
White, B. H., E. B. Royce, and R. N. Keeler, 1968, Bull. Am. Phys. Soc. **13**, 1661.
Wigner, E., and H. B. Huntington, 1935, J. Chem. Phys. **3**, 764.
Wong, J. V., 1969, J. Appl. Phys. **40**, 1789.
Wong, J. V., R. K. Linde, and P. S. DeCarli, 1968, Nature (Lond.) **219**, 713.
Zeldovich, Ya. B., S. B. Kormer, M. V. Sinitsyn, K. B. Yushko, 1961, Sov. Phys.—Dokl. **6**, 494.
Zeldvoich, Ya. B., and Yu. P. Raiser, 1966, in *Physics of Shock Waves and High-Temperature Phenomena Vol. I*, edited by W. D. Hayes and R. F. Probstein (Academic, New York).
Zeldovich, Ya. B., and Yu. P. Raiser, 1967, in *Physics of Shock Waves and High-Temperature Phenomena Vol. II*, edited by W. D. Hayes and R. F. Probstein (Academic, New York).
Zukas, E. G., and C. M. Fowler, 1961, in *Response of Metals to High Velocity Deformation* (Interscience, New York), p. 343.
Zukas, E. G., C. M. Fowler, F. S. Minshall, and J. O'Rourke, 1963, Trans. Metall. Soc. AIME (Am. Inst. Min. Metall. Pet. Eng.) **227**, 746.